IL NUOVO CIMENTO Vol. 36 C, N. 1 Suppl. 1 Gennaio-Febbraio 2013
DOI 10.1393/ncc/i2013-11495-4

Colloquia: 12th Italian-Korean Symposium 2011

On the general relativistic Thomas-Fermi theory of white dwarfs and neutron stars

J. A. Rueda(*) and R. Ruffini(**)

Dipartimento di Fisica and ICRA, Sapienza Università di Roma - P.le Aldo Moro 5 I-00185 Rome, Italy and
ICRANet - P.zza della Repubblica 10, I-65122 Pescara, Italy

ricevuto il 9 Marzo 2012

Summary. — We present a review of the multi-year effort in the formulation of a self-consistent theory for the description of white dwarfs and neutron stars based on the general relativistic extension of the Thomas-Fermi model of the atom.

PACS 04.40.Dg – Relativistic stars: structure, stability, and oscillations.
PACS 26.60.Dd – Neutron star core.
PACS 26.60.Gj – Neutron star crust.
PACS 26.60.Kp – Equations of state of neutron-star matter.

1. – Introduction

That the Thomas-Fermi model originates from the realm of Atomic Physics has been known for a long time [1, 2]. It has been in 1973 that, as a theoretical interest it was proposed that the Thomas-Fermi model could be useful to give an alternative derivation of a self-gravitating system of fermions within Newtonian gravity leading to a description of neutron stars and white dwarfs complementary to the traditional derivation in the perfect fluid approximation [3, 4]. This gravitational treatment needed the special relativistic generalization of the Thomas-Fermi model, which became also a necessity in order to describe the physics of heavy nuclei [5-7]. The Thomas-Fermi treatment from the original realm of Atomic Physics started so to be applied in its special relativistic extension to gravitational and Nuclear Physics.

(*) E-mail: jorge.rueda@icra.it
(**) E-mail: ruffini@icra.it

It has been until [8-11] that all these considerations have been extended to a heuristic simplified Thomas-Fermi model of a neutron star taking into account Nuclear Physics, Newtonian Physics, and β-equilibrium. The evidence for the possible existence of overcritical electric fields at the core of neutron stars was there presented [9]. At this stage a basic theoretical progress in the description of neutron stars with a fully relativistic Thomas-Fermi model with all interactions became a *necessity*. Particularly important has been to use a Wigner Seitz cell: we first solved the relativistic Thomas-Fermi model for compressed atoms [12], generalizing the classical approach of Feynman, Metropolis and Teller (FMT) [13]. This has given as a byproduct a new equation of state for white dwarfs duly expressed in general relativity [14]. We then proved the impossibility of imposing local charge neutrality on chemically equilibrated matter made of neutrons, protons, and electrons, in the simplified case where strong interactions are neglected [15]. This was a critical issue for neutron star matter calculations, since we demonstrated that the equations which describe baryonic matter need to be solved simultaneously in combination with the Einstein-Maxwell equations. The general formulation to the case of strong interactions have been recently achieved in [16]. The present article is the result of the above multi year effort and summarizes and discusses the relevant equations for the description of neutron stars, *i.e.* relativistic mean field theory and the Einstein-Maxwell-Thomas-Fermi system of general relativistic equations, presenting a self-consistent neutron star model including all fundamental interactions: strong, weak, electromagnetic, and gravitational.

It is well-known that the classic works of Tolman [17] and of Oppenheimer and Volkoff [18], for short TOV, address the problem of neutron star equilibrium configurations composed only of neutrons. For the more general case when protons and electrons are also considered, in all of the scientific literature on neutron stars it is assumed that the condition of local charge neutrality applies identically to all points of the equilibrium configuration (see, *e.g.*, [19]). Consequently, the corresponding solutions in this more general case of a non-rotating neutron star, are systematically obtained also on the base of the TOV equations.

In general, the formulation of the equilibrium of systems composed by different particle species must be established within the framework of statistical physics of multicomponent systems; see, *e.g.*, [20]. Thermodynamic equilibrium of these systems is warrantied by demanding the constancy throughout the configuration of the generalized chemical potentials, often called "electro-chemical", of each of the components of the system; see *e.g.* [21-23]. Such generalized potentials include not only the contribution due to kinetic energy but also the contribution due to the potential fields, *e.g.* gravitational and electromagnetic potential energies per particle, and in the case of rotating stars also the centrifugal potential. For such systems in presence of gravitational and Coulomb fields, global electric polarization effects at macroscopic scales occur. The balance of the gravitational and electric forces acting on ions and electrons in ideal electron-ion plasma leading to the occurrence of gravito-polarization was pointed out in the classic work of S. Rosseland [24].

If one turns to consider the gravito-polarization effects in neutron stars, the corresponding theoretical treatment acquires remarkable conceptual and theoretical complexity, since it must be necessarily formulated consistently within the Einstein-Maxwell system of equations. O. Klein, in [21], first introduced the constancy of the general relativistic chemical potential of particles, hereafter "Klein potentials", in the study of the thermodynamic equilibrium of a self-gravitating one-component fluid of neutral particles throughout the configuration within the framework of general relativity. The extension

of the Klein's work to the case of neutral multicomponent degenerate fluids can be found in [22] and to the case of multi-component degenerate fluid of charged particles in [23].

Using the concept of Klein potentials, we have recently proved the impossibility of imposing the condition of local charge neutrality in the simplest case of a self-gravitating system of degenerate neutrons, protons and electrons in β-equilibrium [15]: it has been shown that the consistent treatment of the above system implies the solution of the general relativistic Thomas-Fermi equations, coupled with the Einstein-Maxwell ones, being the TOV equations thus superseded.

We have recently formulated the theory of a system of neutrons, protons and electrons fulfilling strong, electromagnetic, weak and gravitational interactions [16] (see sect. **12** for details). The role of the Klein first integrals has been again evidenced and their theoretical formulation in the Einstein-Maxwell background and in the most general case of finite temperature has been there presented, generalizing the previous results for the "non-interacting" case [15]. The strong interactions, modeled by a relativistic nuclear mean field theory, are there described by the introduction of the σ, ω and ρ virtual mesons.

The equilibrium configurations of non-rotating neutron stars following this new approach (see [15, 16]) have been constructed in [25] where the properties of neutron star matter and neutron stars treated fully self-consistently with strong, weak, electromagnetic, and gravitational interactions have been computed. The full set of the Einstein-Maxwell-Thomas-Fermi equations has been solved numerically for zero temperatures and for selected parameterizations of the nuclear model (see sect. **13** for details).

In this article we present a brief review of all the above literature that led to what we can call a general relativistic Thomas-Fermi theory of white dwarfs and neutron stars which treats in a self-consistent relativistic fashion the strong, weak, electromagnetic, and gravitational interactions inside these high-density objects. We use CGS units throughout the article except in sects. **12** and **13** where units with $\hbar = c = 1$ are employed.

2. – The classical Thomas-Fermi model

Thomas [26] and Fermi [27] published, independently in the 1920s, a simple and elegant approximation to the Schrödinger theory of a many electron atom (after named Thomas-Fermi model), which is useful in providing quick numerical estimates and a physical feel for some atomic phenomena (see, *e.g.*, [1]). This model has been applied to the analysis both of ions and neutral atoms by many classical papers from the Rome group and abroad while Feynman, Metropolis and Teller [13] generalized the applicability of the model to the study of compressed atoms. These results have become of paramount importance in the analysis of the internal constitutions of the stars at the end point of thermonuclear evolution. This section is devoted to the semi-classical Thomas-Fermi theory using the statistics for degenerate fermions. The Thomas-Fermi equation in the non-relativistic formulation is obtained and discussed in order to describe free neutral atoms, positive ions and compressed atoms.

The Thomas-Fermi model assumes that the electrons of an atom constitute a fully degenerate gas of fermions confined in a spherical region by the Coulomb potential of a point-like nucleus of charge $+eN_p$. The condition of equilibrium of the electrons in the atom, in the non-relativistic limit, is expressed by

$$E_e^F = \frac{(P_e^F)^2}{2m_e} - eV = \text{const}, \tag{1}$$

where m_e is the electron mass, V is the electrostatic potential and P_e^F and E_e^F are the electron Fermi momentum and energy.

The electrostatic potential fulfills, for $r > 0$, the Poisson equation

$$\nabla^2 V = 4\pi e n_e, \tag{2}$$

where the electron number density n_e is related to the Fermi momentum P_e^F by

$$n_e = \frac{(P_e^F)^3}{3\pi^2\hbar^3}\,. \tag{3}$$

Introducing the potential $\phi(r)$ through

$$eV(r) + E_e^F = e^2 N_p \frac{\phi(r)}{r}\,, \tag{4}$$

and the dimensionless radial coordinate η as

$$r = b\eta, \qquad b = \frac{(3\pi)^{2/3}}{2^{7/3}} \frac{1}{N_p^{1/3}} \frac{\hbar^2}{e^2 m_e} = \frac{\sigma}{N_p^{1/3}} r_{\mathrm{Bohr}}, \tag{5}$$

where $\sigma = (3\pi)^{2/3}/2^{7/3}$ and $r_{\mathrm{Bohr}} = \hbar^2/(e^2 m_e)$ is the Bohr radius, we obtain the electron number density

$$n_e(\eta) = \frac{N_p}{4\pi b^3} \left[\frac{\phi(\eta)}{\eta}\right]^{3/2}, \tag{6}$$

and eq. (2) can be rewritten in the form

$$\frac{\mathrm{d}^2\phi(\eta)}{\mathrm{d}\eta^2} = \frac{\phi(\eta)^{3/2}}{\eta^{1/2}}\,. \tag{7}$$

Equation (7) is called the classic Thomas-Fermi equation [27] and it can be solved once two boundary conditions are given. The Thomas-Fermi equation is independent on the atomic number N_p and therefore its solution can be used to describe any atom through specific scaling laws.

A first boundary condition for eq. (7) follows from the point-like structure of the nucleus

$$\phi(0) = 1, \tag{8}$$

and a second boundary condition comes from the number of electrons of the system

$$N_e = \int_0^{R_0} 4\pi n_e(r) r^2 \mathrm{d}r = N_p[1 - \phi(\eta_0) + \eta_0 \phi'(\eta_0)], \tag{9}$$

where $R_0 = b\eta_0$ is the radius of the atom, which constrains the value of the first derivative of the Thomas-Fermi function at the origin $\phi'(0)$ depending on the kind of atom we

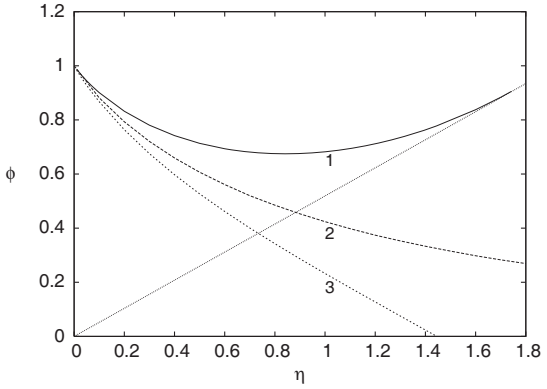

Fig. 1. – Physically relevant solutions of the Thomas-Fermi differential equation (7) with the boundary conditions (8) and (9). The curve 1 refers to a neutral compressed atom. The curve 2 refers to a neutral free atom. The curve 3 refers to a positive ion. The dotted straight line is the tangent to the curve 1 at the point $(\eta_0, \phi(\eta_0))$ corresponding to overall charge neutrality (see eq. (9)).

consider: ionized ($N_e < N_p$, $n_e(R_0) = 0$, $V(R_0) > 0$), free ($N_e = N_p$, $n_e(R_0) = 0$, $V(R_0) = 0$) or compressed ($N_e = N_p$, $n_e(R_0) > 0$, $V(R_0) = 0$), as can be seen in fig. 1. The electron Fermi energy is, respectively, negative, zero or positive.

It is worth to mention that in the case of free neutral atoms $\eta_0 \to \infty$ and $\phi(\eta_0) \to 0$ (see fig. 1).

For compressed atoms, using eqs. (1) and (3), the Fermi energy of electrons satisfies the universal relation (see fig. 2)

$$\frac{\sigma r_{\mathrm{Bohr}}}{e^2} \frac{E_e^F}{N_p^{4/3}} = \frac{\phi(\eta_0)}{\eta_0}\,, \tag{10}$$

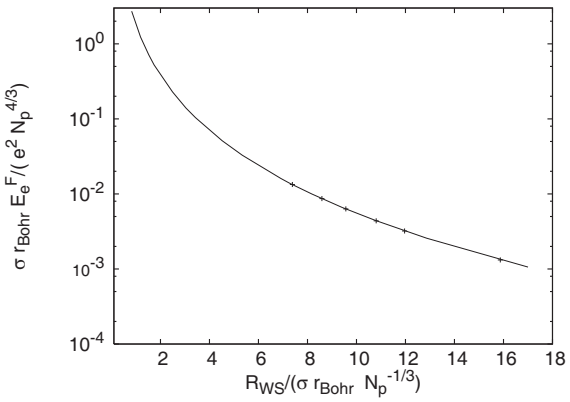

Fig. 2. – The electron Fermi energy E_e^F, in units of $e^2 N_p^{4/3}/(\sigma r_{\mathrm{Bohr}})$ is plotted as a function of the atom radius R_0, in units of $\sigma r_{\mathrm{Bohr}} N_p^{-1/3}$ (see eqs. (10), (11)). Points refer to the numerical integrations of the Thomas-Fermi equation (7) performed originally by Feynman, Metropolis and Teller in [13].

while the atom radius R_0 satisfies the universal relation

$$\frac{R_0}{\sigma r_{\rm Bohr} N_p^{-1/3}} = \eta_0, \tag{11}$$

An analogous Thomas-Fermi approach as the one summarized above in the case of atoms can be used to describe a system of self-gravitating fermions. The relevance of a gravitational Thomas-Fermi model for the understanding of the equilibrium configurations of self-gravitating collapsed objects has been known for a long time (see *e.g.* [3]). We briefly review such a theory in the following Section.

3. – The gravitational non-relativistic Thomas-Fermi model

Let us assume a system of N degenerate fermions of mass m, so the particle number density n is given by

$$n = \frac{(P^F)^3}{3\pi^2\hbar^3}\,, \tag{12}$$

where P^F is the Fermi momentum of the fermions.

The equilibrium condition of the configuration in the non-relativistic case is given by

$$E^F = \frac{(P^F)^2}{2m} - m\Phi = -m\Phi_0 = \text{constant}, \tag{13}$$

where Φ is the gravitational potential which fulfills in this case the Poisson equation

$$\nabla^2\Phi = -4\pi G m n, \tag{14}$$

G is Newton's gravitational constant, and Φ_0 is the gravitational potential at the radius R of the system, so

$$\Phi_0 = \frac{GM}{R}\,, \tag{15}$$

being M the total mass of the configuration.

Introducing the potential $\chi(r)$ through

$$\Phi - \Phi_0 = GmN\frac{\chi(r)}{r}\,, \tag{16}$$

and the dimensionless radial coordinate ξ as

$$r = b_g\xi, \qquad b_g = \frac{(3\pi)^{2/3}}{2^{7/3}}\frac{1}{N^{1/3}}\frac{\hbar^2}{Gm^3}\,, \tag{17}$$

we obtain the electron number density

$$n(\eta) = \frac{N}{4\pi b_g^3}\left[\frac{\chi(\xi)}{\xi}\right]^{3/2}, \tag{18}$$

and eq. (14) can be rewritten in the form

$$\frac{\mathrm{d}^2\chi(\xi)}{\mathrm{d}\xi^2} = -\frac{\chi(\xi)^{3/2}}{\xi^{1/2}}\,. \tag{19}$$

Equation (19) differs from eq. (7) only in the minus sign on the right-hand side and corresponds to the well-known Lane-Emden equation [28]

$$\frac{\mathrm{d}^2\chi(\xi)}{\mathrm{d}\xi^2} = -\frac{\chi(\xi)^{n}}{\xi^{n-1}}\,, \tag{20}$$

for the specific case $n = 3/2$. This gravitational Thomas-Fermi equation must be solved with the boundary conditions

$$\chi(0) = \chi(R) = 0, \tag{21}$$

as required from eq. (16) and the first derivative of the Thomas-Fermi function at the origin $\chi(0)$ is constrained in order to fulfill the normalization condition

$$N = \int_0^R 4\pi r^2 n \mathrm{d}r = N\int_0^{\xi_0} \chi^{3/2}\xi^{1/2}\mathrm{d}\xi, \tag{22}$$

from which we obtain

$$\int_0^{\xi_0} \chi^{3/2}\xi^{1/2}\mathrm{d}\xi = -\xi_0\chi'(\xi_0) = 1, \tag{23}$$

where $\xi_0 = R/b_g$ and we have used eqs. (20) and (21).

It is appropriate to discuss the homothetic property of the Lane-Emden equation (20) with particular attention to the gravitational Thomas-Fermi equation (19). Introducing the transformations

$$\hat{\xi} = A\xi, \qquad \hat{\chi} = B\chi, \tag{24}$$

eq. (20) becomes

$$\frac{\mathrm{d}^2\hat{\chi}(\hat{\xi})}{\mathrm{d}\hat{\xi}^2} = -\frac{A^{n-3}}{B^{n-1}}\frac{\hat{\chi}(\hat{\xi})^{n}}{\hat{\xi}^{n-1}}\,, \tag{25}$$

and thus we obtain from the invariance condition

$$B = A^{(n-3)/(n-1)}, \tag{26}$$

which in the specific case $n = 3/2$ of eq. (19) reads

$$B = \frac{1}{A^3}\,. \tag{27}$$

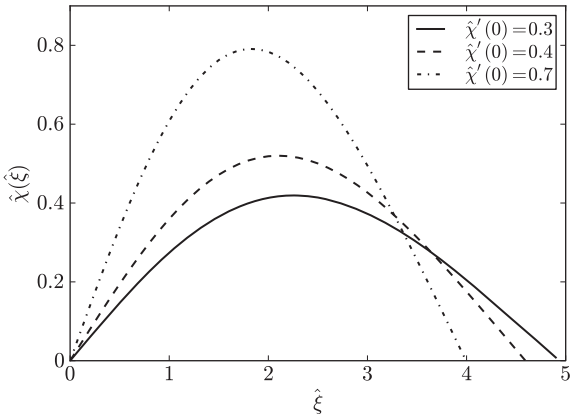

Fig. 3. – Generic solutions of the gravitational Thomas-Fermi differential equation (19) with the boundary condition (21), but not the normalization (23). In order to satisfy the normalization condition (23), these specific solutions must be rescaled using the transformations (24) and the relations (27) and (31) with $A = 0.968679$, $A = 0.901458$ and $A = 0.783765$ for the solid, dashed and dot-dashed curves, respectively.

These transformations are useful to obtain solutions of the gravitational Thomas-Fermi equation (19) that satisfy the normalization condition (23) as follows. For given initial conditions $\hat{\chi}(0)$ and $\hat{\chi}'(0) > 0$ we can solve numerically eq. (23) until the boundary $\hat{\chi}(\hat{\xi}_0) = 0$, as shown in fig. 3.

The solution satisfies at the boundary $\hat{\xi}_0$

$$\int_0^{\hat{\xi}_0} \hat{\chi}^{3/2}\hat{\xi}^{1/2}\mathrm{d}\hat{\xi} = -\hat{\xi}_0\hat{\chi}'(\hat{\xi}_0) = D, \tag{28}$$

which by applying the homothetic transformation becomes

$$A^{3/2}B^{3/2}\int_0^{\xi_0} \chi^{3/2}\xi^{1/2}\mathrm{d}\xi = D, \tag{29}$$

or equivalently

$$\int_0^{\xi_0} \chi^{3/2}\xi^{1/2}\mathrm{d}\xi = DA^3, \tag{30}$$

where we have used eq. (27). Thus, in order to satisfy the normalization condition (23) we find the condition

$$A = \frac{1}{D^{1/3}}\,. \tag{31}$$

3˙1. *Application to neutron stars and white dwarfs.* – For the case of neutron stars we assume first, as a zeroth approximation, a neutron star made only of free neutrons. It is clear that this configuration is unstable with respect to the β-decay of neutrons

and therefore in a realistic configuration both protons and electrons must be necessarily present. In such a case the electromagnetic interactions between the charged particles and the strong interactions between nucleons must be taken properly into account. We shall discuss this general case later on.

In the simplified case of a self-gravitating system of non-relativistic degenerate neutrons, the configurations of equilibrium can be simply constructed using the gravitational Thomas-Fermi model by changing $m \to m_n$ where m_n is the neutron mass. Instead, the application of the above equations to the case of white dwarfs is less straightforward and it must be done as follows.

Both Chandrasekhar [29] and Landau [30] neglected the electromagnetic interactions in the white-dwarf interior. The contribution of the electrons to the density and the one of the nuclei to the pressure are neglected as well, namely

$$\rho \approx \rho_N, \qquad P \approx P_e. \tag{32}$$

The Thomas-Fermi equilibrium condition in the gravitational case given by eq. (13) can be regarded as the condition for the thermodynamic equilibrium of the system. Neglecting the contribution of the nuclei to the kinetic energy and the contribution of the electrons to the mass, eq. (13) becomes

$$E^F = \frac{(P_e^F)^2}{2m_e} - \mu m_N \Phi = -\mu m_N \Phi_0 = \text{const}, \tag{33}$$

where $m_N \approx m_n$ is the nucleon mass, P_e^F is the Fermi momentum of electrons and $\mu = A/Z \approx 2$ is the average molecular weight of the nuclei.

We note here the hybrid character of eq. (33) describing an effective one-component electron-nucleon fluid approach where the kinetic pressure is given by electrons of mass m_e and their gravitational contribution is given by an effective mass μM_N attached to each electron (see, *e.g.*, [31] for details).

In this case the gravitational Poisson equation (14) becomes

$$\nabla^2 \Phi = -4\pi G \mu m_N n_e, \tag{34}$$

where n_e is the electron number density given by

$$n_e = \frac{(P_e^F)^3}{3\pi^2 \hbar^3}\,. \tag{35}$$

Introducing the potential $\chi(r)$ through

$$\Phi - \Phi_0 = G\mu m_N N \frac{\chi(r)}{r}\,, \tag{36}$$

and the dimensionless radial coordinate ξ as

$$r = b_g \xi, \qquad b_g = \frac{(3\pi)^{2/3}}{2^{7/3}} \frac{1}{N^{1/3}} \frac{\hbar^2}{G m_e} \frac{1}{(\mu m_N)^2}\,, \tag{37}$$

eq. (34) can be rewritten in the form

$$\frac{\mathrm{d}^2\chi(\xi)}{\mathrm{d}\xi^2} = -\frac{\chi(\xi)^{3/2}}{\xi^{1/2}}\,, \tag{38}$$

which is the gravitational Thomas-Fermi equation that must be solved with the boundary conditions (21) and (23).

We have so far assumed that the particles inside the stars are non-relativistic. However, it can be seen that such an approximation is in fact not suitable for the interior white dwarfs and neutron stars. Neglecting the contribution of electrons to the density, the Fermi momentum of the electrons in a white dwarf is approximately given by

$$P_e^F = \frac{(3\pi)^{1/3}}{(\mu m_N)^{1/3}}\hbar\rho^{1/3}, \tag{39}$$

where we have used eq. (35). From this expression we can check that at densities $\rho \sim 10^6\,\mathrm{g/cm^3}$ $P_e^F \sim m_e c$ and thus the non-relativistic approximation breaks down. The same situation occurs for the neutrons in neutron stars at densities $\rho \sim 10^{15}\,\mathrm{g/cm^3}$. It is therefore necessary to reformulate the gravitational Thomas-Fermi model in order to include the effects of special relativity.

4. – Gravitational special relativistic Thomas-Fermi model

In analogy with the Thomas-Fermi atom [26, 27], the equilibrium condition of this configuration in the relativistic case can be expressed as

$$E^F = \sqrt{(cP^F)^2 + m^2c^4} - mc^2 - m\Phi = \mathrm{const} = -m\Phi(R), \tag{40}$$

where Φ is the gravitational potential and R is the radius of the configuration at which the Fermi momentum of the fermions vanishes, namely $P^F(R) = 0$. The gravitational potential satisfies the Poisson equation

$$\nabla^2\Phi = -4\pi\, G\,\rho_0, \tag{41}$$

where $\rho_0 = m\,n$ is the rest-mass density.

Introducing the dimensionless radial coordinate

$$r = b\,\xi, \qquad b = \frac{(3\pi)^{2/3}}{2^{7/3}}\frac{1}{N^{1/3}}\frac{\hbar^2}{Gm^3}\,, \tag{42}$$

and a new potential $\chi(r)$ defined by

$$\Phi(r) - \Phi(R) = GmN\frac{\chi(r)}{r}\,, \tag{43}$$

with N the total number of fermions in the system, eq. (41) becomes

$$\frac{\mathrm{d}^2\chi(\xi)}{\mathrm{d}\xi^2} = -\frac{\chi(\xi)^{3/2}}{\xi^{1/2}}\left[1 + \left(\frac{N}{N^*}\right)^{4/3}\frac{\chi(\xi)}{\xi}\right]^{3/2}\,, \tag{44}$$

where N^* is given by

$$N^* = \frac{\sqrt{3\pi}}{2}\left(\frac{m_{\rm Planck}}{m}\right)^3, \tag{45}$$

with $m_{\rm Planck} = \sqrt{\hbar c/G}$ the Planck's mass.

The relativistic Thomas-Fermi equation (44) must be solved subjected to the boundary conditions

$$\chi(0) = \chi(\xi_0) = 0, \qquad \left(\frac{{\rm d}\chi}{{\rm d}\xi}\right)_{\xi=0} > 0, \tag{46}$$

where $\xi_0 = R/b$.

The first derivative of χ at the origin is, at the same time, subjected to the condition that at the radius of the configuration the total number of particles must be equal to N. Mathematically, such a condition can be written as

$$\int_0^{\xi_0} \chi^{3/2}\xi^{1/2}{\rm d}\xi = -\xi_0\left(\frac{{\rm d}\chi}{{\rm d}\xi}\right)_{\xi=\xi_0} = 1. \tag{47}$$

In the extreme relativistic approximation $P^F \gg m\,c$, the equilibrium condition (40) becomes

$$E_F = cP^F - m\Phi = {\rm const} = -m\Phi(R), \tag{48}$$

and the relativistic Thomas-Fermi equation (44) reads simply

$$\frac{{\rm d}^2\chi(\xi)}{{\rm d}\xi^2} = -\left(\frac{N}{N^*}\right)^2\frac{\chi(\xi)^3}{\xi^2}\,. \tag{49}$$

with the following boundary conditions:

$$\chi(0) = 0, \qquad \chi(\xi_0) = 0, \qquad 1 = -\xi_0\left(\frac{{\rm d}\chi}{{\rm d}\xi}\right)_{\xi=\xi_0}. \tag{50}$$

Considering now the transformation $\chi = A\hat{\chi}$, $x = B\hat{x}$ with $A^2(N/N^*)^2 = 1$, eq. (49) becomes

$$\frac{{\rm d}^2\hat{\chi}}{{\rm d}\hat{x}^2} = -\frac{\hat{\chi}^3}{\hat{x}^2}\,, \tag{51}$$

that is the Lane-Emden polytropic equation of index $n = 3$. The boundary conditions are

$$\hat{\chi}(0) = 0, \qquad \hat{\chi}(\hat{x}_0) = 0, \qquad \frac{N}{N^*} = -\hat{x}_0\left(\frac{{\rm d}\hat{\chi}}{{\rm d}\hat{x}}\right)_{\hat{x}=\hat{x}_0}. \tag{52}$$

As we have seen, the eq. (51) is obtained for any value of the factor B, and therefore it is invariant under the scaling $\hat{x} = a\tilde{x}$ with a any constant. Thus, from a given solution

a whole class of solutions can be derived by a simple change of the scale. Consequently the quantity $\hat{x}_0(\frac{\mathrm{d}\hat{\chi}}{\mathrm{d}\hat{x}})_{\hat{x}=\hat{x}_0}$ is a constant. This constant has the value 2.015 (see, *e.g.*, [28]) and gives the following upper limit for the mass of the configuration:

$$M_{\mathrm{crit}} = m\,N = 2.015\,N^* = 2.015\frac{\sqrt{3\pi}}{2}\frac{m_{\mathrm{Planck}}^3}{m^2}\,. \tag{53}$$

4˙1. *Application to white dwarfs and neutron stars.* – Considering that in a white dwarf the electrons of mass m_e are mostly responsible for the pressure (kinetic energy) while the nuclei of molecular weight $\mu = A/Z$ provide the density of the system (gravitational energy), the equilibrium condition (40) can be written as

$$c\sqrt{(cP_e^F)^2 + m_e^2c^2} - m_ec^2 - \mu m_N\Phi = -\mu m_N\Phi(R), \tag{54}$$

where P_e^F is the electron Fermi momentum and m_N is the nucleon rest-mass. We note therefore that all the above gravitational Thomas-Fermi model can be applied to white dwarfs by assuming

$$b = \frac{(3\pi)^{2/3}}{2^{7/3}}\frac{1}{N^{1/3}}\frac{\hbar^2}{Gm_e}\frac{1}{(\mu m_N)^2} \tag{55}$$

and

$$N^* = \frac{\sqrt{3\pi}}{2}\left(\frac{m_{\mathrm{Planck}}}{\mu m_N}\right)^3. \tag{56}$$

The critical mass given by eq. (53) can be then written for white dwarfs as

$$M_{\mathrm{crit}} = m_n\,N = 2.015\,N^* = \frac{\sqrt{3\pi}}{2}\frac{m_{\mathrm{Planck}}^3}{\mu^2 m_N^2} \approx 1.44M_\odot. \tag{57}$$

where for simplicity we have set the average molecular weight $\mu = 2$.

It is interesting at this point to compare this result with the pioneering work of E. C. Stoner [32] who introduced the effect of special relativity into the concept of degenerate stars first introduced by R. H. Fowler [33] in the non-relativistic case. Stoner was indeed the first to discover a critical mass of white dwarfs

$$M_{\mathrm{crit}}^{\mathrm{Stoner}} = \frac{15}{16}\sqrt{5\pi}\frac{m_{\mathrm{Planck}}^3}{\mu^2 m_N^2}\,, \tag{58}$$

assuming a white dwarf of constant density.

Following Stoner's work, Chandrasekhar [29] pointed out the relevance of describing white dwarfs by using an approach, initiated by E. A. Milne [34], of using the mathematical method of the solutions of the Lane-Emden polytropic equations [28]. The same idea of using the Lane-Emden equations taking into account the special relativistic effects to the equilibrium of stellar matter for a degenerate system of fermions, came independently to L. D. Landau [30]. Both the Chandrasekhar and Landau treatments were explicit in

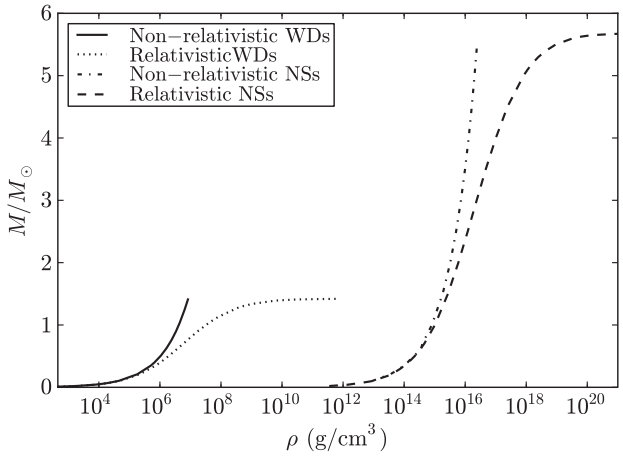

Fig. 4. – Mass *versus* central density of white dwarfs with average molecular weight $\mu = 2$ and of neutron stars in the relativistic case.

pointing out the existence of the critical mass given by the above eq. (57), which is quantitatively smaller than the one obtained first by Stoner due to the inhomogeneity of the density distribution.

For neutron stars, it is enough to change $m \to m_n$ where m_n is the neutron mass. In such a case, the critical mass is given by

$$M_{\rm crit} = m\,N = 2.015\,N^* = \frac{\sqrt{3\pi}}{2}\frac{m_{\rm Planck}^3}{m_n^2} \approx 5.76 M_\odot. \tag{59}$$

It is well known however that special relativistic effects in the determination of the density of the system are important for neutron stars as well as the effects of general relativity. As a result of these additional effects, the critical mass given by eq. (59) is lowered to the a value $\sim 0.7 M_\odot$ for a self-gravitating non-interacting degenerate neutron gas in general relativity (see [18] and sect. **5** below for details).

In fig. 4 we show the mass of the equilibrium configurations of both white dwarfs and neutron stars as a function of the central density in the non-relativistic and relativistic cases.

5. – The TOV equilibrium equations of neutron stars

The importance of special relativity in the description of matter in a compact star such as white dwarfs and neutron stars has been shown in the previous results leading to the concept of critical mass of a self-gravitating object. On the other-hand, the relative importance of general relativistic effects can be estimated from the ratio $GM/(c^2R)$ which gives us the strength of the gravitational field in units of c^2. A roughly estimate of the radii of white dwarfs and neutron stars gives $\sim (m_{\rm Planck}/m_n)(\hbar/(m_e c))$ and $\sim (m_{\rm Planck}/m_n)(\hbar/(m_\pi c))$, respectively, where m_π is the pion mass. We have here assumed a neutron star with an average density of the order of the nuclear one $\sim (\hbar/(m_\pi c))^{-3}$.

Thus, we have

$$\frac{GM}{c^2R} \sim \begin{cases} \dfrac{m_\pi}{m_n} \sim 0.15, & \text{for neutron stars,} \\ \dfrac{m_e}{m_n} \sim 5 \times 10^{-4}, & \text{for white dwarfs.} \end{cases} \tag{60}$$

We can therefore expect the effects of general relativity to be much more important in the description of neutron stars that in the one of white dwarfs. It is however worth mentioning that, as we will show later on, also in the latter case general relativistic effects play an important role.

The earliest general relativistic description of a neutron star date back to 1939 with the seminal work of Oppenheimer & Volkoff [18]. The matter inside a neutron star is considered to be composed only by a gas of degenerate neutrons and the equations of equilibrium are derived for non-rotating neutron stars, *i.e.* in the spherically symmetric case.

The spacetime metric is given by

$$ds^2 = \mathrm{e}^{\nu(r)}c^2dt^2 - \mathrm{e}^{\lambda(r)}dr^2 - r^2d\theta^2 - r^2\sin^2\theta d\varphi^2, \tag{61}$$

and the Einstein equations can be reduced to the hydrostatic equilibrium equation (hereafter TOV equation) [18]

$$\frac{dP(r)}{dr} = -\frac{G[\rho(r) + P(r)/c^2][4\pi r^3P(r)/c^2 + M(r)]}{r^2[1 - 2GM(r)/(c^2r)]}\,, \tag{62}$$

and the equation for the mass function $M(r)$

$$\frac{dM(r)}{dr} = 4\pi r^2\rho(r), \tag{63}$$

where $\rho(r) = \mathcal{E}(r)/c^2$ is the mass-density and the mass $M(r)$ is related to the metric function e^λ thorough $e^{-\lambda(r)} = 1 - 2GM(r)/(c^2r)$.

In fig. 5 we show the mass-radius relation of neutron stars obtained by Oppenheimer & Volkoff [18] and compare it with the results obtained by the non-relativistic Thomas-Fermi theory of sect. **11**.

As we will show later on, such a classic gravitational Thomas-Fermi theory can be duly generalized to general relativistic regimes both in the case of white dwarfs (see sects. **8**–**13**) and neutron stars (see sect. **10**). It is worthy mentioning that the TOV approach needs as well a proper generalization to account for the strong interactions between the nuclear constituents of the neutron star matter (see sects. **12** and **13** for details).

6. – The relativistic Thomas-Fermi atom

In the relativistic generalization of the Thomas-Fermi equation the point-like approximation of the nucleus must be abandoned [6, 7] since the relativistic Thomas-Fermi equilibrium condition

$$E_e^F = \sqrt{(P_e^Fc)^2 + m_e^2c^4} - m_ec^2 - eV(r), \tag{64}$$

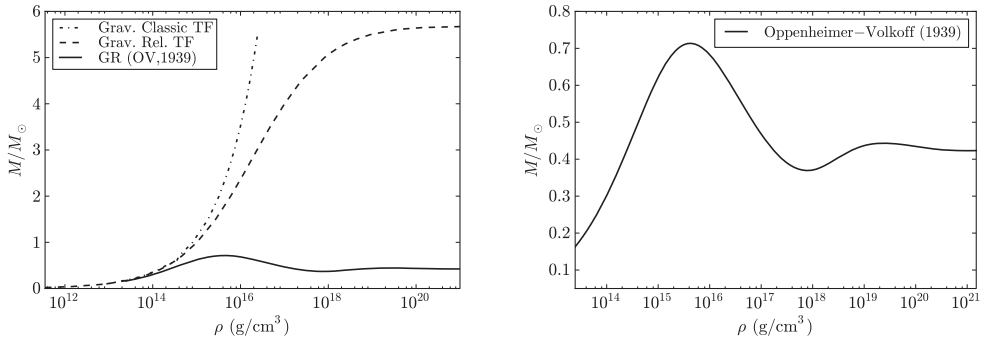

Fig. 5. – Left panel: Mass-Radius relation of neutron stars as given by the gravitational non-relativistic Thomas-Fermi treatment (see sect. **11**), by the gravitational relativistic Thomas-Fermi treatment (see sect. **15**) and by the general relativistic treatment of Oppenheimer & Volkoff [18]. In the right panel it is shown in more detail the Oppenheimer & Volkoff solution.

would lead to a non-integrable expression for the electron density near the origin. Consequently we adopt an extended nucleus. Traditionally the radius of an extended nucleus is given by the phenomenological relation $R_c = r_0 A^{1/3}$, where A is the number of nucleons and $r_0 = 1.2 \times 10^{-13}\,\mathrm{cm}$. Further it is possible to show from the extremization of the semi-empirical Weizsacker mass-formula that the relation between A and N_p is given by

$$N_p \approx \left[\frac{2}{A} + \frac{2a_C}{a_A}\frac{1}{A^{1/3}}\right]^{-1} \approx \left[\frac{2}{A} + \frac{3}{200}\frac{1}{A^{1/3}}\right]^{-1}, \tag{65}$$

where $a_C \approx 0.71\,\mathrm{MeV}$, $a_A \approx 93.15\,\mathrm{MeV}$ are the Coulomb and the asymmetry coefficients respectively. In the limit of small A eq. (65) gives

$$N_p \approx \frac{A}{2}\,. \tag{66}$$

In [11] we have relaxed the condition $N_p \approx A/2$ adopted, *e.g.*, in [5] as well as the condition $N_p \approx [2/A + 3/(200A^{1/3})]^{-1}$ adopted *e.g.* in [6, 7] by imposing explicitly the β-decay equilibrium between neutrons, protons and electrons.

In particular, following the previous treatments (see, *e.g.*, [11]), we have assumed a constant distribution of protons confined in a radius R_c defined by

$$R_c = \Delta \frac{\hbar}{m_\pi c} N_p^{1/3}, \tag{67}$$

where m_π is the pion mass and Δ is a parameter such that $\Delta \approx 1$ ($\Delta < 1$) corresponds to nuclear (supranuclear) densities when applied to ordinary nuclei. Consequently, the proton density can be written as

$$n_p(r) = \frac{N_p}{\frac{4}{3}\pi R_c^3}\theta(R_c - r) = \frac{3}{4\pi}\frac{m_\pi^3 c^3}{\hbar^3}\frac{1}{\Delta^3}\theta(R_c - r), \tag{68}$$

where $\theta(x)$ is the Heaviside function which by definition is given by

$$\theta(x) = \begin{cases} 0, & x < 0, \\ 1, & x > 0. \end{cases} \tag{69}$$

The electron density is given by

$$n_e(r) = \frac{(P_e^F)^3}{3\pi^2\hbar^3} = \frac{1}{3\pi^2\hbar^3 c^3}\left[e^2V^2(r) + 2m_e c^2 eV(r)\right]^{3/2}, \tag{70}$$

where V is the Coulomb potential.

The overall Coulomb potential satisfies the Poisson equation

$$\nabla^2 V(r) = -4\pi e\left[n_p(r) - n_e(r)\right], \tag{71}$$

with the boundary conditions $V(\infty) = 0$ (due to global charge neutrality) and finiteness of $V(0)$.

Using eqs. (4), (5) and replacing the particle densities (68) and (70) into the Poisson equation (71) we obtain the relativistic Thomas-Fermi equation

$$\frac{\mathrm{d}^2\phi(\eta)}{\mathrm{d}\eta^2} = -\frac{3\eta}{\eta_c^3}\theta(\eta_c - \eta) + \frac{\phi^{3/2}}{\eta^{1/2}}\left[1 + \left(\frac{N_p}{N_p^{\mathrm{crit}}}\right)^{4/3}\frac{\phi}{\eta}\right]^{3/2}, \tag{72}$$

where $\phi(0) = 0$, $\phi(\infty) = 0$ and $\eta_c = R_c/b$. The critical number of protons N_p^{crit} is defined by

$$N_p^{\mathrm{crit}} = \sqrt{\frac{3\pi}{4}}\alpha^{-3/2}, \tag{73}$$

where, as usual, $\alpha = e^2/(\hbar c)$.

It is interesting that by introducing the new dimensionless variable

$$x = \frac{r}{\lambda_\pi} = \frac{b}{\lambda_\pi}\eta, \tag{74}$$

and the function

$$\chi = \alpha N_p \phi, \tag{75}$$

where $\lambda_\pi = \hbar/(m_\pi c)$, eq. (72) assumes a canonical form, the master relativistic Thomas-Fermi equation (see [9])

$$\frac{1}{3x}\frac{\mathrm{d}^2\chi(x)}{\mathrm{d}x^2} = -\frac{\alpha}{\Delta^3}\theta(x_c - x) + \frac{4\alpha}{9\pi}\left[\frac{\chi^2(x)}{x^2} + 2\frac{m_e}{m_\pi}\frac{\chi}{x}\right]^{3/2}, \tag{76}$$

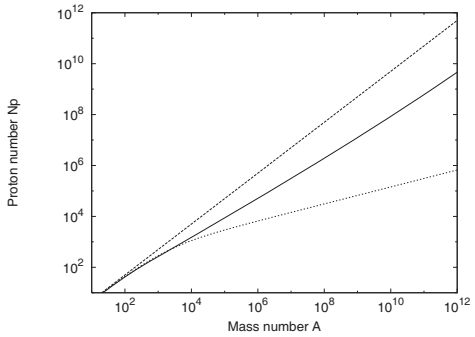

Fig. 6. – The A-N_p relation at nuclear density (solid line) obtained from first principles compared with the phenomenological expressions given by $N_p \approx A/2$ (dashed line) and eq. (65) (dotted line). The asymptotic value, for $A \to (m_{\rm Planck}/m_n)^3$, is $N_p \approx 0.0046A$.

where $x_c = R_c/\lambda_\pi$ with the boundary conditions $\chi(0) = 0$, $\chi(\infty) = 0$. The neutron density $n_n(r)$, related to the neutron Fermi momentum $P_n^F = (3\pi^2\hbar^3 n_n)^{1/3}$, is determined, as in the previous case [11], by imposing the condition of β-equilibrium

$$E_n^F = \sqrt{(P_n^F c)^2 + m_n^2 c^4} - m_n c^2 = \sqrt{(P_p^F c)^2 + m_p^2 c^4} - m_p c^2 + eV(r), \tag{77}$$

which in turn is related to the proton density n_p and the electron density by eqs. (70), (71). Integrating numerically these equations we have obtained a new generalized relation between A and N_p for any value of A. In the limit of small A this result agrees with the phenomenological relations given by eqs. (65), (66), as is clearly shown in fig. 6.

7. – The relativistic Feynman-Metropolis-Teller treatment

Some of the basic assumptions adopted by Chandrasekhar [29] and Landau [30] in their idealized approach of white dwarfs such as the treatment of the electron as a free-gas without taking into due account the electromagnetic interactions, as well as the stability of the distribution of the nuclei against the gravitational interaction led to some criticisms by Eddington [35]. We will show here how the solution of the conceptual problems of the white dwarf models, left open for years, can be duly addressed by considering the relativistic Thomas-Fermi model of the compressed atom.

One of the earliest alternative approaches to the Chandrasekhar-Landau work was proposed by E. E. Salpeter in 1961 [36]. He followed an idea originally proposed by Y. I. Frenkel [37]: to adopt in the study of white dwarfs the concept of a Wigner-Seitz cell. Salpeter introduced to the lattice model of a point-like nucleus surrounded by a uniform cloud of electrons, corrections due to the non-uniformity of the electron distribution (see subsect. **7**˙3 for details). In this way Salpeter [36] obtained an analytic formula for the total energy in a Wigner-Seitz cell and derived the corresponding equation of state of matter composed by such cells, pointing out explicitly the relevance of the Coulomb interaction.

There are different approaches to model the equation of state of nuclei surrounded by electrons, each one characterized by a different way of treating or neglecting the Coulomb interactions, which we will briefly review here. Particular attention is given to the calculation of the self-consistent chemical potential of the Wigner-Seitz cell $\mu_{\rm ws}$, which plays a crucial role in the determination of the equilibrium condition governing white dwarfs.

7˙1. *The uniform approximation.* – In the uniform approximation used, *e.g.*, by Chandrasekhar [29], the electron distribution as well as the nucleons are assumed to be locally constant and therefore the condition of local charge neutrality

$$n_e = \frac{Z}{A_r} n_N, \tag{78}$$

where A_r is the average atomic weight of the nucleus, is applied. Here n_N denotes the nucleon number density and Z is the number of protons of the nucleus. The electrons are considered as a fully degenerate free-gas and then described by Fermi-Dirac statistics. Thus, their number density n_e is related to the electron Fermi-momentum P_e^F by

$$n_e = \frac{(P_e^F)^3}{3\pi^2\hbar^3}\,, \tag{79}$$

and the total electron energy-density and electron pressure are given by

$$\begin{aligned} \mathcal{E}_e &= \frac{2}{(2\pi\hbar)^3}\int_0^{P_e^F} \sqrt{c^2p^2 + m_e^2c^4}\, 4\pi p^2 \mathrm{d}p \\ &= \frac{m_e^4c^5}{8\pi^2\hbar^3}\left[x_e\sqrt{1+x_e^2}(1+2x_e^2) - \operatorname{arcsinh}(x_e)\right], \end{aligned} \tag{80}$$

$$\begin{aligned} P_e &= \frac{1}{3}\frac{2}{(2\pi\hbar)^3}\int_0^{P_e^F} \frac{c^2p^2}{\sqrt{c^2p^2 + m_e^2c^4}}\, 4\pi p^2 \mathrm{d}p \\ &= \frac{m_e^4c^5}{8\pi^2\hbar^3}\left[x_e\sqrt{1+x_e^2}\left(\frac{2}{3}x_e^2 - 1\right) + \operatorname{arcsinh}(x_e)\right], \end{aligned} \tag{81}$$

where we have introduced the dimensionless Fermi momentum $x_e = P_e^F/(m_ec)$, often called relativistic parameter, being m_e the electron rest-mass.

The kinetic energy of nucleons is neglected and therefore the pressure is assumed to be only due to electrons. Thus the equation of state can be written as

$$\mathcal{E}_{\rm unif} = \mathcal{E}_N + \mathcal{E}_e \approx \frac{A_r}{Z} M_u c^2 n_e + \mathcal{E}_e, \tag{82}$$

$$P_{\rm unif} \approx P_e, \tag{83}$$

where $M_u = 1.6604 \times 10^{-24}\,\mathrm{g}$ is the unified atomic mass and $\mathcal{E}_e$ and P_e are given by eqs. (80)–(81).

Within this approximation, the total self-consistent chemical potential is given by

$$\mu_{\rm unif} = A_r M_u c^2 + Z\mu_e, \tag{84}$$

where

$$\mu_e = \frac{\mathcal{E}_e + P_e}{n_e} = \sqrt{c^2 (P_e^F)^2 + m_e^2 c^4}, \tag{85}$$

is the electron free-chemical potential.

As a consequence of this effective approach which does not take into any account the Coulomb interaction, it is obtained an effective one-component electron-nucleon fluid approach where the kinetic pressure is given by electrons of mass m_e and their gravitational contribution is given by an effective mass $(A_r/Z)M_u$ attached to each electron (see *e.g.* [31]). This is even more evident when the electron contribution to the energy-density in eq. (82) is neglected and therefore the energy-density is attributed only to the nuclei. In this approach followed by Chandrasekhar [29], the equation of state reduces to

$$\mathcal{E}_{\mathrm{Ch}} = \frac{A_r}{Z} M_u c^2 n_e, \tag{86}$$

$$P_{\mathrm{Ch}} = P_e. \tag{87}$$

It is worth to note that, in this simple case, no thermodynamically self-consistent chemical potential can be constructed since the chemical potential of electrons must satisfy eq. (85) which needs the presence of the electron contribution to the energy of the system.

7˙2. *The lattice model.* – The first correction to the above uniform model, corresponds to abandon the assumption of the electron-nucleon fluid through the "lattice" model which introduces the concept of Wigner-Seitz cell: each cell contains a point-like nucleus of charge $+eZ$ with A nucleons surrounded by a uniformly distributed cloud of Z fully degenerate electrons. The global neutrality of the cell is guaranteed by the condition

$$Z = V_{\mathrm{ws}} n_e = \frac{n_e}{n_{\mathrm{ws}}}\,, \tag{88}$$

where $n_{\mathrm{ws}} = 1/V_{\mathrm{ws}}$ is the Wigner-Seitz cell density and $V_{\mathrm{ws}} = 4\pi R_{\mathrm{ws}}^3/3$ is the cell volume.

The total energy of the Wigner-Seitz cell is modified by the inclusion of the Coulomb energy, *i.e.*

$$E_{\mathrm{ws}}^{\mathrm{L}} = \mathcal{E}_{\mathrm{unif}} V_{\mathrm{ws}} + E_C, \tag{89}$$

being

$$E_C = E_{e\text{-}N} + E_{e\text{-}e} = -\frac{9}{10}\frac{Z^2 e^2}{R_{\mathrm{ws}}}\,, \tag{90}$$

where $\mathcal{E}_{\mathrm{unif}}$ is given by eq. (82) and $E_{e\text{-}N}$ and $E_{e\text{-}e}$ are the electron-nucleus and the electron-electron Coulomb energies

$$E_{e\text{-}N} = -\int_0^{R_{\mathrm{ws}}} 4\pi r^2 \left(\frac{Ze}{r}\right) e n_e \mathrm{d}r = -\frac{3}{2}\frac{Z^2 e^2}{R_{\mathrm{ws}}}\,, \tag{91}$$

$$E_{e\text{-}e} = \frac{3}{5}\frac{Z^2 e^2}{R_{\mathrm{ws}}}\,, \tag{92}$$

being the latter simply the energy of a uniform distribution of charge.

The self-consistent pressure of the Wigner-Seitz cell is then given by

$$P_{\rm ws}^{\rm L} = -\frac{\partial E_{\rm ws}^{\rm L}}{\partial V_{\rm ws}} = P_{\rm unif} + \frac{1}{3}\frac{E_C}{V_{\rm ws}}\,, \tag{93}$$

where $P_{\rm unif}$ is given by eq. (83). It is worth to recall that the point-like assumption of the nucleus is incompatible with a relativistic treatment of the degenerate electron fluid (see [6, 7] for details). Such an inconsistency has been traditionally ignored by applying, within a point-like nucleus model, the relativistic formulas (80) and (81) and their corresponding ultrarelativistic limits (see, *e.g.*, [36]).

The Wigner-Seitz cell chemical potential is in this case

$$\mu_{\rm ws}^{\rm L} = E_{\rm ws}^{\rm L} + P_{\rm ws}^{\rm L} V_{\rm ws} = \mu_{\rm unif} + \frac{4}{3}E_C, \tag{94}$$

where $\mu_{\rm unif}$ is given by eq. (84).

By comparing eqs. (83) and (93) we can see that the inclusion of the Coulomb interaction results in a decreasing of the pressure of the cell due to the negative lattice energy E_C. The same conclusion is achieved for the chemical potential from eqs. (84) and (94).

7˙3. *Salpeter approach.* – A further development to the lattice model came from Salpeter [36] who studied the corrections due to the non-uniformity of the electron distribution inside a Wigner-Seitz cell.

Following the Chandrasekhar [29] approximation, Salpeter also neglects the electron contribution to the energy-density. Thus, the first term in the Salpeter formula for the energy of the cell comes from the nuclei energy (86). The second contribution is given by the Coulomb energy of the lattice model (90). The third contribution is obtained as follows: the electron density is assumed as $n_e[1+\epsilon(r)]$, where $n_e = 3Z/(4\pi R_{\rm ws}^3)$ is the average electron density as given by eq. (88), and $\epsilon(r)$ is considered infinitesimal. The Coulomb potential energy is assumed to be the one of the point-like nucleus surrounded by a uniform distribution of electrons, so the correction given by $\epsilon(r)$ on the Coulomb potential is neglected. The electron distribution is then calculated at first-order by expanding the relativistic electron kinetic energy

$$\begin{aligned}\epsilon_k &= \sqrt{[cP_e^F(r)]^2 + m_e^2c^4} - m_ec^2 \\ &= \sqrt{\hbar^2c^2(3\pi^2 n_e)^{2/3}[1+\epsilon(r)]^{2/3} + m_e^2c^4} - m_ec^2,\end{aligned} \tag{95}$$

about its value in the uniform approximation

$$\epsilon_k^{\rm unif} = \sqrt{\hbar^2c^2(3\pi^2 n_e)^{2/3} + m_e^2c^4} - m_ec^2, \tag{96}$$

considering as infinitesimal the ratio eV/E_e^F between the Coulomb potential energy eV and the electron Fermi energy

$$E_e^F = \sqrt{[cP_e^F(r)]^2 + m_e^2c^4} - m_ec^2 - eV. \tag{97}$$

The influence of the Dirac electron-exchange correction [38] on the equation of state was also considered by Salpeter [36]. However, adopting the general approach of Migdal

et al. [5], it has been shown that these effects are negligible in the relativistic regime [12]. We will then consider here only the major correction of the Salpeter treatment.

The total energy of the Wigner-Seitz cell is then given by (see [36] for details)

$$E_{\rm ws}^{\rm S} = E_{\rm Ch} + E_C + E_S^{TF}, \tag{98}$$

being

$$E_S^{TF} = -\frac{162}{175}\left(\frac{4}{9\pi}\right)^{2/3}\alpha^2 Z^{7/3}\mu_e, \tag{99}$$

where $E_{\rm Ch} = \mathcal{E}_{\rm Ch}V_{\rm ws}$, E_C is given by eq. (90), μ_e is given by eq. (85), and $\alpha = e^2/(\hbar c)$ is the fine structure constant. It is appropriate to note that in eq. (98) we use $E_{\rm Ch} + E_C$ instead of the lattice energy $E_{\rm ws}^{\rm L}$ given by eq. (89). This is due to the fact that Salpeter [36] followed the Chandrasekhar approximation of neglecting the contribution of the electrons to the energy density, which we keep in the description of the lattice model.

The self-consistent pressure of the Wigner-Seitz cell is

$$P_{\rm ws}^{\rm S} = P_{\rm ws}^{\rm L} + P_{TF}^{S}, \tag{100}$$

where $P_{\rm ws}^{\rm L}$ is the pressure of the lattice model (93) and

$$P_{TF}^{S} = \frac{1}{3}\left(\frac{P_e^F}{\mu_e}\right)^2 \frac{E_S^{TF}}{V_{\rm ws}}\,. \tag{101}$$

In Salpeter's approximation, as in the Chandrasekhar one, no thermodynamically self-consistent chemical potential can be constructed for the Wigner-Seitz cells due to the neglect of the contribution of the electron component to the energy of the cells. If the electron energy were not neglected, the self-consistent Wigner-Seitz cell chemical potential can be computed as

$$\mu_{\rm ws}^{\rm S} = \mu_{\rm ws}^{\rm L} + E_{TF}^{S}\left[1 + \frac{1}{3}\left(\frac{P_e^F}{\mu_e}\right)^2\right], \tag{102}$$

where $\mu_{\rm ws}^{\rm L}$ is the chemical potential of the cell (94) within the lattice model.

It is clear from eqs. (100) and (102), that the inclusion of each additional Coulomb correction results in a further decreasing of the pressure and of the chemical potential of the cell. The Salpeter approach is very interesting in identifying the piecewise contribution of the Coulomb interactions to the total energy, to the total pressure and, to the chemical potential of the Wigner-Seitz cells. However, it does not have the full consistency of the global solutions obtained with the FMT approach [13] and its generalization to relativistic regimes [12] which we will discuss in detail below.

7˙4. *The Feynman-Metropolis-Teller treatment*. – Feynman, Metropolis and Teller [13] showed how to derive the equation of state of matter at high pressures by considering a Thomas-Fermi model confined in a Wigner-Seitz cell of radius $R_{\rm ws}$.

The Thomas-Fermi equilibrium condition for degenerate non-relativistic electrons in the cell is expressed by

$$E_e^F = \frac{(P_e^F)^2}{2m_e} - eV = \text{constant} > 0, \tag{103}$$

where V denotes the Coulomb potential and E_e^F denotes the Fermi energy of electrons, which is positive for configurations subjected to external pressure, namely, for compressed cells.

Defining the function $\phi(r)$ by $eV(r) + E_e^F = e^2 Z\phi(r)/r$, and introducing the dimensionless radial coordinate η by $r = b\eta$, where $b = (3\pi)^{2/3}(\lambda_e/\alpha)2^{-7/3}Z^{-1/3}$, being $\lambda_e = \hbar/(m_e c)$ the electron Compton wavelength; the Poisson equation from which the Coulomb potential V is calculated self-consistently becomes

$$\frac{\mathrm{d}^2\phi(\eta)}{\mathrm{d}\eta^2} = \frac{\phi(\eta)^{3/2}}{\eta^{1/2}}\,. \tag{104}$$

The boundary conditions for eq. (104) follow from the point-like structure of the nucleus $\phi(0) = 1$ and, from the global neutrality of the Wigner-Seitz cell $\phi(\eta_0) = \eta_0 d\phi/d\eta|_{\eta=\eta_0}$, where η_0 defines the dimensionless radius of the Wigner-Seitz cell by $\eta_0 = R_{\rm ws}/b$.

For each value of the compression, *e.g.* η_0, it corresponds a value of the electron Fermi energy E_e^F and a different solution of eq. (104), which determines the self-consistent Coulomb potential energy eV as well as the self-consistent electron distribution inside the cell through

$$n_e(\eta) = \frac{Z}{4\pi b^3}\left[\frac{\phi(\eta)}{\eta}\right]^{3/2}. \tag{105}$$

In the non-relativistic Thomas-Fermi model, the total energy of the Wigner-Seitz cell is given by

$$E_{\rm ws}^{\rm FMT} = E_N + E_k^{(e)} + E_C, \tag{106}$$

being

$$E_N = M_N(Z,A)c^2, \tag{107}$$

$$E_k^{(e)} = \int_0^{R_{\rm ws}} 4\pi r^2 \mathcal{E}_e[n_e(r)]\mathrm{d}r = \frac{3}{7}\frac{Z^2e^2}{b}\left[\frac{4}{5}\eta_0^{1/2}\phi^{5/2}(\eta_0) - \phi'(0)\right], \tag{108}$$

$$E_C = E_{e\text{-}N} + E_{e\text{-}e} = -\frac{6}{7}\frac{Z^2e^2}{b}\left[\frac{1}{3}\eta_0^{1/2}\phi^{5/2}(\eta_0) - \phi'(0)\right], \tag{109}$$

where $M_N(Z,A)$ is the nucleus mass, $\mathcal{E}_e[n_e(r)]$ is given by eq. (80) and $E_{e\text{-}N}$ and $E_{e\text{-}e}$ are the electron-nucleus Coulomb energy and the electron-electron Coulomb energy, which

are given by

$$E_{e\text{-}N} = -\int_0^{R_{\rm ws}} 4\pi r^2 \left(\frac{Ze}{r}\right) e n_e(r) \mathrm{d}r, \tag{110}$$

$$E_{e\text{-}e} = \frac{1}{2}\int_0^{R_{\rm ws}} 4\pi r^2 e n_e(\vec{r}) \mathrm{d}r \times \int_0^{R_{\rm ws}} 4\pi r'^2 \frac{e n_e(\vec{r}\,')}{|\vec{r} - \vec{r}\,'|} \mathrm{d}r'. \tag{111}$$

From eqs. (108) and (109) we recover the well-known relation between the total kinetic energy and the total Coulomb energy in the Thomas-Fermi model [13]

$$E_k^{(e)} = E_k^{\rm unif}[n_e(R_{\rm ws})] - \frac{1}{2}E_C, \tag{112}$$

where $E_k^{\rm unif}[n_e(R_{\rm ws})]$ is the non-relativistic kinetic energy of a uniform electron distribution of density $n_e(R_{\rm ws})$, *i.e.*

$$E_k^{\rm unif}[n_e(R_{\rm ws})] = \frac{3}{5} Z^* \mu_e(R_{\rm ws}), \tag{113}$$

with Z^* defined by

$$Z^* = V_{\rm ws} n_e(R_{\rm ws}), \tag{114}$$

and $\mu_e(R_{\rm ws}) = \hbar^2[3\pi^2 n_e(R_{\rm ws})]^{2/3}/(2m_e)$.

The self-consistent pressure of the Wigner-Seitz cell given by the non-relativistic Thomas-Fermi model is (see [13] for details)

$$P_{\rm ws}^{\rm FMT} = \frac{\partial E_{\rm ws}^{\rm FMT}}{\partial V_{\rm ws}} = \frac{2}{3}\frac{E_k^{\rm unif}[n_e(R_{\rm ws})]}{V_{\rm ws}}\,. \tag{115}$$

The pressure of the Thomas-Fermi model (115) is equal to the pressure of a free-electron distribution of density $n_e(R_{\rm ws})$. Being the electron density inside the cell a decreasing function of the distance from the nucleus, the electron density at the cell boundary, $n_e(R_{\rm ws})$, is smaller than the average electron distribution $3Z/(4\pi R_{\rm ws}^3)$. Then, the pressure given by (115) is smaller than the one given by the non-relativistic version of eq. (81) of the uniform model of subsect. **7**˙1. Such a smaller pressure, although faintfully given by the expression of a free-electron gas, contains in a self-consistent fashion all the Coulomb interaction effects inside the Wigner-Seitz cell.

The chemical potential of the Wigner-Seitz cell of the non-relativistic Thomas-Fermi model can be then written as

$$\mu_{\rm ws}^{\rm FMT} = M_N(Z,A)c^2 + Z^*\mu_e(R_{\rm ws}) + \frac{1}{2}E_C, \tag{116}$$

where we have used eqs. (112)–(114).

Integrating by parts the total number of electrons

$$Z = \int_0^{R_{\rm ws}} 4\pi r^2 n_e(r) \mathrm{d}r = Z^* + I(R_{\rm ws}), \tag{117}$$

where

$$I(R_{\rm ws}) = \int_0^{R_{\rm ws}} \frac{4\pi}{3} r^3 \frac{\partial n_e(r)}{\partial r} {\rm d}r, \tag{118}$$

we can rewrite finally the following semi-analytical expression of the chemical potential (116) of the cell

$$\mu_{\rm ws}^{\rm FMT} = M_N(Z,A)c^2 + Z\mu_e^{\rm unif}\left[1+\frac{I(R_{\rm ws})}{Z}\right]^{2/3} + \mu_e^{\rm unif} I(R_{\rm ws})\left[1+\frac{I(R_{\rm ws})}{Z}\right]^{2/3} + \frac{1}{2}E_C, \tag{119}$$

where $\mu_e^{\rm unif}$ is the electron free-chemical potential (85) calculated with the average electron density, namely, the electron chemical potential of the uniform approximation. The function $I(R_{\rm ws})$ depends explicitly on the gradient of the electron density, *i.e.* on the non-uniformity of the electron distribution.

In the limit of absence of Coulomb interaction both the last term and the function $I(R_{\rm ws})$ in eq. (119) vanish and therefore in this limit $\mu_{\rm TF}$ reduces to

$$\mu_{\rm ws}^{\rm FMT} \to \mu_{\rm unif}, \tag{120}$$

where $\mu_{\rm unif}$ is the chemical potential in the uniform approximation (84).

7˙5. *The relativistic Feynman-Metropolis-Teller treatment.* – We recall now how the above classic FMT treatment of compressed atoms has been recently generalized to relativistic regimes (see [12] for details). One of the main differences in the relativistic generalization of the Thomas-Fermi equation is that, the point-like approximation of the nucleus, must be abandoned since the relativistic equilibrium condition of compressed atoms

$$E_e^F = \sqrt{c^2(P_e^F)^2 + m_e^2c^4} - m_ec^2 - eV(r) = {\rm const} > 0, \tag{121}$$

would lead to a non-integrable expression for the electron density near the origin (see, *e.g.*, [6, 7]).

It is then assumed a constant distribution of protons confined in a radius R_c defined by

$$R_c = \Delta\lambda_\pi Z^{1/3}, \tag{122}$$

where $\lambda_\pi = \hbar/(m_\pi c)$ is the pion Compton wavelength. If the system is at nuclear density $\Delta \approx (r_0/\lambda_\pi)(A/Z)^{1/3}$ with $r_0 \approx 1.2\,{\rm fm}$. Thus, in the case of ordinary nuclei (*i.e.*, for $A/Z \approx 2$) we have $\Delta \approx 1$. Consequently, the proton density can be written as

$$n_p(r) = \frac{Z}{\frac{4}{3}\pi R_c^3}\theta(r-R_c) = \frac{3}{4\pi}\left(\frac{1}{\Delta\lambda_\pi}\right)^3\theta(r-R_c), \tag{123}$$

where $\theta(r-R_c)$ denotes the Heaviside function centered at R_c. The electron density can be written as

$$n_e(r) = \frac{(P_e^F)^3}{3\pi^2\hbar^3} = \frac{1}{3\pi^2\hbar^3c^3}\left[\hat{V}^2(r) + 2m_ec^2\hat{V}(r)\right]^{3/2}, \tag{124}$$

where $\hat{V} = eV + E_e^F$ and we have used eq. (121).

The overall Coulomb potential satisfies the Poisson equation

$$\nabla^2 V(r) = -4\pi e\left[n_p(r) - n_e(r)\right], \tag{125}$$

with the boundary conditions $dV/dr|_{r=R_{\rm ws}} = 0$ and $V(R_{\rm ws}) = 0$ due to the global charge neutrality of the cell.

By introducing the dimensionless quantities $x = r/\lambda_\pi$, $x_c = R_c/\lambda_\pi$, $\chi/r = \hat{V}(r)/(\hbar c)$ and replacing the particle densities (123) and (124) into the Poisson equation (125), it is obtained the relativistic Thomas-Fermi equation [9]

$$\frac{1}{3x}\frac{\mathrm{d}^2\chi(x)}{\mathrm{d}x^2} = -\frac{\alpha}{\Delta^3}\theta(x_c - x) + \frac{4\alpha}{9\pi}\left[\frac{\chi^2(x)}{x^2} + 2\frac{m_e}{m_\pi}\frac{\chi(x)}{x}\right]^{3/2}, \tag{126}$$

which must be integrated subjected to the boundary conditions

$$\chi(0) = 0, \quad \chi(x_{\rm ws}) \geq 0\,, \quad \left.\frac{\mathrm{d}\chi}{\mathrm{d}x}\right|_{x=x_{\rm ws}} = \frac{\chi(x_{\rm ws})}{x_{\rm ws}}\,, \tag{127}$$

where $x_{\rm ws} = R_{\rm ws}/\lambda_\pi$.

The neutron density $n_n(r)$, related to the neutron Fermi momentum $P_n^F = (3\pi^2\hbar^3 n_n)^{1/3}$, is determined by imposing the condition of β-equilibrium

$$E_n^F = \sqrt{c^2(P_n^F)^2 + m_n^2c^4} - m_nc^2 = \sqrt{c^2(P_p^F)^2 + m_p^2c^4} - m_pc^2 + eV(r) + E_e^F, \tag{128}$$

subjected to the baryon number conservation equation

$$A = \int_0^{R_c} 4\pi r^2[n_p(r) + n_n(r)]\mathrm{d}r. \tag{129}$$

In fig. 7 we see how the relativistic generalization of the FMT treatment leads to electron density distributions markedly different from the constant electron density approximation. The electron distribution is far from being uniform as a result of the solution of eq. (126), which takes into account the electromagnetic interaction between electrons and between the electrons and the finite sized nucleus. Additional details are given in [12].

V. S. Popov *et al.* [11,10] have shown how the solution of the relativistic Thomas-Fermi equation (126) together with the self-consistent implementation of the β-equilibrium condition (128) leads, in the case of zero electron Fermi energy ($E_e^F = 0$), to a theoretical prediction of the β-equilibrium line, namely a theoretical Z-A relation. Within this model the mass to charge ratio A/Z of nuclei is overestimated, *e.g.* in the case of ^{4}He the overestimate is $\sim 3.8\%$, for ^{12}C $\sim 7.9\%$, for ^{16}O $\sim 9.52\%$, and for ^{56}Fe $\sim 13.2\%$.

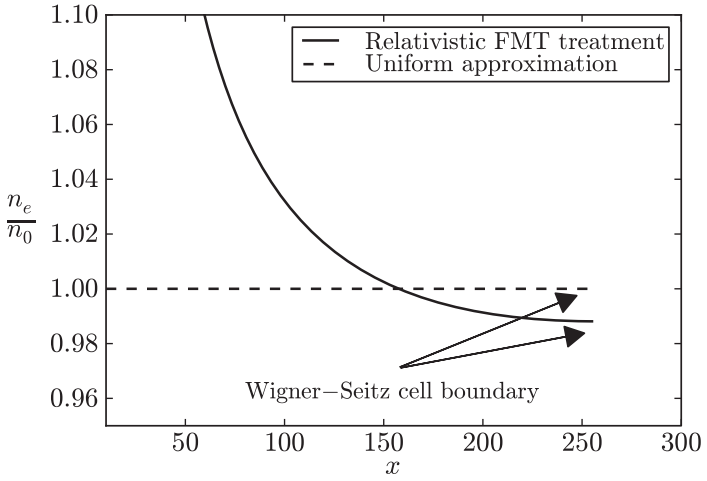

Fig. 7. – The electron number density n_e in units of the average electron number density $n_0 = 3Z/(4\pi R_{\rm ws}^3)$ inside a Wigner-Seitz cell of ^{12}C. The dimensionless radial coordinate is $x = r/\lambda_\pi$ and Wigner-Seitz cell radius is $x_{\rm ws} \approx 255$ corresponding to a density of $\sim 10^8\,{\rm g/cm^3}$. The solid curve corresponds to the relativistic FMT treatment and the dashed curve to the uniform approximation. The electron distribution for different levels of compression as well as for different nuclear compositions can be found in [12].

These discrepancies are corrected when the model of the nucleus considered above is improved by explicitly including the effects of strong interactions. This model, however, illustrates how a self-consistent calculation of compressed nuclear matter can be done including electromagnetic, weak, strong as well as special relativistic effects without any approximation. This approach promises to be useful when theoretical predictions are essential, for example in the description of nuclear matter at very high densities, *e.g.*, nuclei close and beyond the neutron drip line.

The densities in white dwarf interiors are not highly enough to require such theoretical predictions. Therefore, in order to ensure the accuracy of our results we use for (Z, A), needed to solve the relativistic Thomas-Fermi equation (126), as well as for the nucleus mass $M_N(Z, A)$, their known experimental values. In this way we take into account all the effects of the nuclear interaction.

Thus, the total energy of the Wigner-Seitz cell in the present case can be written as

$$E_{\rm ws}^{\rm relFMT} = E_N + E_k^{(e)} + E_C, \tag{130}$$

being

$$E_N = M_N(Z, A)c^2, \tag{131}$$

$$E_k^{(e)} = \int_0^{R_{\rm ws}} 4\pi r^2(\mathcal{E}_e - m_e n_e){\rm d}r, \tag{132}$$

$$E_C = \frac{1}{2}\int_{R_c}^{R_{\rm ws}} 4\pi r^2 e[n_p(r) - n_e(r)]V(r){\rm d}r, \tag{133}$$

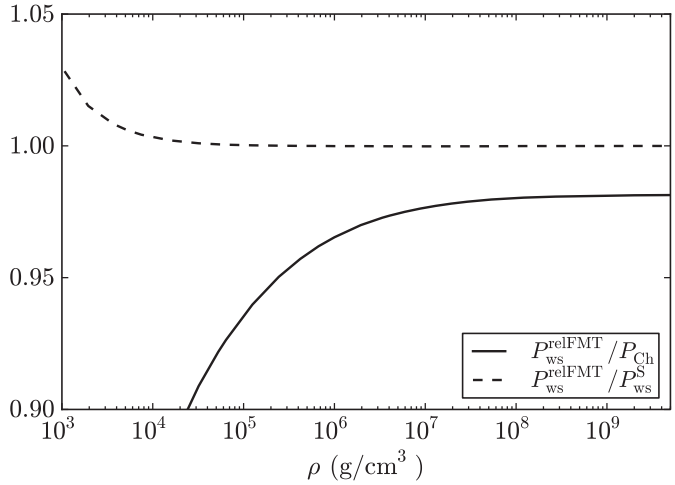

Fig. 8. – Ratio of the pressures in the different treatments as a function of the density for ^{12}C white dwarfs (see table I). The solid curve corresponds to the ratio between the relativistic FMT pressure $P_{\rm ws}^{\rm relFMT}$ given by eq. (134) and the Chandrasekhar pressure $P_{\rm Ch}$ given by eq. (81). The dashed curve corresponds to the ratio between the relativistic FMT pressure $P_{\rm ws}^{\rm relFMT}$ given by eq. (134) and the Salpeter pressure $P_{\rm ws}^{\rm S}$ given by eq. (100).

where $M_N(Z,A) = A_r M_u$ is the experimental nucleus mass, *e.g.* for ^{4}He, ^{12}C, ^{16}O and ^{56}Fe we have $A_r = 4.003$, 12.01, 16.00 and 55.84, respectively. In eq. (133) the integral is evaluated only outside the nucleus (*i.e.* for $r > R_c$) in order to avoid a double counting with the Coulomb energy of the nucleus already taken into account in the nucleus mass (131). In order to avoid another double counting we subtract to the electron energy-density $\mathcal{E}_e$ in eq. (132) the rest-energy density $m_e c^2 n_e$ which is also taken into account in the nucleus mass (131).

The total pressure of the Wigner-Seitz cell is given by

$$P_{\rm ws}^{\rm relFMT} = P_e[n_e(R_{\rm ws})], \tag{134}$$

where $P_e[n_e(R_{\rm ws})]$ is the relativistic pressure (81) computed with the value of the electron density at the boundary of the cell.

The electron density at the boundary $R_{\rm ws}$ in the relativistic FMT treatment is smaller with respect to the one given by the uniform density approximation (see fig. 7). Thus, the relativistic pressure (134) gives systematically smaller values with respect to the uniform approximation pressure (81) as well as with respect to the Salpeter pressure (100).

In fig. 8 we show the ratio between the relativistic FMT pressure $P_{\rm ws}^{\rm relFMT}$ (134) and the Chandrasekhar pressure $P_{\rm Ch}$ (81) and the Salpeter pressure $P_{\rm ws}^{\rm S}$ (100) in the case of ^{12}C. It can be seen how $P_{\rm ws}^{\rm relFMT}$ is smaller than $P_{\rm Ch}$ for all densities as a consequence of the Coulomb interaction. With respect to the Salpeter case, we have that the ratio $P_{\rm ws}^{\rm relFMT}/P_{\rm ws}^{\rm S}$ approaches unity from below at large densities as one should expect.

However, at low densities $\lesssim 10^4$–10^5 g/cm^3, the ratio becomes larger than unity due to the defect of the Salpeter treatment which, in the low-density non-relativistic regime, leads to a drastic decrease of the pressure and even to negative pressures at densities $\lesssim 10^2$ g/cm^3 or higher for heavier nuclear compositions, *e.g.*, ^{56}Fe (see [36,12] and table I).

TABLE I. – *Equation of state for* ^{12}C *within the different treatments. The pressure in the uniform approximation for* $\mu = 2$ *is* $P_{\rm Ch}$*, the Salpeter pressure is* $P_{\rm ws}^{\rm S}$ *and the relativistic FMT pressure is* $P_{\rm ws}^{\rm relFMT}$*. The units for the density are* g/cm^3 *and for the pressure* dyn/cm^2*.*

ρ	$P_{\rm Ch}$	$P_{\rm ws}^{\rm S}$	$P_{\rm ws}^{\rm relFMT}$
10	1.46731×10^{14}	-1.35282×10^{13}	4.54920×10^{14}
40	1.47872×10^{15}	4.60243×10^{14}	7.09818×10^{14}
70	3.75748×10^{15}	1.60860×10^{15}	2.05197×10^{15}
10^2	6.80802×10^{15}	3.34940×10^{15}	3.90006×10^{15}
10^3	3.15435×10^{17}	2.40646×10^{17}	2.44206×10^{17}
10^4	1.45213×10^{19}	1.28976×10^{19}	1.28965×10^{19}
10^5	6.50010×10^{20}	6.14494×10^{20}	6.13369×10^{20}
10^6	2.62761×10^{22}	2.54932×10^{22}	2.54431×10^{22}
10^7	8.46101×10^{23}	8.28899×10^{23}	8.27285×10^{23}
10^8	2.15111×10^{25}	2.11375×10^{25}	2.10896×10^{25}
10^9	4.86236×10^{26}	4.78170×10^{26}	4.76613×10^{26}
10^{10}	1.05977×10^{28}	1.04239×10^{28}	1.03668×10^{28}

This is in contrast with the relativistic FMT treatment which matches smoothly the classic FMT equation of state in that regime (see [12] for details).

No analytic expression of the Wigner-Seitz cell chemical potential can be given in this case, so we only write its general expression

$$\mu_{\rm ws}^{\rm relFMT} = E_{\rm ws}^{\rm relFMT} + P_{\rm ws}^{\rm relFMT} V_{\rm ws}, \tag{135}$$

where $E_{\rm ws}^{\rm relFMT}$ and $P_{\rm ws}^{\rm relFMT}$ are given by eqs. (130) and (134), respectively. The above equation, contrary to the non-relativistic formula (116), in no way can be simplified in terms of its uniform counterparts. However, it is easy to check that, in the limit of no Coulomb interaction $n_e(R_{\rm ws}) \to 3Z/(4\pi R_{\rm ws}^3)$, $E_C \to 0$, and $E_k \to \mathcal{E}_{\rm Ch} V_{\rm ws}$ and, neglecting the nuclear binding and the proton-neutron mass difference, we finally obtain

$$\mu_{\rm ws}^{\rm relFMT} \to \mu_{\rm unif}, \tag{136}$$

as it should be expected.

Now we summarize how the equation of state of compressed nuclear matter can be computed in the Salpeter case and in the relativistic FMT case, parameterized by the total density of the system:

i) For a given radius $R_{\rm ws}$ of the Wigner-Seitz cell the relativistic Thomas-Fermi equation (126) is integrated numerically and the density of the configuration is computed as $\rho = E_{\rm ws}^{\rm relFMT}/(c^2 V_{\rm ws})$ where $E_{\rm ws}^{\rm relFMT}$ is the energy of the cell given by eq. (130).

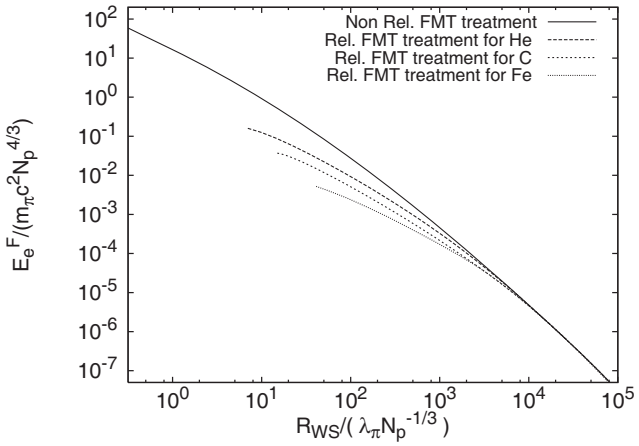

Fig. 9. – The electron Fermi energies in units of $m_\pi c^2 N_p^{4/3}$ for ^{4}He, ^{12}C and ^{56}Fe are plotted as a function of the ratio $R_{WS}/(\lambda_\pi N_p^{-1/3})$ respectively in the non-relativistic and in the relativistic FMT treatment. The dimensionless quantities have been chosen in order to obtain the universal curve in the non relativistic treatment following eqs. (10) and (11). The relativistic treatment leads to results of the electron Fermi energy dependent on the nuclear composition and systematically smaller than the non-relativistic ones. The electron Fermi energy can attain arbitrary large values, in the non-relativistic treatment, as the point-like nucleus is approached.

ii) For that value of the density, the radius of the Wigner-Seitz cell in the Salpeter treatment is

$$R_{\rm ws} = \left(\frac{3A_r M_u}{4\pi\rho}\right)^{1/3}, \tag{137}$$

where eq. (86) has been used. On the contrary, in the relativistic FMT treatment no analytic expression relating Wigner-Seitz cell radius and density can be written.

iii) From this Wigner-Seitz cell radius, or equivalently using the value of the density, the electron density in the Salpeter model is computed from the assumption of uniform electron distribution and the charge neutrality condition, *i.e.* eq. (86). In the relativistic FMT treatment, the electron number density at the boundary of the Wigner-Seitz cell is, following eq. (124), given by

$$n_e^{\rm relFMT} = \frac{1}{3\pi^2\lambda_\pi^3}\left[\frac{\chi^2(x_{\rm ws})}{x_{\rm ws}^2} + 2\frac{m_e}{m_\pi}\frac{\chi(x_{\rm ws})}{x_{\rm ws}}\right]^{3/2}, \tag{138}$$

where the function $\chi(x)$ is the solution of the relativistic Thomas-Fermi equation (126).

iv) Finally, with the knowledge of the electron density at $R_{\rm ws}$, the pressure can be calculated. In the Salpeter approach it is given by eq. (100) while in the relativistic FMT case it is given by eq. (134).

7˙6. *Relativistic FMT treatment vs. non-relativistic FMT treatment.* – In fig. 9 we compare and contrast the electron Fermi energy in a compressed atom in the non-relativistic FMT case (103) and in the relativistic one (121).

There are major differences:

1) The electron Fermi energy in the relativistic treatment is strongly dependent on the nuclear composition, while the non-relativistic treatment presents a universal behavior in the units of fig. 9. In the limit of low densities the relativistic curves approach the universal non-relativistic curve. In the non relativistic treatment the ratio $E_e^F/(m_\pi c^2 N_p^{4/3})$ does not depend on the number of protons N_p if the Wigner-Seitz cell radius R_{WS} is multiplied by $N_p^{1/3}$ (see eqs. (10), (11)). This universality is lost in the relativistic treatment since there is no way to eliminate the dependence of the electron Fermi energy on the nuclear composition.

2) The relativistic treatment leads to values of the electron Fermi energy consistently smaller than the ones of the non-relativistic treatment.

3) While in the non-relativistic treatment the electron Fermi energy can reach, by compression, infinite values as $R_{WS} \to 0$, in the relativistic treatment it reaches a perfectly finite value attained when R_{WS} coincides with the nuclear radius R_c.

It is clear then, from above considerations, the relativistic treatment of the Thomas-Fermi equation introduces significant differences from current approximations in the literature: a) the uniform electron distribution (*e.g.* [29]); b) the approximate perturbative solutions departing from the uniform distribution [36]; and c) the non-relativistic treatment [13].

8. – The relativistic Feynman-Metropolis-Teller theory for white dwarfs in general relativity

Outside each Wigner-Seitz cell the system is electrically neutral, thus no overall electric field exists. Therefore, the relativistic FMT equation of state can be used to calculate the structure of the star through the Einstein equations. Introducing the spherically symmetric metric (61), the Einstein equations can be written in the Tolman-Oppenheimer-Volkoff form [17, 18]

$$\frac{\mathrm{d}\nu(r)}{\mathrm{d}r} = \frac{2G}{c^2}\frac{4\pi r^3 P(r)/c^2 + M(r)}{r^2\left[1 - \frac{2GM(r)}{c^2 r}\right]}, \tag{139}$$

$$\frac{\mathrm{d}M(r)}{\mathrm{d}r} = 4\pi r^2 \frac{\mathcal{E}(r)}{c^2}, \tag{140}$$

$$\frac{\mathrm{d}P(r)}{\mathrm{d}r} = -\frac{1}{2}\frac{\mathrm{d}\nu(r)}{\mathrm{d}r}[\mathcal{E}(r) + P(r)], \tag{141}$$

where we have introduced the mass enclosed at the distance r through $e^{\lambda(r)} = 1 - 2GM(r)/(c^2 r)$, $\mathcal{E}(r)$ is the energy-density and $P(r)$ is the total pressure.

We turn now to find, from eq. (141), the general relativistic equation of equilibrium for the self-consistent chemical potential μ_{ws} of the Wigner-Seitz cells inside a white dwarf. The first law of thermodynamics for a zero temperature fluid of N particles, total energy E, total volume V, total pressure $P = -\partial E/\partial V$, and chemical potential $\mu = \partial E/\partial N$ reads

$$\mathrm{d}E = -P\mathrm{d}V + \mu \mathrm{d}N, \tag{142}$$

where the differentials denote arbitrary but simultaneous changes in the variables. Since for a system whose surface energy can be neglected with respect to volume energy, the

total energy per particle E/N depends only on the particle density $n = N/V$, we can assume E/N as a homogeneous function of first-order in the variables N and V and hence, the well-known thermodynamic relation follows:

$$E = -PV + \mu N. \tag{143}$$

In the case of the Wigner-Seitz cells, eq. (143) reads

$$E_{\rm ws} = -P_{\rm ws}V_{\rm ws} + \mu_{\rm ws}, \tag{144}$$

where we have introduced the fact that the Wigner-Seitz cells are the building blocks of the configuration and therefore we must put in eq. (143) $N_{\rm ws} = 1$. Through the entire article we have used eq. (144) to obtain from the knowns energy and pressure, the Wigner-Seitz cell chemical potential (see, *e.g.*, eqs. (84) and (94)). From eqs. (142) and (143) we obtain the so-called Gibbs-Duhem relation

$$\mathrm{d}P = n\mathrm{d}\mu. \tag{145}$$

In a white dwarf the pressure P and the chemical potential μ are decreasing functions of the distance from the origin. Thus, the differentials in the above equations can be assumed as the gradients of the variables which, in the present spherically symmetric case, become just derivatives with respect to the radial coordinate r. From eq. (145) it follows the relation

$$\frac{\mathrm{d}P_{\rm ws}}{\mathrm{d}r} = n_{\rm ws}\frac{\mathrm{d}\mu_{\rm ws}}{\mathrm{d}r}\,. \tag{146}$$

From eqs. (141), (144) and (146) we obtain

$$n_{\rm ws}(r)\frac{\mathrm{d}\mu_{\rm ws}(r)}{\mathrm{d}r} = -\frac{1}{2}\frac{\mathrm{d}\nu(r)}{\mathrm{d}r}n_{\rm ws}(r)\mu_{\rm ws}(r), \tag{147}$$

which can be straightforwardly integrated to obtain the first integral

$$e^{\nu(r)/2}\mu_{\rm ws}(r) = \text{const.} \tag{148}$$

The above equilibrium condition is general and it also applies for non-zero temperature configurations (see [21] for details). In such a case, it can be shown that, in addition to the equilibrium condition (148), the temperature of the system satisfies the general relativistic Tolman isothermality condition [39]

$$e^{\nu(r)/2}T(r) = \text{const.} \tag{149}$$

8˙1. *The weak-field non-relativistic limit.* – In the weak-field limit we have $e^{\nu/2} \approx 1 + \Phi/c^2$, where Φ denotes the Newtonian gravitational potential. In the non-relativistic mechanics limit $c \to \infty$, the chemical potential $\mu_{\rm ws} \to \tilde{\mu}_{\rm ws} + M_{\rm ws}c^2$, where $\tilde{\mu}_{\rm ws}$ denotes the non-relativistic free-chemical potential of the Wigner-Seitz cell and $M_{\rm ws}$ is the rest-mass of the Wigner-Seitz cell, namely, the rest-mass of the nucleus plus the rest-mass of the electrons. Applying these considerations to eq. (148) we obtain

$$e^{\nu/2}\mu_{\rm ws} \approx M_{\rm ws}c^2 + \tilde{\mu}_{\rm ws} + M_{\rm ws}\Phi = \text{const.} \tag{150}$$

Absorbing the Wigner-Seitz rest-mass energy $M_{\rm ws}c^2$ in the constant on the right-hand-side we obtain

$$\tilde{\mu}_{\rm ws} + M_{\rm ws}\Phi = \text{const.} \tag{151}$$

In the weak-field non-relativistic limit, the Einstein equations (139)–(141) reduce to

$$\frac{\mathrm{d}\Phi(r)}{\mathrm{d}r} = \frac{GM(r)}{r^2}\,, \tag{152}$$

$$\frac{\mathrm{d}M(r)}{\mathrm{d}r} = 4\pi r^2\rho(r), \tag{153}$$

$$\frac{\mathrm{d}P(r)}{\mathrm{d}r} = -\frac{GM(r)}{r^2}\rho(r), \tag{154}$$

where $\rho(r)$ denotes the rest-mass density. Equations (152)–(153) can be combined to obtain the gravitational Poisson equation

$$\frac{\mathrm{d}^2\Phi(r)}{\mathrm{d}r^2} + \frac{2}{r}\frac{\mathrm{d}\Phi(r)}{\mathrm{d}r} = 4\pi G\rho(r). \tag{155}$$

In the uniform approximation (see subsect. **7**˙1), the equilibrium condition given by eq. (151) reads

$$\tilde{\mu}_e + \frac{A_r}{Z}M_u\Phi = \text{const}, \tag{156}$$

where we have neglected the electron rest-mass with respect to the nucleus rest-mass and we have divided the equation by the total number of electrons Z. This equilibrium equation is the classical condition of thermodynamic equilibrium assumed for non-relativistic white dwarf models (see, *e.g.*, [31] for details).

Introducing the above equilibrium condition (156) into eq. (155), and using the relation between the non-relativistic electron chemical potential and the particle density $n_e = (2m_e)^{3/2}\tilde{\mu}_e^{3/2}/(3\pi^2\hbar^3)$, we obtain

$$\frac{\mathrm{d}^2\tilde{\mu}_e(r)}{\mathrm{d}r^2} + \frac{2}{r}\frac{\mathrm{d}\tilde{\mu}_e(r)}{\mathrm{d}r} = -\frac{2^{7/3}m_e^{3/2}(A_r/Z)^2m_N^2G}{3\pi\hbar^3}\tilde{\mu}_e^{3/2}(r), \tag{157}$$

which is the correct equation governing the equilibrium of white dwarfs within Newtonian gravitational theory [31]. It is remarkable that the equation of equilibrium (157), obtained from the correct application of the Newtonian limit, does not coincide with the equation given by [29, 40], which, as correctly pointed out by [35], is a mixture of both relativistic and non-relativistic approaches. Indeed, the consistent relativistic equations should be eq. (148). Therefore a dual relativistic and non-relativistic equation of state was used by Chandrasekhar. The pressure on the left-hand-side of eq. (154) is taken to be given by relativistic electrons while, the term on the right-hand-side of eq. (153) and (154) (or the source of eq. (155)), is taken to be the rest-mass density of the system instead of the total relativistic energy-density. Such a hybrid approach is also present in the gravitational special relativistic Thomas-Fermi theory summarized in sect. **4**. This is equivalent to assume the chemical potential in eq. (151) as a relativistic quantity. As we have seen,

this is inconsistent with the weak-field non-relativistic limit of the general relativistic equations.

8˙2. *The Post-Newtonian limit.* – Indeed, if one were to treat the problem of white dwarfs approximately without going to the sophistications of general relativity, but including the effects of relativistic mechanics, one should use at least the equations in the post-Newtonian limit. The first-order post-Newtonian expansion of the Einstein equations (139)–(141) in powers of $P/\mathcal{E}$ and $GM/(c^2 r)$ leads to the equilibrium equations [41]

$$\frac{\mathrm{d}\Phi(r)}{\mathrm{d}r} = -\frac{1}{\mathcal{E}(r)}\left[1 - \frac{P(r)}{\mathcal{E}(r)}\right]\frac{\mathrm{d}P(r)}{\mathrm{d}r}\,, \tag{158}$$

$$\frac{\mathrm{d}M(r)}{\mathrm{d}r} = 4\pi r^2 \frac{\mathcal{E}(r)}{c^2}\,, \tag{159}$$

$$\frac{\mathrm{d}P(r)}{\mathrm{d}r} = -\frac{GM(r)}{r^2}\frac{\mathcal{E}(r)}{c^2}\left[1 + \frac{P(r)}{\mathcal{E}(r)} + \frac{4\pi r^3 P(r)}{M(r)c^2} + \frac{2GM(r)}{c^2 r}\right], \tag{160}$$

where eq. (160) is the post-Newtonian version of the Tolman-Oppenheimer-Volkoff equation (141).

Replacing eq. (146) into eq. (158) we obtain

$$\left[1 - \frac{P(r)}{\mathcal{E}(r)}\right]\frac{\mathrm{d}\mu_{\mathrm{ws}}(r)}{\mathrm{d}r} + \frac{\mathcal{E}(r)/c^2}{n_{\mathrm{ws}}(r)}\frac{\mathrm{d}\Phi(r)}{\mathrm{d}r} = 0. \tag{161}$$

It is convenient to split the energy-density as $\mathcal{E} = c^2\rho + U$, where $\rho = M_{\mathrm{ws}} n_{\mathrm{ws}}$ is the rest-energy density and U the internal energy-density. Thus, eq. (161) becomes

$$\frac{\mathrm{d}\mu_{\mathrm{ws}}(r)}{\mathrm{d}r} + M_{\mathrm{ws}}\frac{\mathrm{d}\Phi(r)}{\mathrm{d}r} - \frac{P(r)}{\mathcal{E}(r)}\frac{\mathrm{d}\mu_{\mathrm{ws}}(r)}{\mathrm{d}r} + \frac{U/c^2}{n_{\mathrm{ws}}(r)}\frac{\mathrm{d}\Phi(r)}{\mathrm{d}r} = 0, \tag{162}$$

which is the differential post-Newtonian version of the equilibrium equation (148) and where the post-Newtonian corrections of equilibrium can be clearly seen. Applying the non-relativistic limit $c \to \infty$ to eq. (162): $P/\mathcal{E} \to 0$, $U/c^2 \to 0$, and $\mu_{\mathrm{ws}} \to M_{\mathrm{ws}}c^2 + \tilde{\mu}_{\mathrm{ws}}$, we recover the Newtonian equation of equilibrium (151).

8˙3. *Mass and radius of general relativistic stable white dwarfs*

8˙3.1. Inverse β-decay instability. It is known that white dwarfs may become unstable against the inverse β-decay process $(Z, A) \to (Z-1, A)$ through the capture of energetic electrons (see, *e.g.*, [42-45]). In order to trigger such a process, the electron Fermi energy must be larger than the mass difference between the initial nucleus (Z, A) and the final nucleus $(Z-1, A)$. We denote this threshold energy as ϵ^{β}_{Z}. Usually it is satisfied $\epsilon^{\beta}_{Z-1} < \epsilon^{\beta}_{Z}$ and therefore the initial nucleus undergoes two successive decays, *i.e.* $(Z, A) \to (Z-1, A) \to (Z-2, A)$ (see, *e.g.*, [36, 48]). Some of the possible decay channels in white dwarfs with the corresponding known experimental threshold energies ϵ^{β}_{Z} are listed in table II. The electrons in the white dwarf may eventually reach the threshold energy to trigger a given decay at some critical density $\rho^{\beta}_{\mathrm{crit}}$. Configurations with $\rho > \rho^{\beta}_{\mathrm{crit}}$ become unstable (see [36] for details).

TABLE II. – *Onset of inverse beta decay instability for* ^{4}He, ^{12}C, ^{16}O *and* ^{56}Fe. *The experimental inverse* β*-decay energies* ϵ_Z^β *are given in MeV and they have been taken from table 1 of* [46]. *The corresponding critical density for the uniform electron density model,* $\rho_{\rm crit}^{\beta,{\rm unif}}$ *given by eq.* (163), *is given in* g/cm^3 *as well as the critical density* $\rho_{\rm crit}^{\beta,{\rm relFMT}}$ *for the relativistic FMT case. The numerical values of* ϵ_Z^β *are taken from* [47], *see also* [48].

Decay	ϵ_Z^β	$\rho_{\rm crit}^{\beta,{\rm relFMT}}$	$\rho_{\rm crit}^{\beta,{\rm unif}}$
$^4{\rm He} \rightarrow ^3{\rm H} + {\rm n} \rightarrow 4{\rm n}$	20.596	1.39×10^{11}	1.37×10^{11}
$^{12}{\rm C} \rightarrow ^{12}{\rm B} \rightarrow ^{12}{\rm Be}$	13.370	3.97×10^{10}	3.88×10^{10}
$^{16}{\rm O} \rightarrow ^{16}{\rm N} \rightarrow ^{16}{\rm C}$	10.419	1.94×10^{10}	1.89×10^{10}
$^{56}{\rm Fe} \rightarrow ^{56}{\rm Mn} \rightarrow ^{56}{\rm Cr}$	3.695	1.18×10^{9}	1.14×10^{9}

Within the uniform approximation, *e.g.* in the case of the Salpeter equation of state [36], the critical density for the onset of inverse β-decay is given by

$$\rho_{\rm crit}^{\beta,{\rm unif}} = \frac{A_r}{Z}\frac{M_u}{3\pi^2\hbar^3c^3}\left[(\epsilon_Z^\beta)^2 + 2m_ec^2\epsilon_Z^\beta\right]^{3/2}, \tag{163}$$

where eq. (86) has been used.

Because the computation of the electron Fermi energy within the relativistic FMT approach [12] involves the numerical integration of the relativistic Thomas-Fermi equation (126), no analytic expression for $\rho_{\rm crit}^\beta$ can be found in this case. The critical density $\rho_{\rm crit}^{\beta,{\rm relFMT}}$ is then obtained numerically by looking for the density at which the electron Fermi energy (121) equals ϵ_Z^β.

In table II we show, correspondingly to each threshold energy ϵ_Z^β, the critical density both in the Salpeter case $\rho_{\rm crit}^{\beta,{\rm unif}}$ given by eq. (163) and in the relativistic FMT case $\rho_{\rm crit}^{\beta,{\rm relFMT}}$. It can be seen that $\rho_{\rm crit}^{\beta,{\rm relFMT}} > \rho_{\rm crit}^{\beta,{\rm unif}}$ as one should expect from the fact that, for a given density, the electron density at the Wigner-Seitz cell boundary satisfies $n_e^{\rm relFMT} < n_e^{\rm unif}$. This means that, in order to reach a given energy, the electrons within the relativistic FMT approach must be subjected to a larger density with respect to the one given by the approximated Salpeter analytic formula (163).

8˙3.2. General relativistic instability. The concept of the critical mass has played a major role in the theory of stellar evolution. For Newtonian white dwarfs the critical mass is reached asymptotically at infinite central densities of the object. One of the most important general relativistic effects is to shift this critical point to some finite density $\rho_{\rm crit}^{\rm GR}$.

This general relativistic effect is an additional source of instability with respect to the already discussed instability due to the onset of inverse β-decay which, contrary to the present general relativistic one, applies also in the Newtonian case by shifting the maximum mass of Newtonian white dwarfs to finite densities.

8˙3.3. Numerical results. In figs. 10–17 we have plotted the mass-central density relation and the mass-radius relation of general relativistic ^{4}He, ^{12}C, ^{16}O and ^{56}Fe white dwarfs. In particular, we show the results for the Newtonian white dwarfs of Hamada and Salpeter [49], for the Newtonian white dwarfs of Chandrasekhar [29] and the general

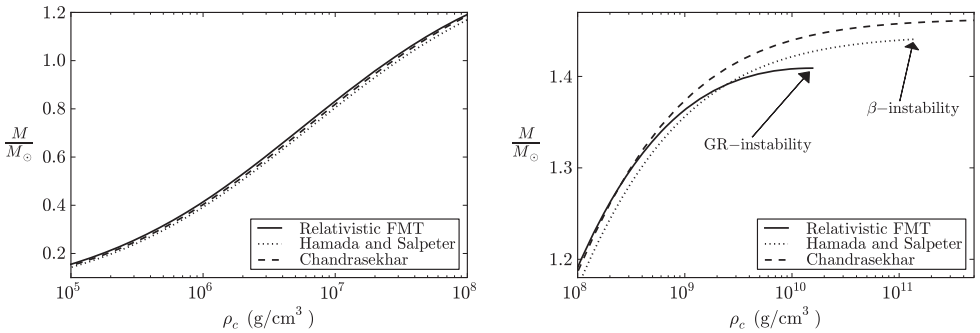

Fig. 10. – Mass in solar masses as a function of the central density in the range (left panel) 10^5–10^8 g/cm^3 and in the range (right panel) 10^8–5×10^{11} g/cm^3 for ^{4}He white dwarfs. The solid curve corresponds to the present work, the dotted curves are the Newtonian configurations of Hamada and Salpeter and the dashed curve are the Newtonian configurations of Chandrasekhar.

relativistic configurations obtained in this work based on the relativistic FMT equation of state [12].

Since our approach takes into account self-consistently both β-decay equilibrium and general relativity, we can determine if the critical mass is reached due either to inverse β-decay instability or to the general relativistic instability.

A comparison of the numerical value of the critical mass as given by Stoner [32], eq. (58), by Chandrasekhar [29] and Landau [30], eq. (57), by Hamada and Salpeter [49] and, by the treatment presented here can be found in table III.

From the numerical integrations we have obtained:

1. ^{4}He and ^{12}C white dwarfs satisfy $\rho_{\rm crit}^{\rm GR} < \rho_{\rm crit}^{\beta}$ (see figs. 10–13 and tables II and III), so they are unstable with respect to general relativistic effects. The critical density of ^{12}C white dwarfs is $\sim 2.12\times10^{10}$ g/cm^3, to be compared with the value 2.65×10^{10} g/cm^3 obtained from calculations based on general relativistic corrections to the theory of polytropes (see, *e.g.*, [48]).

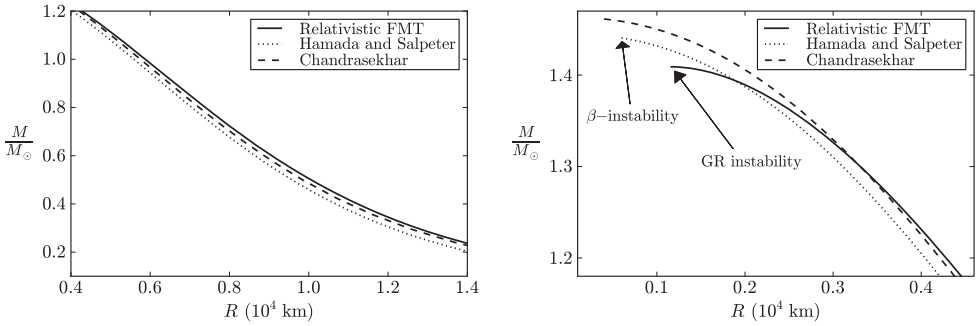

Fig. 11. – Mass in solar masses as a function of the radius in units of 10^4 km for ^{4}He white dwarfs. The left and right panels show the configurations for the same range of central densities of the corresponding panels of fig. 10. The solid curve corresponds to the present work, the dotted curves are the Newtonian configurations of Hamada and Salpeter and the dashed curve are the Newtonian configurations of Chandrasekhar.

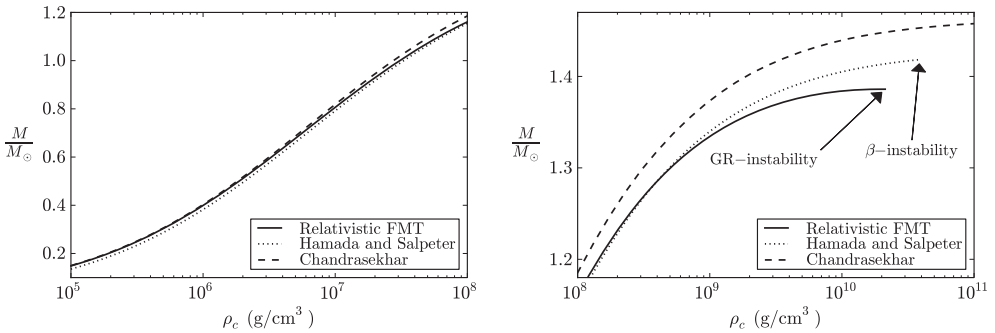

Fig. 12. – Mass in solar masses as a function of the central density in the range (left panel) 10^5–10^8 g/cm^3 and in the range (right panel) 10^8–10^{11} g/cm^3 for ^{12}C white dwarfs. The solid curve corresponds to the present work, the dotted curves are the Newtonian configurations of Hamada and Salpeter and the dashed curve are the Newtonian configurations of Chandrasekhar.

2. White dwarfs composed of heavier material than ^{12}C, *e.g.* ^{16}O and ^{56}Fe are unstable due to inverse β-decay of the nuclei (see figs. 14–17 and tables II and III). It is worth to notice that the correct evaluation of general relativistic effects and of the combined contribution of the electrons to the energy-density of the system introduce, for ^{12}C white dwarfs, a critical mass not due to the inverse beta decay. When the contribution of the electrons to the energy-density is neglected (*e.g.* Chandrasekhar [29] and Hamada and Salpeter [49], see eq. (86)) the critical density for Carbon white dwarfs is determined by inverse beta decay irrespective of the effects of general relativity.

3. It can be seen from figs. 10–17 that the drastic decrease of the Salpeter pressure at low densities (see [36, 12] and table I for details) produces an underestimate of the mass and the radius of low density (low mass) white dwarfs.

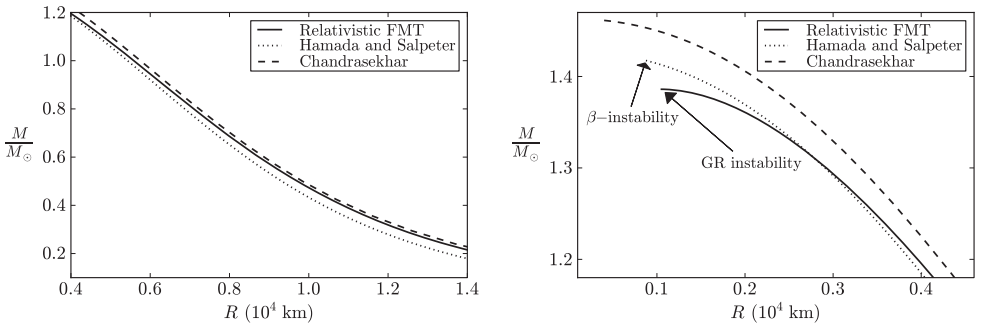

Fig. 13. – Mass in solar masses as a function of the radius in units of 10^4 km for ^{12}C white dwarfs. The left and right panels show the configurations for the same range of central densities of the corresponding panels of fig. 12. The solid curve corresponds to the present work, the dotted curves are the Newtonian configurations of Hamada and Salpeter and the dashed curve are the Newtonian configurations of Chandrasekhar.

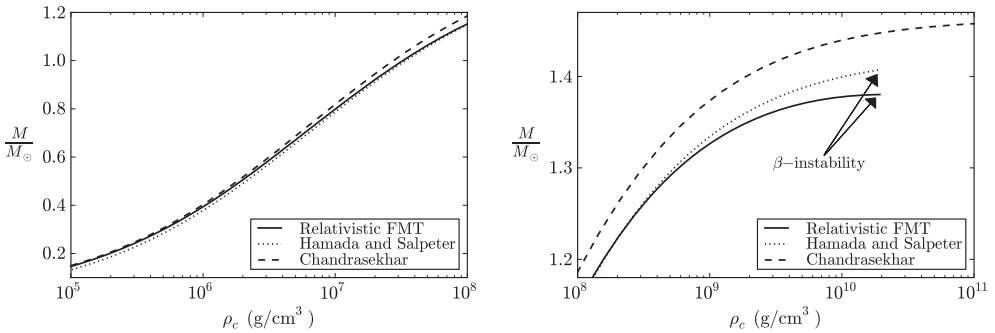

Fig. 14. – Mass in solar masses as a function of the central density in the range (left panel) 10^5–10^8 g/cm^3 and in the range (right panel) 10^8–10^{11} g/cm^3 for ^{16}O white dwarfs. The solid curve corresponds to the present work, the dotted curves are the Newtonian configurations of Hamada and Salpeter and the dashed curve are the Newtonian configurations of Chandrasekhar.

4. The Coulomb effects are much more pronounced in the case of white dwarfs with heavy nuclear compositions, *e.g.*, ^{56}Fe (see figs. 16 and 17).

We have addressed the theoretical physics aspects of the white dwarf configurations of equilibrium, quite apart from the astrophysical application. The recently accomplished description of a compressed atom within the global approach of the relativistic FMT treatment [12] has been here solved within the Wigner-Seitz cell and applied to the construction of white dwarfs in the framework of general relativity. From a theoretical physics point of view, this is the first unified approach of white dwarfs taking into account consistently the gravitational, the weak, the strong and the electromagnetic interactions, and it answers open theoretical physics issues in this matter. No analytic formula for the critical mass of white dwarfs can be derived and, on the contrary, the critical mass can obtained only through the numerical integration of the general relativistic equations of equilibrium together with the relativistic FMT equation of state.

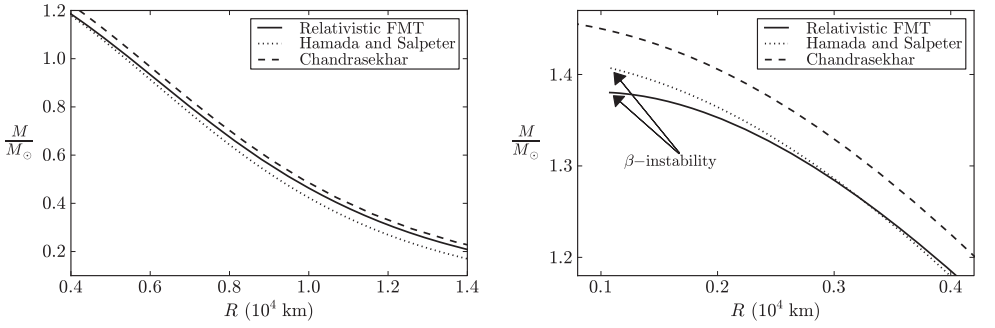

Fig. 15. – Mass in solar masses as a function of the radius in units of 10^4 km for ^{16}O white dwarfs. The left and right panels show the configurations for the same range of central densities of the corresponding panels of fig. 14. The solid curve corresponds to the present work, the dotted curves are the Newtonian configurations of Hamada and Salpeter and the dashed curve are the Newtonian configurations of Chandrasekhar.

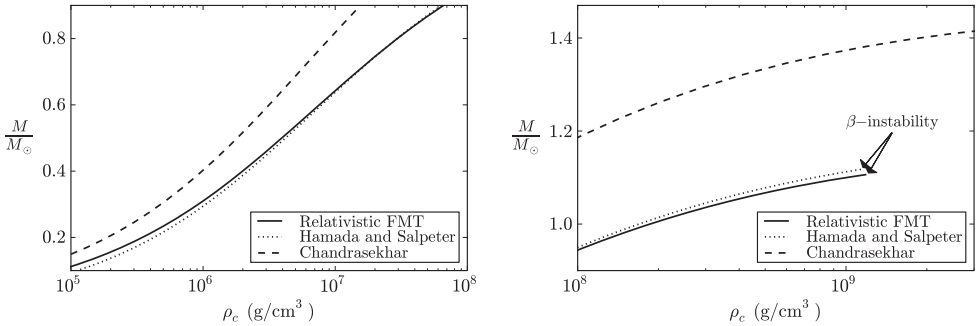

Fig. 16. – Mass in solar masses as a function of the central density in the range (left panel) 10^5–10^8 g/cm^3 and in the range (right panel) 10^8–3×10^9 g/cm^3 for ^{56}Fe white dwarfs. The solid curve corresponds to the present work, the dotted curves are the Newtonian configurations of Hamada and Salpeter and the dashed curve are the Newtonian configurations of Chandrasekhar.

The value of the critical mass and the radius of white dwarfs in our treatment and in the Hamada and Salpeter [49] treatment becomes a function of the composition of the star. Specific examples have been given in the case of white dwarfs composed of ^{4}He, ^{12}C, ^{16}O and ^{56}Fe. The results of Chandrasekhar, of Hamada and Salpeter and ours have been compared and contrasted (see table III and figs. 10–17).

The critical mass is a decreasing function of Z and Coulomb effects are more important for heavy nuclear compositions. The validity of the Salpeter approximate formulas increases also with Z, namely for heavy nuclear compositions the numerical values of the masses as well as of the radii of white dwarfs obtained using the Salpeter equation of state are closer to the ones obtained from the full numerical integration of the general relativistic treatment presented here.

Turning now to astrophysics, the critical mass of white dwarfs is today acquiring a renewed interest in view of its central role in the explanation of the supernova phenomena [50-53]. The central role of the critical mass of white dwarfs as related to supernova

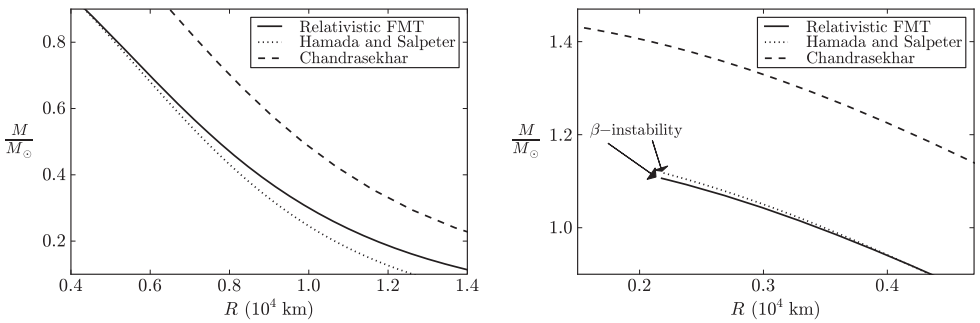

Fig. 17. – Mass in solar masses as a function of the radius in units of 10^4 km for ^{56}Fe white dwarfs. The left and right panels show the configurations for the same range of central densities of the corresponding panels of fig. 16. The solid curve corresponds to the present work, the dotted curves are the Newtonian configurations of Hamada and Salpeter and the dashed curve are the Newtonian configurations of Chandrasekhar.

TABLE III. – *Critical density and corresponding critical mass for the onset of gravitational collapse of the Newtonian* ^{4}He, ^{12}C, ^{16}O *and* ^{56}Fe *white dwarfs of Hamada* [49]*, based on the Salpeter equation of state* [36]*, and of the corresponding general relativistic configurations obtained in this work based on the relativistic FMT equation of state* [12]*. Densities are in g/cm*^{3} *and masses in solar masses. For the sake of comparison, the critical mass of Stoner* (58) *and of the one of Chandrasekhar-Landau* (57) *are* $M_{\rm crit}^{\rm Stoner} \sim 1.72 M_\odot$ *and* $M_{\rm crit}^{\rm Ch-L} \sim 1.45 M_\odot$*, for the average molecular weight* $\mu = A_r/Z = 2$*.*

	$\rho_{\rm crit}^{\rm H\&S}$	$M_{\rm crit}^{\rm H\&S}/M_\odot$	$\rho_{\rm crit}^{\rm FMTrel}$	$M_{\rm crit}^{\rm FMTrel}/M_\odot$
^{4}He	1.37×10^{11}	1.44064	1.56×10^{10}	1.40906
^{12}C	3.88×10^{10}	1.41745	2.12×10^{10}	1.38603
^{16}O	1.89×10^{10}	1.40696	1.94×10^{10}	1.38024
^{56}Fe	1.14×10^{9}	1.11765	1.18×10^{9}	1.10618

was presented by F. Hoyle and W. A. Fowler [54] explaining the difference between type-I and type-II Supernova. This field has developed in the intervening years to a topic of high precision research in astrophysics and, very likely, both the relativistic and the Coulomb effects outlined in this article will become topic of active confrontation between theory and observation. For instance, the underestimate of the mass and the radius of low density white dwarfs within the Hamada and Salpeter treatment [49] (see figs. 10–17) leads to the possibility of a direct confrontation with observations in the case of low mass white dwarfs, *e.g.* the companion of the Pulsar J1141-6545.

We have finally obtained a general formula in eq. (148) as a "first integral" of the general relativistic equations of equilibrium. This formula relates the chemical potential of the Wigner-Seitz cells, duly obtained from the relativistic FMT model [12] taking into account weak, nuclear and electromagnetic interactions, to the general relativistic gravitational potential at each point of the configuration. Besides its esthetic value, this is an important tool to examine the radial dependence of the white dwarf properties and it can be also applied to the crust of a neutron star as it approaches to the physical important regime of neutron star cores.

The formalism we have introduced allows in principle to evaluate subtle effects of a nuclear density distribution as a function of the radius and of the Fermi energy of the electrons and of the varying depth of the general relativistic gravitational potential. The theoretical base presented in this article establishes also the correct framework for the formulation of the more general case when finite temperatures and magnetic fields are present. This treatment naturally opens the way to a more precise description of the crust of neutron stars, which will certainly become an active topic of research in view of the recent results by S. Goriely *et al.* [55] and by J. M. Pearson *et al.* [56] on the importance of the Coulomb effects in the r-process nucleosynthesis of the crust material during its post-ejection evolution in the process of gravitational collapse and/or in the merging of neutron star binaries.

9. – The ultra-relativistic Thomas-Fermi equation and nuclear matter cores of stellar dimensions

We have generalized the FMT treatment of compressed atoms to the relativistic regimes (see [12] and sect. **7**). The application of this approach to general relativistic white dwarfs has been presented in sect. **8**. Thanks to the existence of scaling laws of

the ultrarelativistic Thomas-Fermi equation [9-12] this treatment can be extrapolated to what can be called compressed nuclear matter cores of stellar dimensions: objects with mass numbers $A \simeq (m_{\rm Planck}/m_n)^3 \sim 10^{57}$ or $M_{\rm core} \sim M_\odot$. As we will show below, such configurations fulfill global but not local charge neutrality and have electric fields on their core surfaces reaching values much larger than the critical value $E_c = m_e^2 c^3/(e\hbar)$. A constant distribution of protons at nuclear densities is assumed to simulate the confinement due to the strong interactions in the case of nuclei and heavy nuclei and due to both the gravitational field and the strong interactions in the case of nuclear matter cores of stellar sizes.

In the ultrarelativistic limit, the relativistic Thomas-Fermi equation admits an analytic solution. Introducing the new function ϕ defined by $\phi = \frac{4^{1/3}}{(9\pi)^{1/3}} \Delta \frac{\chi}{x}$ and the new variables $\hat{x} = (12/\pi)^{1/6} \sqrt{\alpha} \Delta^{-1} x$, $\xi = \hat{x} - \hat{x}_c$, where $\hat{x}_c = (12/\pi)^{1/6} \sqrt{\alpha} \Delta^{-1} x_c$, then eq. (126) becomes

$$\frac{{\rm d}^2 \hat{\phi}(\xi)}{{\rm d}\xi^2} = -\theta(-\xi) + \hat{\phi}(\xi)^3, \tag{164}$$

where $\hat{\phi}(\xi) = \phi(\xi + \hat{x}_c)$. The boundary conditions on $\hat{\phi}$ are: $\hat{\phi}(\xi) \to 1$ as $\xi \to -\hat{x}_c \ll 0$ (at the massive nuclear density core center) and $\hat{\phi}(\xi) \to 0$ as $\xi \to \infty$. The function $\hat{\phi}$ and its first derivative $\hat{\phi}'$ must be continuous at the surface $\xi = 0$ of the massive nuclear density core. Equation (164) admits an exact solution

$$\hat{\phi}(\xi) = \begin{cases} 1 - 3\left[1 + 2^{-1/2} \sinh(a - \sqrt{3}\xi)\right]^{-1}, & \xi < 0, \\ \dfrac{\sqrt{2}}{(\xi + b)}, & \xi > 0, \end{cases} \tag{165}$$

where the integration constants a and b have the values $a = \operatorname{arcsinh}(11\sqrt{2}) \approx 3.439$, $b = (4/3)\sqrt{2} \approx 1.886$. Next we evaluate the Coulomb potential energy function

$$eV(\xi) = \left(\frac{9\pi}{4}\right)^{1/3} \frac{1}{\Delta} m_\pi c^2 \hat{\phi}(\xi), \tag{166}$$

and by differentiation, the electric field

$$E(\xi) = -\left(\frac{3^5\pi}{4}\right)^{1/6} \frac{\sqrt{\alpha}}{\Delta^2} \frac{m_\pi^2 c^3}{e\hbar} \hat{\phi}'(\xi). \tag{167}$$

Details are given in figs. 18 and 19.

We now estimate three crucial quantities: 1) the Coulomb potential at the center of the configuration,

$$eV(0) \approx \left(\frac{9\pi}{4}\right)^{1/3} \frac{1}{\Delta} m_\pi c^2, \tag{168}$$

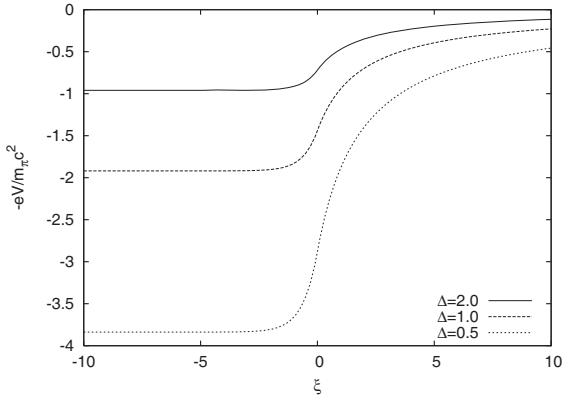

Fig. 18. – The electron Coulomb potential energy $-eV$, in units of pion mass m_π is plotted as a function of the radial coordinate $\xi = \hat{x} - \hat{x}_c$, for selected values of the density parameter Δ.

2) the electric field at the surface of the core

$$E_{\max} \approx 0.95\sqrt{\alpha}\frac{1}{\Delta^2}\frac{m_\pi^2 c^3}{e\hbar} = 0.95\frac{\sqrt{\alpha}}{\Delta^2}\left(\frac{m_\pi}{m_e}\right)^2 E_c, \tag{169}$$

3) the Coulomb electrostatic energy of the core

$$\mathcal{E}_{\rm em} = \int \frac{E^2}{8\pi}\mathrm{d}^3 r \approx 0.15\frac{3\hbar c(3\pi)^{1/2}}{4\Delta\sqrt{\alpha}}A^{2/3}\frac{m_\pi c}{\hbar}\left(\frac{N_p}{A}\right)^{2/3}. \tag{170}$$

These three quantities are functions only of the pion mass m_π, the density parameter Δ and of the fine structure constant α. Their formulas apply over the entire range from superheavy nuclei with $N_p \sim 10^3$ all the way up to massive cores with $N_p \approx (m_{\rm Planck}/m_n)^3$.

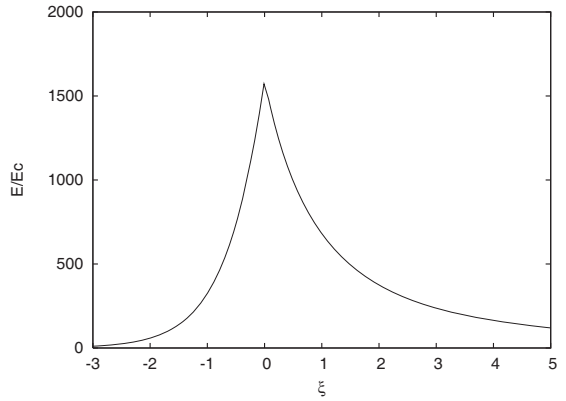

Fig. 19. – The electric field is plotted in units of the critical field E_c as a function of the radial coordinate ξ for $\Delta = 2$, showing a sharp peak at the core radius.

Starting from the analytic solutions of the previous section we obtain the following new results:

a) Using the solution (165), we have obtained a new generalized relation between A and N_p for any value of A. In the limit of small A this result agrees well with the phenomenological relations given by eqs. (65) and (66). It seems that the explicit evaluation of the β-equilibrium, in contrast with the previously adopted equations, leads to an effect comparable in magnitude and qualitatively similar to the asymmetry energy in the phenomenological liquid drop model.

b) The charge-to-mass ratio of the effective charge Q at the core surface to the core mass M is given by

$$\frac{Q}{\sqrt{G}M} \approx \frac{E_{\max} R_c^2}{\sqrt{G} m_n A} \approx \frac{m_{\mathrm{Planck}}}{m_n} \left(\frac{1}{N_p}\right)^{1/3} \frac{N_p}{A}\,. \tag{171}$$

For superheavy nuclei with $N_p \approx 10^3$, the charge-to-mass ratio for the nucleus is

$$\frac{Q}{\sqrt{G}M} > \frac{1}{20} \frac{m_{\mathrm{Planck}}}{m_n} \sim 10^{18}. \tag{172}$$

Gravitation obviously plays no role in the stabilization of these nuclei.

Instead for massive nuclear density cores where $N_p \approx (m_{\mathrm{Planck}}/m_n)^3$, the ratio $Q/\sqrt{G}M$ given by eq. (171) is simply

$$\frac{Q}{\sqrt{G}M} \approx \frac{N_p}{A}\,, \tag{173}$$

which is approximatively 0.0046. It is well-known that the charge-to-mass-ratio (173) smaller than 1 evidences the equilibrium of self-gravitating mass-charge system both in Newtonian gravity and general relativity.

c) For a massive core at nuclear density the criterion of stability against fission ($\mathcal{E}_{em} < 2\mathcal{E}_s$) is satisfied:

$$\frac{\mathcal{E}_{em}}{2\mathcal{E}_s} \approx 0.15 \frac{3}{8} \sqrt{\frac{3\pi}{\alpha}} \frac{1}{\Delta} \left(\frac{N_p}{A}\right)^{2/3} \frac{m_\pi c^2}{17.5\,\mathrm{MeV}} \sim 0.1 < 1. \tag{174}$$

9˙1. *Estimates of gravitational effects in a Newtonian approximation.* – In order to investigate the possible effects of gravitation on these massive nuclear density cores we proceed to some qualitative and quantitative estimates based on the Newtonian approximation.

a) The *maximum* Coulomb energy per proton is given by eq. (168) where the potential is evaluated at the center of the core. The Newtonian gravitational potential energy per proton (of mass m_p) in the field of a massive nuclear density core with $A \approx (m_{\mathrm{Planck}}/m_n)^3$ is given by

$$\mathcal{E}_g = -G\frac{M m_p}{R_c} = -\frac{1}{\Delta} \frac{m_{\mathrm{Planck}}}{m_n} \frac{m_\pi c^2}{N_p^{1/3}} \simeq -\frac{m_\pi c^2}{\Delta} \left(\frac{A}{N_p}\right)^{1/3}. \tag{175}$$

Since $A/N_p \sim 0.0046$ for any value of Δ, the gravitational energy is larger in magnitude than and opposite in sign to the Coulomb potential energy per proton of eq. (168) so the system should be gravitationally stable.

b) There is yet a more accurate derivation of the gravitational stability based on the analytic solution of the Thomas-Fermi equation eq. (164). The Coulomb energy $\mathcal{E}_{\rm em}$ given by (170) is mainly distributed within a thin shell of width $\delta R_c \approx \hbar\Delta/(\sqrt{\alpha} m_\pi c)$ and proton number $\delta N_p = n_p 4\pi R_c^2 \delta R_c$ at the surface. To ensure the stability of the system, the attractive gravitational energy of the thin proton shell

$$\mathcal{E}_{\rm gr} \approx -3\frac{G}{\Delta}\frac{A^{4/3}}{\sqrt{\alpha}}\left(\frac{N_p}{A}\right)^{1/3} m_n^2 \frac{m_\pi c}{\hbar} \tag{176}$$

has to be larger than the repulsive Coulomb energy (170). For small A, the gravitational energy is always negligible. However, since the gravitational energy increases proportionally to $A^{4/3}$ while the Coulomb energy only increases proportionally to $A^{2/3}$, the two must eventually cross, which occurs at

$$A_R = 0.039\left(\frac{N_p}{A}\right)^{1/2}\left(\frac{m_{\rm Planck}}{m_n}\right)^3 . \tag{177}$$

This establishes a *lower* limit for the mass number A_R necessary for the existence of an island of stability for massive nuclear density cores. The *upper* limit of the island of stability will be determined by general relativistic effects.

c) Having established the role of gravity in stabilizing the Coulomb interaction of the massive nuclear density core, we outline the importance of the strong interactions in determining its surface. We find for the neutron pressure at the surface:

$$P_n = \frac{9}{40}\left(\frac{3}{2\pi}\right)^{1/3}\left(\frac{m_\pi}{m_n}\right)\frac{m_\pi c^2}{(\hbar/m_\pi c)^3}\left(\frac{A}{N_p}\right)^{5/3}\frac{1}{\Delta^5} , \tag{178}$$

and for the surface tension, as extrapolated from nuclear scattering experiments,

$$P_s = -\left(\frac{0.13}{4\pi}\right)\frac{m_\pi c^2}{(\hbar/m_\pi c)^3}\left(\frac{A}{N_p}\right)^{2/3}\frac{1}{\Delta^2} . \tag{179}$$

We then obtain

$$\frac{|P_s|}{P_n} = 0.39\cdot\Delta^3\left(\frac{N_p}{A}\right) = 0.24\cdot\frac{\rho_{\rm nucl}}{\rho_{\rm surf}} , \tag{180}$$

where $\rho_{\rm nucl} = 3m_n A/4\pi R_c^3$. The relative importance of the nuclear pressure and nuclear tension is a very sensitive function of the density $\rho_{\rm surf}$ at the surface.

It is important to emphasize a major difference between nuclei and the massive nuclear density cores treated here: the gravitational binding energy in these massive nuclear density cores is instead $\mathcal{E}_{\rm gr} \approx GM_\odot m_n/R_c \approx 0.1 m_n c^2 \approx 93.8\,{\rm MeV}$. Namely, it is much bigger than the nuclear energy in ordinary nuclei $\mathcal{E}_{\rm nuclear} \approx \hbar^2/m_n r_0^2 \approx 28.8\,{\rm MeV}$.

9·2. *Compressed nuclear matter cores of stellar dimensions.* – Following the above treatment, we use the existence of scaling laws and proceed to the ultra-relativistic limit of the above equations for positive values of the electron Fermi energy E_e^F. We then introduce the new function $\phi = 4^{1/3}(9\pi)^{-1/3}\chi\Delta/x$ and the new variable $\hat{x} = kx$ where $k = (12/\pi)^{1/6}\sqrt{\alpha}\Delta^{-1}$, as well as the variable $\xi = \hat{x} - \hat{x}_c$ in order to describe better the region around the core radius.

Thus, eq. (126) becomes

$$\frac{\mathrm{d}^2\hat{\phi}(\xi)}{\mathrm{d}\xi^2} = -\theta(-\xi) + \hat{\phi}(\xi)^3, \tag{181}$$

where $\hat{\phi}(\xi) = \phi(\xi + \hat{x}_c)$ and the curvature term $2\hat{\phi}'(\xi)/(\xi + \hat{x}_c)$ has been neglected.

The Coulomb potential energy is given by

$$eV(\xi) = \left(\frac{9\pi}{4}\right)^{1/3} \frac{1}{\Delta} m_\pi c^2 \hat{\phi}(\xi) - E_e^F, \tag{182}$$

corresponding to the electric field

$$E(\xi) = -\left(\frac{3^5\pi}{4}\right)^{1/6} \frac{\sqrt{\alpha}}{\Delta^2} \frac{m_\pi^2 c^3}{e\hbar} \hat{\phi}'(\xi), \tag{183}$$

and the electron number-density

$$n_e(\xi) = \frac{1}{3\pi^2\hbar^3 c^3} \left(\frac{9\pi}{4}\right) \frac{1}{\Delta^3} (m_\pi c^2)^3 \hat{\phi}^3(\xi). \tag{184}$$

In the core center we must have $n_e = n_p$. From eqs. (68) and (184) we than have that, for $\xi = -\hat{x}_c$, $\hat{\phi}(-\hat{x}_c) = 1$.

In order to consider a compressed nuclear density core of stellar dimensions, we then introduce a Wigner-Seitz cell determining the outer boundary of the electron distribution which, in the new radial coordinate ξ is characterized by ξ^{WS}. In view of the global charge neutrality of the system the electric field goes to zero at $\xi = \xi^{WS}$. This implies, from eq. (183), $\hat{\phi}'(\xi^{WS}) = 0$.

We turn now to the determination of the Fermi energy of the electrons in this compressed core. The function $\hat{\phi}$ and its first derivative $\hat{\phi}'$ must be continuous at the surface $\xi = 0$ of the nuclear density core.

This boundary-value problem can be solved analytically and indeed eq. (181) has the first integral,

$$2[\hat{\phi}'(\xi)]^2 = \begin{cases} \hat{\phi}^4(\xi) - 4\hat{\phi}(\xi) + 3, & \xi < 0, \\ \hat{\phi}^4(\xi) - \phi^4(\xi^{WS}), & \xi > 0, \end{cases} \tag{185}$$

with boundary conditions at $\xi = 0$:

$$\hat{\phi}(0) = \frac{\hat{\phi}^4(\xi^{WS}) + 3}{4}, \tag{186}$$

$$\hat{\phi}'(0) = -\sqrt{\frac{\hat{\phi}^4(0) - \hat{\phi}^4(\xi^{WS})}{2}}.$$

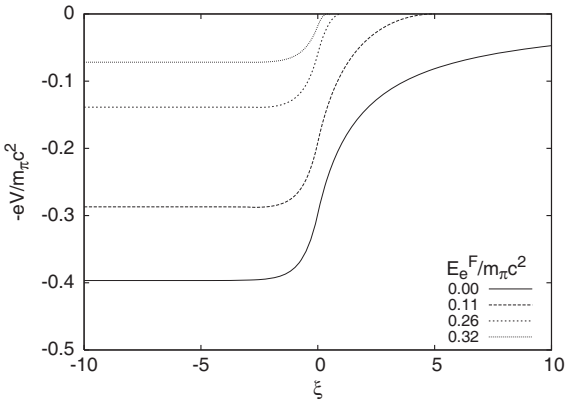

Fig. 20. – The electron Coulomb potential energies in units of the pion rest energy in a nuclear matter core of stellar dimensions with $A \simeq 10^{57}$ or $M_{core} \sim M_\odot$ and $R_c \approx 10^6$ cm, are plotted as a function of the dimensionless variable ξ, for different values of the electron Fermi energy also in units of the pion rest energy. The solid line corresponds to the case of null electron Fermi energy. By increasing the value of the electron Fermi energy the electron Coulomb potential energy depth is reduced.

Having fullfilled the continuity condition we integrate eq. (185) obtaining for $\xi \leq 0$

$$\hat{\phi}(\xi) = 1 - 3\left[1 + 2^{-1/2}\sinh(a - \sqrt{3}\xi)\right]^{-1}, \tag{187}$$

where the integration constant a has the value

$$\sinh(a) = \sqrt{2}\left(\frac{11 + \hat{\phi}^4(\xi^{WS})}{1 - \hat{\phi}^4(\xi^{WS})}\right). \tag{188}$$

In the interval $0 \leq \xi \leq \xi^{WS}$, the field $\hat{\phi}(\xi)$ is implicitly given by

$$F\left(\arccos\frac{\hat{\phi}(\xi^{WS})}{\hat{\phi}(\xi)}, \frac{1}{\sqrt{2}}\right) = \hat{\phi}(\xi^{WS})(\xi - \xi^{WS}), \tag{189}$$

where $F(\varphi, k)$ is the elliptic function of the first kind, and $F(0, k) \equiv 0$. For $F(\varphi, k) = u$, the inverse function $\varphi = F^{-1}(u, k) = \mathrm{am}(u, k)$ is the well known Jacobi amplitude. In terms of it, we can express the solution (189) for $\xi > 0$ as,

$$\hat{\phi}(\xi) = \hat{\phi}(\xi^{WS})\left\{\cos\left[\mathrm{am}\left(\hat{\phi}(\xi^{WS})(\xi - \xi^{WS}), \frac{1}{\sqrt{2}}\right)\right]\right\}^{-1}. \tag{190}$$

In the present case of $E_e^F > 0$ the ultra-relativistic approximation is indeed always valid up to $\xi = \xi^{WS}$ for high compression factors, *i.e.* for $R_{WS} \simeq R_c$. In the case $E_e^F = 0$, $\xi^{WS} \to \infty$, there is a breakdown of the ultra-relativistic approximation when $\xi \to \xi^{WS}$.

Details are given in figs. 20, 21, 22.

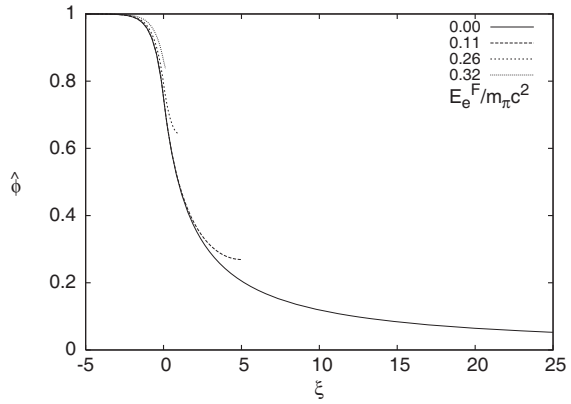

Fig. 21. – Solutions of the ultra-relativistic Thomas-Fermi equation (181) for different values of the Wigner-Seitz cell radius R_{WS} and correspondingly of the electron Fermi energy in units of the pion rest energy as in fig. 20, near the core surface. The solid line corresponds to the case of null electron Fermi energy.

We can now estimate two crucial quantities of the solutions: the Coulomb potential at the center of the configuration and the electric field at the surface of the core

$$eV(0) \simeq \left(\frac{9\pi}{4}\right)^{1/3} \frac{1}{\Delta} m_\pi c^2 - E_e^F, \tag{191}$$

$$E_{\max} \simeq 2.4 \frac{\sqrt{\alpha}}{\Delta^2} \left(\frac{m_\pi}{m_e}\right)^2 E_c |\hat{\phi}'(0)|, \tag{192}$$

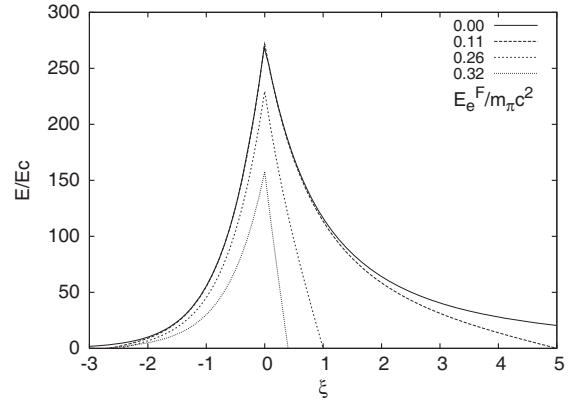

Fig. 22. – The electric field in units of the critical field for vacuum polarization $E_c = m_e^2 c^3/(e\hbar)$ is plotted as a function of the coordinate ξ, for different values of the electron Fermi energy in units of the pion rest energy. The solid line corresponds to the case of null electron Fermi energy. To an increase of the value of the electron Fermi energy it is found a reduction of the peak of the electric field.

where $E_c = m_e^2 c^3/(e\hbar)$ is the critical electric field for vacuum polarization. These functions depend on the value $\hat{\phi}(\xi^{WS})$ via eqs. (185)–(189). At the boundary $\xi = \xi^{WS}$, due to the global charge neutrality, both the electric field $E(\xi^{WS})$ and the Coulomb potential $eV(\xi^{WS})$ vanish. From eq. (182), we determine the value of $\hat{\phi}(\xi)$ at $\xi = \xi^{WS}$

$$\hat{\phi}(\xi^{WS}) = \Delta \left(\frac{4}{9\pi}\right)^{1/3} \frac{E_e^F}{m_\pi c^2}\,, \tag{193}$$

as a function of the electron Fermi energies E_e^F. From the above eq. (193), one can see that there exists a solution, characterized by the value of electron Fermi energy

$$\frac{(E_e^F)_{max}}{m_\pi c^2} = \frac{1}{\Delta}\left(\frac{9\pi}{4}\right)^{1/3}, \tag{194}$$

such that $\hat{\phi}(\xi^{WS}) = 1$. From eq. (189) and $\xi = 0$, we also have

$$\xi^{WS}(\hat{\phi}(\xi^{WS})) = \left\{\frac{1}{\hat{\phi}(0)} F\left[\arccos\left(4 - \frac{3}{\hat{\phi}(0)}\right), \frac{1}{\sqrt{2}}\right]\right\}. \tag{195}$$

For $\hat{\phi}(\xi^{WS}) = 1$, from eq. (186) there follows $\hat{\phi}(0) = 1$, hence eq. (195) becomes

$$\xi^{WS}(\hat{\phi}(0)) = F\left[0, \frac{1}{\sqrt{2}}\right]. \tag{196}$$

It is well known that if the inverse Jacobi amplitude $F[0, 1/\sqrt{2}]$ is zero, then

$$\xi^{WS}(\hat{\phi}(\xi^{WS}) = \hat{\phi}(0) = 1) = 0. \tag{197}$$

Indeed from $\hat{\phi}(\xi^{WS}) = 1$ follows $\hat{\phi}(0) = 1$ and $\xi^{WS} = 0$. When $\xi^{WS} = 0$ from eq. (186) follows $\hat{\phi}'(0) = 0$ and, using eq. (192), $E_{\max} = 0$. In other words for the value of E_e^F fulfilling eq. (193) no electric field exists on the boundary of the core and from eq. (184) and eqs. (67), (68) it follows that indeed this is the solution fulfilling both global $N_e = N_p$ and local $n_e = n_p$ charge neutrality. In this special case we obtain

$$(E_e^F)_{max}^{3/2} = \frac{\frac{9\pi}{4}(\hbar c)^3 \frac{A}{R_c^3} - (E_e^F)_{max}^3}{2^{3/2}\left[\left(\frac{9\pi}{4}(\hbar c)^3 \frac{A}{R_c^3} - (E_e^F)_{max}^3\right)^{2/3} + m_n^2 c^4\right]^{3/4}}. \tag{198}$$

In the ultra-relativistic approximation $(E_e^F)_{max}^3 / \frac{9\pi}{4}(\hbar c)^3 \frac{A}{R_c^3} \ll 1$ so eq. (198) can be approximated to

$$(E_e^F)_{max} = 2^{1/3} \frac{m_n}{m_\pi} \gamma \left[-1 + \sqrt{1 + \frac{\beta}{2\gamma^3}}\right]^{2/3} m_\pi c^2, \tag{199}$$

where $A = N_p + N_n$ and

$$\beta = \frac{9\pi}{4}\left(\frac{\hbar}{m_n c}\right)^3 \frac{A}{R_c^3}\,, \qquad \gamma = \sqrt{1+\beta^{2/3}}. \tag{200}$$

The corresponding limiting value to the N_p/A ratio is

$$\frac{N_p}{A} = \frac{2\gamma^3}{\beta}\left[-1+\sqrt{1+\frac{\beta}{2\gamma^3}}\right]^2. \tag{201}$$

The N_p-independence in the limiting case of maximum electron Fermi energy attained when $R_{WS} = R_c$, in which the ultra-relativistic treatment approaches the uniform one, and the N_p-dependence for smaller compressions $R_{WS} > R_c$ can be understood as follows. Let see the solution to the ultra-relativistic equation (181) for small $\xi > 0$. Analogously to the FMT approach to the non-relativistic Thomas-Fermi equation, we solve the ultra-relativistic equation (181) for small ξ. Expanding $\hat{\phi}(\xi)$ about $\xi = 0$ in a semiconvergent power series,

$$\frac{\hat{\phi}(\xi)}{\hat{\phi}(0)} = 1 + \sum_{n=2}^{\infty} a_n \xi^{n/2} \tag{202}$$

and substituting it into the ultra-relativistic equation (181), we have

$$\sum_{k=3}^{\infty} a_k \frac{k(k-2)}{4}\xi^{(k-4)/2} = \phi^2(0)\exp\left[3\ln(1+\sum_{n=2}^{\infty} a_n \xi^{n/2})\right]. \tag{203}$$

This leads to a recursive determination of the coefficients:

$$\begin{aligned} &a_3 = 0, \qquad a_4 = \phi^2(0)/2, \qquad a_5 = 0, \qquad a_6 = \phi^2(0)a_2/2, \\ &a_7 = 0, \qquad a_8 = \phi^2(0)(1-a_2^2)/8, \ldots, \end{aligned} \tag{204}$$

with $a_2 = \hat{\phi}'(0)/\hat{\phi}(0)$ determined by the initial slope, namely, the boundary condition $\hat{\phi}'(0)$ and $\hat{\phi}(0)$ in eq. (186):

$$\hat{\phi}(0) = \frac{\hat{\phi}^4(\xi^{WS})+3}{4}, \qquad \hat{\phi}'(0) = -\sqrt{\frac{\hat{\phi}^4(0)-\hat{\phi}^4(\xi^{WS})}{2}} \tag{205}$$

Thus the series solution (202) is uniquely determined by the boundary value $\hat{\phi}(\xi^{WS})$ at the Wigner-Seitz cell radius.

Now we consider the solution up to the leading orders

$$\hat{\phi}(\xi) = \hat{\phi}(0) + \hat{\phi}'(0)\xi + \frac{1}{2}\hat{\phi}^3(0)\xi^2 + \frac{1}{2}\hat{\phi}^3(0)a_2\xi^3 + \frac{1}{8}\hat{\phi}^3(0)(1-a_2^2)\xi^4 + \ldots\,. \tag{206}$$

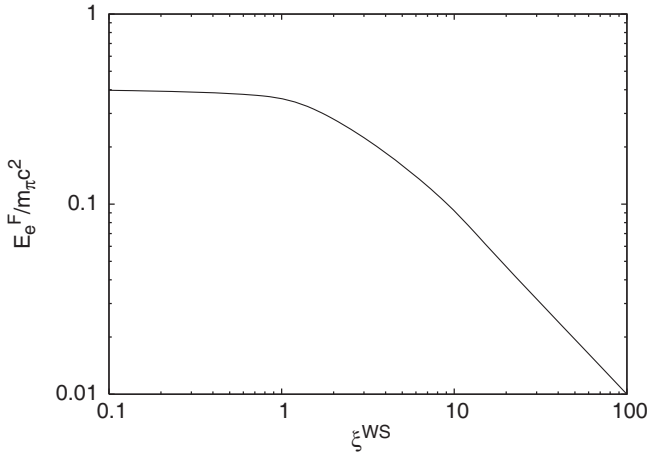

Fig. 23. – The Fermi energy of electrons in units of the pion rest energy is plotted for different Wigner-Seitz cell dimensions (*i.e.* for different compressions) ξ^{WS} in the ultra-relativistic approximation. In the limit $\xi^{WS} \to 0$ the electron Fermi energy approaches asymptotically the value $(E_e^F)_{max}$ given by eq. (199).

Using eq. (206), the electron Fermi energy (193) becomes

$$E_e^F = (E_e^F)_{max}\left[1 + a_2\xi^{WS} + \frac{1}{2}\hat{\phi}^2(0)(\xi^{WS})^2 + \frac{1}{2}\hat{\phi}^2(0)a_2(\xi^{WS})^3 + \frac{1}{8}\hat{\phi}^2(0)(1-a_2^2)(\xi^{WS})^4 + \cdots\right]\hat{\phi}(0), \tag{207}$$

where $(E_e^F)_{max} = (9\pi/4)^{1/3}\Delta^{-1}$ is the maximum Fermi energy which is attained when the Wigner-Seitz cell radius equals the nucleus radius R_c (see eq. 194). For $\hat{\phi}(\xi^{WS}) < 1$, we approximately have $\hat{\phi}(0) = 3/4$, $\hat{\phi}'(0) = -(3/4)^2/\sqrt{2}$ and the initial slope $a_2 = \hat{\phi}'(0)/\hat{\phi}(0) = -(3/4)/\sqrt{2}$. Therefore eq. (207) becomes

$$E_e^F \approx (E_e^F)_{max}\left[1 - \frac{3}{4\sqrt{2}}\xi^{WS} + \frac{1}{2}\left(\frac{3}{4}\right)^2(\xi^{WS})^2 - \frac{1}{2^{3/2}}\left(\frac{3}{4}\right)^3(\xi^{WS})^3 + \frac{1}{8}\left(\frac{3}{4}\right)^2\left(\frac{41}{32}\right)(\xi^{WS})^4 + \cdots\right]. \tag{208}$$

By the definition of the coordinate ξ, we know all terms except the first term in the square bracket depend on the values of N_p. In the limit of maximum compression when the electron Fermi energy acquires its maximum value, namely when $\xi^{WS} = 0$, the electron Fermi energy (208) is the same as the one obtained from the uniform approximation which is independent of N_p. For smaller compressions, namely for $\xi^{WS} > 0$ the electron Fermi energy deviates from the one given by the uniform approximation becoming N_p-dependent.

In fig. 23 we plot the Fermi energy of electrons, in units of the pion rest energy, as a function of the dimensionless parameter ξ^{WS} and, as $\xi^{WS} \to 0$, the limiting value given by eq. (199) is clearly displayed.

In Alcock, Farhi and Olinto [57], in order to study the electrodynamical properties of strange stars, the ultra-relativistic Thomas-Fermi equation was numerically solved in the case of bare strange stars as well as in the case of strange stars with a crust (see *e.g.* curves (a) and (b) in fig. 6 of [57]). In fig. 6 of [57] was plotted what they called the Coulomb potential energy, which we will denote as $V_{\rm Alcock}$. The potential $V_{\rm Alcock}$ was plotted for different values of the electron Fermi momentum at the edge of the crust. Actually, such potential $V_{\rm Alcock}$ is not the Coulomb potential eV but it coincides with our function $e\hat{V} = eV + E_e^F$. Namely, the potential $V_{\rm Alcock}$ corresponds to the Coulomb potential shifted by the Fermi energy of the electrons. We then have from eq. (182)

$$e\hat{V}(\xi) = \left(\frac{9\pi}{4}\right)^{1/3} \frac{1}{\Delta} m_\pi c^2 \hat{\phi}(\xi) = V_{\rm Alcock}. \tag{209}$$

This explains why in [57], for different values of the Fermi momentum at the crust the depth of the potential $V_{\rm Alcock}$ remains unchanged. Instead, the correct behaviour of the Coulomb potential is quite different and, indeed, its depth decreases with increasing of compression as can be seen in fig. 20.

9˙2.1. Compressional energy of nuclear matter cores of stellar dimensions. We turn now to the compressional energy of these family of compressed nuclear matter cores of stellar dimensions each characterized by a different Fermi energy of the electrons. The kinematic energy-spectra of complete degenerate electrons, protons and neutrons are

$$\epsilon^i(p) = \sqrt{(pc)^2 + m_i^2 c^4}, \quad p \le P_i^F, \quad i = e, p, n. \tag{210}$$

So the compressional energy of the system is given by

$$\mathcal{E} = \mathcal{E}_B + \mathcal{E}_e + \mathcal{E}_{\rm em}, \qquad \mathcal{E}_B = \mathcal{E}_p + \mathcal{E}_n, \tag{211}$$

$$\mathcal{E}_{\rm i} = 2 \int_i \frac{{\rm d}^3 r {\rm d}^3 p}{(2\pi\hbar)^3} \epsilon^i(p), \quad i = e, p, n, \qquad \mathcal{E}_{\rm em} = \int \frac{E^2}{8\pi} {\rm d}^3 r. \tag{212}$$

Using the analytic solution (190) we calculate the energy difference between two systems, I and II,

$$\Delta\mathcal{E} = \mathcal{E}(E_e^F(II)) - \mathcal{E}(E_e^F(I)), \tag{213}$$

with $E_e^F(II) > E_e^F(I) \ge 0$, at fixed A and R_c.

We first consider the infinitesimal variation of the total energy $\delta\mathcal{E}_{\rm tot}$ with respect to the infinitesimal variation of the electron Fermi energy δE_e^F

$$\delta\mathcal{E} = \left[\frac{\partial\mathcal{E}}{\partial N_p}\right]_{V^{WS}} \left[\frac{\partial N_p}{\partial E_e^F}\right] \delta E_e^F + \left[\frac{\partial\mathcal{E}}{\partial V^{WS}}\right]_{N_p} \left[\frac{\partial V^{WS}}{\partial E_e^F}\right] \delta E_e^F. \tag{214}$$

For the first term of this relation we have

$$\begin{aligned} \left[\frac{\partial\mathcal{E}}{\partial N_p}\right]_{V^{WS}} &= \left[\frac{\partial\mathcal{E}_{\rm p}}{\partial N_p} + \frac{\partial\mathcal{E}_{\rm n}}{\partial N_p} + \frac{\partial\mathcal{E}_{\rm e}}{\partial N_p} + \frac{\partial\mathcal{E}_{\rm em}}{\partial N_p}\right]_{V^{WS}} \\ &\simeq \left[E_p^F - E_n^F + E_e^F + \frac{\partial\mathcal{E}_{\rm em}}{\partial N_p}\right]_{V^{WS}}, \end{aligned} \tag{215}$$

where the general definition of chemical potential $\partial\epsilon_i/\partial n_i = \partial\mathcal{E}_i/\partial N_i$ is used ($i = e$, p, n) neglecting the mass defect $m_n - m_p - m_e$. Further using the condition of the β-equilibrium between neutrons, protons, and electrons we have

$$\left[\frac{\partial\mathcal{E}}{\partial N_p}\right]_{V^{WS}} = \left[\frac{\partial\mathcal{E}_{\mathrm{em}}}{\partial N_p}\right]_{V^{WS}}. \tag{216}$$

For the second term of eq. (214) we have

$$\begin{aligned}\left[\frac{\partial\mathcal{E}}{\partial V^{WS}}\right]_{N_p} &= \left[\frac{\partial\mathcal{E}_{\mathrm{p}}}{\partial V^{WS}} + \frac{\partial\mathcal{E}_{\mathrm{n}}}{\partial V^{WS}} + \frac{\partial\mathcal{E}_{\mathrm{e}}}{\partial V^{WS}} + \frac{\partial\mathcal{E}_{\mathrm{em}}}{\partial V^{WS}}\right]_{N_p} \\ &= \left[\frac{\partial\mathcal{E}_{\mathrm{e}}}{\partial V^{WS}}\right]_{N_p} + \left[\frac{\partial\mathcal{E}_{\mathrm{em}}}{\partial V^{WS}}\right]_{N_p},\end{aligned} \tag{217}$$

since in the process of increasing the electron Fermi energy namely, by decreasing the radius of the Wigner-Seitz cell, the system by definition maintains the same number of baryons A and the same core radius R_c.

Now $\delta\mathcal{E}$ reads

$$\delta\mathcal{E} = \left\{\left[\frac{\partial\mathcal{E}_{\mathrm{e}}}{\partial V^{WS}}\right]_{N_p}\frac{\partial V^{WS}}{\partial E_e^F} + \left[\frac{\partial\mathcal{E}_{\mathrm{em}}}{\partial V^{WS}}\right]_{N_p}\frac{\partial V^{WS}}{\partial E_e^F} + \left[\frac{\partial\mathcal{E}_{\mathrm{em}}}{\partial N_p}\right]_{V^{WS}}\frac{\partial N_p}{\partial E_e^F}\right\}\delta E_e^F, \tag{218}$$

so only the electromagnetic energy and the electron energy give non-null contributions.

From this equation it follows that

$$\Delta\mathcal{E} = \Delta\mathcal{E}_{\mathrm{em}} + \Delta\mathcal{E}_{\mathrm{e}}, \tag{219}$$

where $\Delta\mathcal{E}_{\mathrm{em}} = \mathcal{E}_{\mathrm{em}}(E_e^F(II)) - \mathcal{E}_{\mathrm{em}}(E_e^F(I))$ and $\Delta\mathcal{E}_{\mathrm{e}} = \mathcal{E}_{\mathrm{e}}(E_e^F(II)) - \mathcal{E}_{\mathrm{e}}(E_e^F(I))$.

In the particular case in which $E_e^F(II) = (E_e^F)_{max}$ and $E_e^F(I) = 0$ we obtain

$$\Delta\mathcal{E} \simeq 0.75\frac{3^{5/3}}{2}\left(\frac{\pi}{4}\right)^{1/3}\frac{1}{\Delta\sqrt{\alpha}}\left(\frac{\pi}{12}\right)^{1/6}N_p^{2/3}m_\pi c^2, \tag{220}$$

which is positive.

The compressional energy of a nuclear matter core of stellar dimensions increases with its electron Fermi energy as expected.

10. – The self-gravitating system of degenerate neutrons, protons and electrons in β-equilibrium

In the earliest description of neutron stars in the work of Oppenheimer and Volkoff in 1939 [18] only a gas of neutrons was considered and the equation of equilibrium was written in the Schwarzschild metric (see sect. **5** for details). They considered the model of a degenerate gas of neutrons to hold from the center to the border, with the density monotonically decreasing away from the center. In the intervening years a more realistic model has been presented challenging the original considerations of [17, 18]. Their TOV equations considered the existence of neutrons all the way to the surface of the star. The

presence of neutrons, protons and electrons in β equilibrium were instead introduced in [45]. Still more important the neutron stars have been shown to be composed of two sharply different components: the core at nuclear and/or supra-nuclear density consisting of neutrons, protons and electrons and a crust of white dwarf like material, namely of degenerate electrons in a nuclei lattice [45, 58]. The pressure and the density of the core are mainly due to the baryons while the pressure of the crust is mainly due to the electrons with the density due to the nuclei and possibly with some free neutrons due to neutron drip (see *e.g.* [58]). Further works describing the nuclear interactions where later introduced (see *e.g.* [59]). Clearly all these considerations departed profoundly from the TOV approximation. The matching between the core component and the crust is the major unsolved problem. To this issue the model studied here introduce some preliminary results in a simplified way which has the advantage to present explicit analytic solutions.

In nearly all the scientific literature on neutron stars, in order to close the system of equations, the condition of local charge neutrality $n_e = n_p$ was adopted without a proof. The considerations of massive neutron density cores presented before offer an alternative to the local charge neutrality condition. In a specific example which can be solved also analytically such condition is substituted by the Thomas-Fermi relativistic equations implying $n_e \neq n_p$ and an overall charge neutral system, $N_e = N_p$. The condition of global charge neutrality as opposed to the local one, leads to the existence of overcritical electric fields at the core surface which may be relevant in the description of neutron stars.

Both the relativistic extension of the FMT treatment and its application to general relativistic white dwarfs and to nuclear matter cores of stellar sizes open the way to a new general relativistic theory of neutron stars. The first steps towards such a theory have been accomplished in [15]. The previous considerations for nuclear matter cores have been made for an isolated massive core at constant proton density whose boundary has been sharply defined by a step function. Both the free case and the compressed one have been duly considered. In [15] the effects of the gravitational field have been considered explicitly in the most simplified nontrivial but rigorous treatment of a general relativistic system of degenerate neutrons, protons and electrons in β-equilibrium.

10˙1. *The impossibility of a solution with local charge neutrality.* – We consider the equilibrium configurations of a degenerate gas of neutrons, protons and electrons with total matter energy density and total matter pressure

$$\mathcal{E} = \sum_{i=n,p,e} \frac{2}{(2\pi\hbar)^3} \int_0^{P_i^F} \epsilon_i(p)\, 4\pi p^2 \mathrm{d}p, \tag{221}$$

$$P = \sum_{i=n,p,e} \frac{1}{3} \frac{2}{(2\pi\hbar)^3} \int_0^{P_i^F} \frac{p^2}{\epsilon_i(p)}\, 4\pi p^2 \mathrm{d}p, \tag{222}$$

where $\epsilon_i(p) = \sqrt{c^2p^2 + m_i^2c^4}$ is the relativistic single particle energy. In addition, we require the condition of β-equilibrium between neutrons, protons and electrons

$$\mu_n = \mu_p + \mu_e, \tag{223}$$

where P_i^F denotes the Fermi momentum and $\mu_i = \partial\mathcal{E}/\partial n_i = \sqrt{c^2(P_i^F)^2 + m_i^2c^4}$ is the free-chemical potential of particle-species with number density $n_i = (P_i^F)^3/(3\pi^2\hbar^3)$.

We now introduce the extension to general relativity of the Thomas-Fermi equilibrium condition on the generalized Fermi energy E_e^F of the electron component

$$E_e^F = \mathrm{e}^{\nu/2}\mu_e - m_e c^2 - eV = \text{const}, \tag{224}$$

where e is the fundamental charge, V is the Coulomb potential of the configuration and we have introduced the metric given by (61) for a spherically symmetric non-rotating neutron star. The metric function λ is related to the mass $M(r)$ and the electric field $E(r) = -\mathrm{e}^{-(\nu+\lambda)/2}V'$ (a prime stands for radial derivative) through

$$\mathrm{e}^{-\lambda} = 1 - \frac{2GM(r)}{c^2 r} + \frac{G}{c^4} r^2 E^2(r). \tag{225}$$

Thus the equations for the neutron star equilibrium configuration consist of the following Einstein-Maxwell equations and general relativistic Thomas-Fermi equation:

$$M' = 4\pi r^2 \frac{\mathcal{E}}{c^2} - \frac{4\pi r^3}{c^2}\mathrm{e}^{-\nu/2}\hat{V}'(n_p - n_e), \tag{226}$$

$$\nu' = \frac{2G}{c^2}\frac{4\pi r^3 P/c^2 + M - r^3 E^2/c^2}{r^2\left(1 - \frac{2GM}{c^2 r} + \frac{Gr^2}{c^4}E^2\right)}, \tag{227}$$

$$P' + \frac{\nu'}{2}(\mathcal{E} + P) = -(P^{\mathrm{em}})' - \frac{4P^{\mathrm{em}}}{r}, \tag{228}$$

$$\hat{V}'' + \hat{V}'\left[\frac{2}{r} - \frac{(\nu' + \lambda')}{2}\right] = - 4\pi\alpha\hbar c\,\mathrm{e}^{\nu/2}\mathrm{e}^{\lambda}\left\{n_p - \frac{[\hat{V}^2 + 2m_e c^2\hat{V} - m_e^2 c^4(\mathrm{e}^{\nu} - 1)]^{3/2}}{3\pi^2\mathrm{e}^{3\nu/2}}\right\}, \tag{229}$$

where α denotes the fine structure constant, $\hat{V} = E_e^F + eV$, $P^{\mathrm{em}} = -E^2/(8\pi)$ and we have used eq. (224) to obtain eq. (229).

It can be demonstrated that the assumption of the equilibrium condition (224) together with the β-equilibrium condition (223) and the hydrostatic equilibrium (228) is enough to guarantee the constancy of the generalized Fermi energy

$$E_i^F = \mathrm{e}^{\nu/2}\mu_i - m_i c^2 + q_i V, \qquad i = n, p, e, \tag{230}$$

for all particle species separately. Here q_i denotes the particle unit charge of the i-species. Indeed, as shown by Olson and Bailyn [23,60], when the fermion nature of the constituents and their degeneracy is taken into account, in the configuration of minimum energy the generalized Fermi energies E_i^F defined by (230) must be constant over the entire configuration. These minimum energy conditions generalize the equilibrium conditions of Klein [21] and of Kodama and Yamada [22] to the case of degenerate multicomponent fluids with particle species with non-zero unit charge.

If one were to assume, as often done in literature, the local charge neutrality condition $n_e(r) = n_p(r)$ instead of assuming the equilibrium condition (224), this would lead to

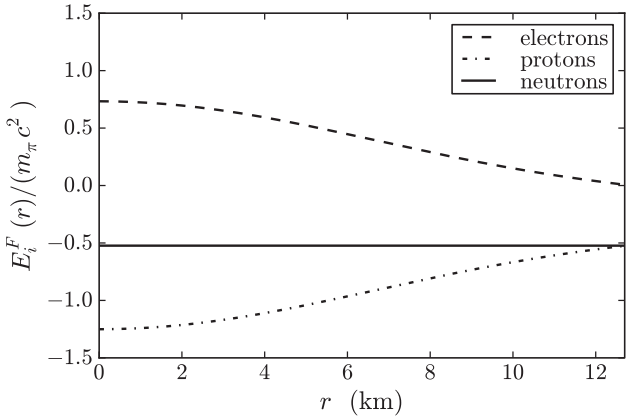

Fig. 24. – Fermi energies for neutrons, protons and electrons in units of the pion rest-energy for a locally neutral configuration with central density $\rho(0) = 3.94\rho_{\rm nuc}$, where $\rho_{\rm nuc} = 2.7\times10^{14}\,{\rm g\,cm^{-3}}$ denotes the nuclear density.

$V = 0$ identically (since there will be no electric fields generated by the neutral matter distribution) implying via eqs. (223) and (228)

$$E_e^F + E_p^F = {\rm e}^{\nu/2}(\mu_e + \mu_p) - (m_e + m_p)c^2 = E_n^F + (m_n - m_e - m_p)c^2 = \text{const.} \tag{231}$$

Thus the neutron Fermi energy would be constant throughout the configuration as well as the sum of the proton and electron Fermi energies but not the individual Fermi energies of each component. In fig. 24 we show the results of the Einstein equations for a selected value of the central density of a system of degenerate neutrons, protons, and electrons in β-equilibrium under the constraint of local charge neutrality. In particular, we have plotted the Fermi energy of the particle species in units of the pion rest-energy. It can be seen that indeed the Fermi energies of the protons and electrons are not constant throughout the configuration which would lead to microscopic instability. This proves the impossibility of having a self-consistent configuration fulfilling the condition of local charge neutrality for our system. This result is complementary to the conclusion of eq. (4.6) of [23] who found that, at zero temperature, only a dust solution with zero particle kinetic energy can satisfy the condition of local charge neutrality and such a configuration is clearly unacceptable for an equilibrium state of a self-gravitating system.

10˙2. *The solution with global charge neutrality.* – We turn now to describe the equilibrium configurations fulfilling only global charge neutrality. We solve self-consistently eqs. (226) and (227) for the metric, eq. (228) for the hydrostatic equilibrium of the three degenerate fermions and, in addition, we impose eq. (223) for the β-equilibrium. The crucial equation relating the proton and the electron distributions is then given by the general relativistic Thomas-Fermi equation (229). The boundary conditions are: for eq. (226) the regularity at the origin: $M(0) = 0$, for eq. (228) a given value of the central density, and for eq. (229) the regularity at the origin $n_e(0) = n_p(0)$, and a second condition at infinity which results in an eigenvalue problem determined by imposing the

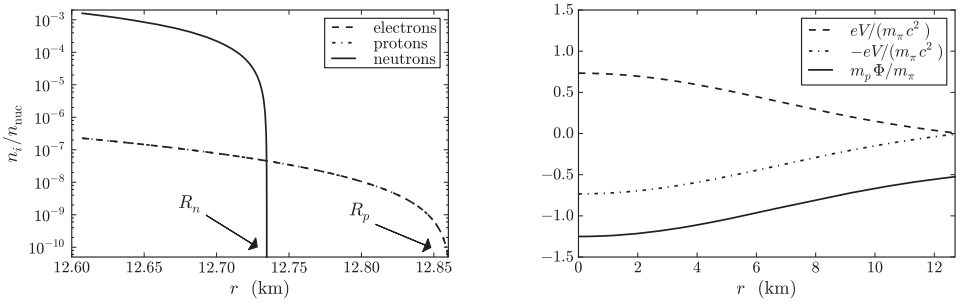

Fig. 25. – Left panel: particle number density of neutrons, protons, and electrons approaching the boundary of the configuration in units of the nuclear density $n_{\rm nuc} \simeq 1.6 \times 10^{38}\,{\rm cm}^{-3}$. Right panel: proton and electron Coulomb potentials in units of the pion rest-energy $eV/(m_\pi c^2)$ and $-eV/(m_\pi c^2)$ respectively and the proton gravitational potential in units of the pion mass $m_p\Phi/m_\pi$ where $\Phi = ({\rm e}^{\nu/2} - 1)$.

global charge neutrality conditions

$$\hat{V}(R_e) = E_e^F, \qquad \hat{V}'(R_e) = 0, \tag{232}$$

at the radius R_e of the electron distribution defined by

$$P_e^F(R_e) = 0, \tag{233}$$

from which there follows:

$$E_e^F = m_e c^2 {\rm e}^{\nu(R_e)/2} - m_e c^2 = m_e c^2 \sqrt{1 - \frac{2GM(R_e)}{c^2 R_e}} - m_e c^2. \tag{234}$$

Then the eigenvalue problem consists in determining the gravitational potential and the Coulomb potential at the center of the configuration that satisfy the conditions (232)–(234) at the boundary.

10˙3. *Numerical integration of the equilibrium equations.* – The solution for the particle densities, the gravitational potential, the Coulomb potential and the electric field are shown in fig. 25 for a configuration with central density $\rho(0) = 3.94\rho_{\rm nuc}$. In order to compare our results with those obtained in the case of nuclear matter cores of stellar dimensions [12] as well as to analyze the gravito-electrodynamical stability of the configuration we have plotted the electric potential in units of the pion rest-energy and the gravitational potential in units of the pion-to-proton mass ratio. One particular interesting new feature is the approach to the boundary of the configuration: three different radii are present corresponding to distinct radii at which the individual particle Fermi pressure vanishes. The radius R_e for the electron component corresponding to $P_e^F(R_e) = 0$, the radius R_p for the proton component corresponding to $P_p^F(R_p) = 0$ and the radius R_n for the neutron component corresponding to $P_n^F(R_n) = 0$.

The smallest radius R_n is due to the threshold energy for β-decay which occurs at a density $\sim 10^7\,{\rm g\,cm}^{-3}$. The radius R_p is larger than R_n because the proton mass is

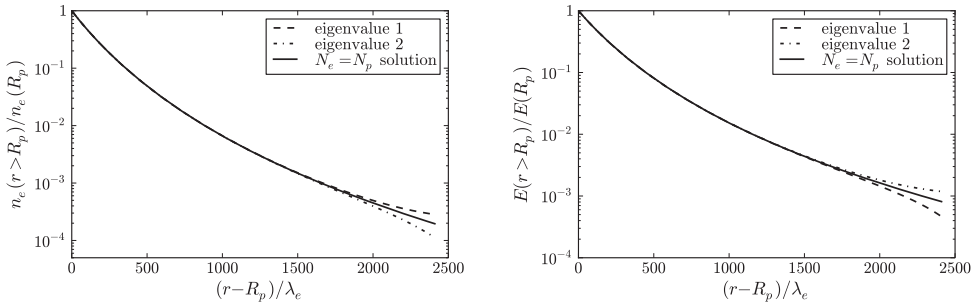

Fig. 26. – Left panel: electron number density for $r \geq R_p$ normalized to its value at $r = R_p$. Right panel: electric field for $r \geq R_p$ normalized to its value at $r = R_p$. We have shown also the behavior of the solution of the general relativistic Thomas-Fermi equation (229) for two different eigenvalues close to the one which gives the globally neutral configuration.

slightly smaller than the neutron mass. Instead, $R_e > R_p$ due to a combined effect of the difference between the proton and electron masses and the implementation of the global charge neutrality condition through the Thomas-Fermi equilibrium conditions.

For the configuration of fig. 25 we found $R_n \simeq 12.735\,\mathrm{km}$, $R_p \simeq 12.863\,\mathrm{km}$ and $R_e \simeq R_p + 10^3\lambda_e$ where $\lambda_e = \hbar/(m_e c)$ denotes the electron Compton wavelength. We find that the electron component follows closely the proton component up to the radius R_p and neutralizes the configuration at R_e without having a net charge (see fig. 26), contrary to the results, *e.g.*, in [60].

It can be seen from fig. 25 that the negative proton gravitational potential energy is indeed always larger than the positive proton electric potential energy. Therefore the configuration is stable against Coulomb repulsion. This confirms the results in the simplified case analyzed by M. Rotondo *et al.* in [12].

From eq. (230) and the relation between Fermi momentum and the particle density $P_i^F = (3\pi^2\hbar^3 n_i)^{1/3}$, we obtain the proton-to-electron and proton-to-neutron ratio for any value of the radial coordinate

$$\frac{n_p(r)}{n_e(r)} = \left[\frac{f^2(r)\mu_e^2(r) - m_p^2c^4}{\mu_e^2(r) - m_e^2c^4}\right]^{3/2}, \quad \frac{n_p(r)}{n_n(r)} = \left[\frac{g^2(r)\mu_n^2(r) - m_p^2c^4}{\mu_n^2(r) - m_n^2c^4}\right]^{3/2}, \tag{235}$$

where $f(r) = (E_p^F + m_pc^2 - eV)/(E_e^F + m_ec^2 + eV)$, $g(r) = (E_p^F + m_pc^2 - eV)/(E_n^F + m_nc^2)$ and the constant values of the generalized Fermi energies are given by

$$E_n^F = m_nc^2\mathrm{e}^{\nu(R_n)/2} - m_nc^2, \tag{236}$$

$$E_p^F = m_pc^2\mathrm{e}^{\nu(R_p)/2} - m_pc^2 + eV(R_p), \tag{237}$$

$$E_e^F = m_ec^2\mathrm{e}^{\nu(R_e)/2} - m_ec^2. \tag{238}$$

A novel situation occurs: the determination of the quantities given in eqs. (235) and (236) necessarily require the prior knowledge of the global electrodynamical and gravitational potential from the center of the configuration all the way out to the boundary defined by the radii R_e, R_p and R_n. This necessity is an outcome of the solution for the eigenfunction of the general relativistic Thomas-Fermi equation (229).

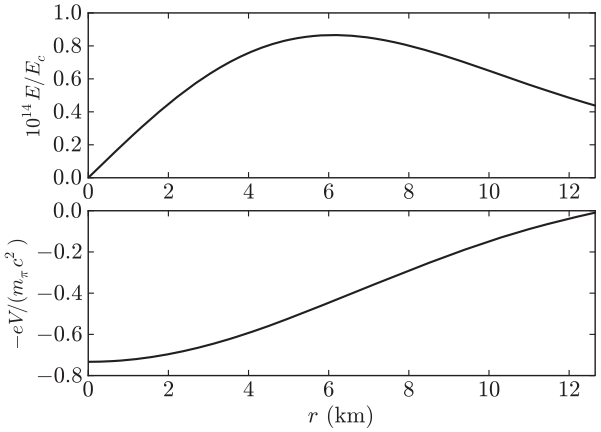

Fig. 27. – Electric field and electron Coulomb potential energy of the configuration of neutrons, protons, and electrons in β-equilibrium studied here and in [15].

From the regularity condition at the center of the star $n_e(0) = n_p(0)$ together with eq. (235) we obtain the Coulomb potential at the center of the configuration

$$eV(0) = \frac{(m_p - m_e)c^2}{2}\left[1 + \frac{E_p^F - E_e^F}{(m_p - m_e)c^2} - \frac{(m_p + m_e)c^2}{E_n^F + m_n c^2}\mathrm{e}^{\nu(0)}\right], \tag{239}$$

which after some algebraic manipulation and defining the central density in units of the nuclear density $\eta = \rho(0)/\rho_{\mathrm{nuc}}$ can be estimated as

$$\begin{aligned} eV(0) &\simeq \frac{1}{2}\left[m_p c^2 \mathrm{e}^{\nu(R_p)/2} - m_e c^2 \mathrm{e}^{\nu(R_e)/2} - \frac{m_n c^2 \mathrm{e}^{\nu(R_n)/2}}{1 + [P_n^F(0)/(m_n c)]^2}\right] \\ &\simeq \frac{1}{2}\left[\frac{(3\pi^2\eta/2)^{2/3} m_p}{(3\pi^2\eta/2)^{2/3} m_\pi + m_n^2/m_\pi}\right] m_\pi c^2, \end{aligned} \tag{240}$$

where we have approximated the gravitational potential at the boundary as $\mathrm{e}^{\nu(R_e)/2} \simeq \mathrm{e}^{\nu(R_p)/2} \simeq \mathrm{e}^{\nu(R_n)/2} \simeq 1$. Then for configurations with central densities larger than the nuclear density we necessarily have $eV(0) \gtrsim 0.35 m_\pi c^2$. In particular, for the configuration we have exemplified with $\eta = 3.94$ in fig. 25, from the above expression (240) we obtain $eV(0) \simeq 0.85 m_\pi c^2$. This value of the central potential agrees with the one obtained in the simplified case of nuclear matter cores with constant proton density [12].

It can be seen from fig. 25 that the depth of the Coulomb potential is of the order of $\lesssim m_\pi c^2$. In fig. 27 we have plotted the Coulomb potential and the corresponding electric field of the configuration studied here. A Coulomb potential $\sim m_\pi c^2/e$ decreasing in a typical macroscopic neutron star radius $R \sim \lambda_\pi (m_{\mathrm{Planck}}/m_p)$ creates an electric field $\sim (m_p/m_{\mathrm{Planck}})(m_\pi/m_e)^2 E_c \sim 10^{-14} E_c$, being $E_c = m_e^2 c^3/(e\hbar)$ the critical electric field for vacuum polarization.

11. – Newtonian limit

Despite the fact that the strong gravitational field of neutron stars requires a general relativistic treatment, it is interesting to explore the Newtonian limit of all the above considerations. This can help to elucidate if the gravito-electromagnetic effects we have found are of general relativistic nature or to prove their validity in a Newtonian regime.

The Newtonian limit of the equilibrium equations can be obtained by the weak-field non-relativistic limit. We expand the gravitational potential at first-order $e^{\nu/2} \approx 1 + \Phi/c^2$, where Φ is the Newtonian gravitational potential. In the non-relativistic mechanics limit $c \to \infty$, the particle chemical potential becomes $\mu_i \to \tilde{\mu}_i + m_i c^2$, where $\tilde{\mu}_i = (P_i^F)^2/(2m_i)$ denotes the non-relativistic free-chemical potential. Applying these considerations, the electron and proton equilibrium law (224) becomes

$$E_p^{F,\mathrm{Newt}} = \tilde{\mu}_p + m_p\Phi + eV = \mathrm{const}, \tag{241}$$

$$E_e^{F,\mathrm{Newt}} = \tilde{\mu}_e + m_e\Phi - eV = \mathrm{const}, \tag{242}$$

which is the classical condition of thermodynamic equilibrium of a fluid of charged particles in presence of external gravitational an electrostatic fields.

The condition of β-equilibrium is, in this case, given by

$$E_n^{F,\mathrm{Newt}} = E_p^{F,\mathrm{Newt}} + E_e^{F,\mathrm{Newt}}, \tag{243}$$

which links the constants $E_p^{F,\mathrm{Newt}}$ and $E_e^{F,\mathrm{Newt}}$ to the constant neutron Fermi energy $E_n^{F,\mathrm{Newt}}$.

From the constancy of the proton and electron Fermi energies it follows the relation

$$\tilde{\mu}_p - \tilde{\mu}_e + (m_p - m_e)\Phi + 2eV = \mathrm{constant}, \tag{244}$$

which in the case of an ideal electron-ion gas becomes the Rosseland relation of equilibrium (see eq. (7) in [24]). It is interesting to obtain from the above equation an estimate of the Coulomb potential well inside the configuration. Evaluating eq. (244) at the radius of the configuration where the particle free chemical potentials go to zero, we obtain an estimate of the ratio of the Coulomb potential energy and the gravitational energy close to the surface of the configuration

$$\frac{eV(R)}{\Phi(R)} \sim -\frac{m_p - m_e}{2}\,. \tag{245}$$

Assuming that the system is at nuclear density, $\rho \sim m_p/\lambda_\pi^3$ where $\lambda_\pi = \hbar/(m_\pi c)$ is the pion Compton wavelength, the mass and the radius of the configuration are roughly given by $M \sim m_{\mathrm{Planck}}^3/m_p^2$ and $R \sim \lambda_\pi(m_{\mathrm{Planck}}/m_p)$ and therefore the gravitational potential will be $\Phi(R) = -GM/R \sim (m_\pi/m_p)c^2$. Consequently, the Coulomb potential energy close to the border is approximately $eV(R) \sim m_\pi c^2/2$. Assuming a constant charge density approximation, the Coulomb potential energy at the center of the configuration is 3/2 times its value at the surface, thus we obtain approximately

$$eV(0) \sim \frac{3}{4} m_\pi c^2, \tag{246}$$

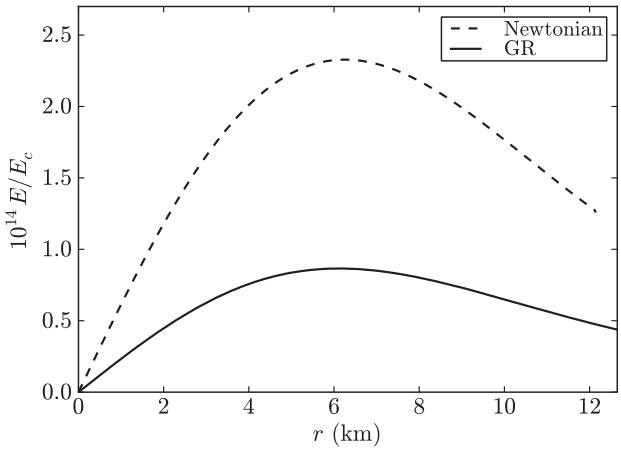

Fig. 28. – Electric field (multiplied by 10^{14}) in units of the critical field $E_c = m_e^2c^3/(e\hbar) \sim 10^{16}$ Volt/cm in the region $r < R_n$ both for the Newtonian and the general relativistic configurations. The central density of both systems is $\rho(0) = 3.94\rho_{\rm nuc}$ where $\rho_{\rm nuc} = 2.7 \times 10^{14}\,{\rm g\,cm^{-3}}$ is the nuclear density.

which is in full agreement with both with the numerical results and with the general relativistic formulas given by eqs. (21) and (22) of [15]. This numerical value is also in line with the Coulomb potential well obtained from the idealized treatment presented in [10-12].

In the weak-field non-relativistic limit, the Einstein-Maxwell equations (226)–(229) become

$$M' = 4\pi r^2 \rho(r), \tag{247}$$

$$\Phi' = \frac{GM}{r^2}\,, \tag{248}$$

$$P' = -\frac{GM}{r^2}\rho - \left[n_p - \frac{(2m_e)^{3/2}}{3\pi^2\hbar^3}(\hat{V} - m_e\Phi)^{3/2}\right]\hat{V}', \tag{249}$$

$$\hat{V}'' + \frac{2}{r}\hat{V}' = -4\pi e^2\left[n_p - \frac{(2m_e)^{3/2}}{3\pi^2\hbar^3}(\hat{V} - m_e\Phi)^{3/2}\right], \tag{250}$$

where ρ in this case is the rest-mass density

$$\rho = \sum_{i=n,p,e} m_i n_i. \tag{251}$$

The solution of eqs. (241), (247)–(250) together with the β-equilibrium condition (243) leads to qualitatively similar electrodynamical properties as the one obtained in the general relativistic case. In fig. 28 we show the electric field in the region $r < R_n$ ($R_n^{\rm Newt} < R_n^{\rm GR}$) both for the Newtonian as well as for the General Relativistic configuration for the given central density $\rho(0) = 3.94\rho_{\rm nuc}$. From the quantitative point of view, the

electric field of the Newtonian configuration is larger than the electric field of the general relativistic configuration.

12. – Introducing the strong interactions

It is clear now that if one considers a fluid of only neutrons, protons, and electrons in β equilibrium neglecting the effects of strong interactions and the presence of a crust, then the electromagnetic structure is the one shown in figs. 27 and 28. The effect of having different radii R_n, R_p, and R_e needs to be also studied in the more general case when strong interactions and the presence of the crust of the neutron star are included. The complete study of such a problem must to be necessarily done within a fully relativistic approach taking into account the strong, weak, electromagnetic, and gravitational interactions. Indeed, an essential step forward in this direction has been given in [16] by formulating such a treatment.

Since neutron stars cores may reach densities of order $\sim 10^{16}$–$10^{17}\,\mathrm{g/cm^3}$, much larger than the nuclear density $\rho_{\mathrm{nuc}} \sim 2.7 \times 10^{14}\,\mathrm{g/cm^3}$, approaches for nuclear interactions based on phenomenological potentials and non-relativistic many-body theories become inapplicable (see [61, 62], for instance). Based on the pioneering work of Johnson and Teller [63], Duerr [64] and later on Miller and Green [65] formulated the basis of what is now known as Relativistic Mean-Field Theory of nuclear matter. They constructed the simplest relativistic model that accounts for the binding of symmetric nuclear matter at saturation density by introducing the interaction of one scalar field and one vector field with nucleons through Yukawa couplings. A nuclear model with only the scalar field with a self-interacting potential up to quartic order based on the sigma-model was considered in [66, 67]. The repulsive contribution of nuclear force was there introduced by hand through a *hard-sphere* model that artificially increases the nucleon Fermi momentum emulating the effect of a massive vector field coupled to nucleons. The relevance of such interactions as well as relativistic effects in the determination of the equation of state and in the nuclear matter properties such as compressibility and the nucleon effective mass was clearly pointed out in [65, 68, 69]. The importance of allowing scalar meson self-interactions (cubic and quartic terms in the scalar field potential) as adjustable parameters to reproduce physical nuclear properties and not due to renormalization (see *e.g.* [70]) was stressed in [69, 71-73]. The necessity of introducing additional isovector fields to match the empirical symmetry energy of nuclear matter at saturation density was recognized in [69].

Assuming that the nucleons interact with σ, ω and ρ meson fields through Yukawa-like couplings and assuming flat spacetime the equation of state of nuclear matter can be determined. However, it has been clearly stated in [15, 16] that, when we turn into a neutron star configuration at nuclear and supranuclear densities, the global description of the Einstein-Maxwell-Thomas-Fermi equations is mandatory. Associated to this system of equations there is a sophisticated eigenvalue problem, especially the one for the general relativistic Thomas-Fermi equation is necessary in order to fulfill the global charge neutrality of the system and to consistently describe the confinement of the ultrarelativistic electrons.

We here adopt the phenomenological relativistic mean field nuclear model of Boguta and Bodmer [69] by assuming nucleons interacting in minimal coupling approximation with a σ isoscalar meson field that provides the attractive long-range part of the nuclear force and a massive vector field ω that models the repulsive short range. The self-interacting scalar field potential $U(\sigma)$ is assumed as a quartic polynom with adjustable

coefficients. In addition, a massive isovector field ρ is introduced to accounts for surface as well as isospin effects of nuclei.

The total Lagrangian density of the system is given by

$$\mathcal{L} = \mathcal{L}_g + \mathcal{L}_f + \mathcal{L}_\sigma + \mathcal{L}_\omega + \mathcal{L}_\rho + \mathcal{L}_\gamma + \mathcal{L}_{\rm int}, \tag{252}$$

where the Lagrangian densities for the free-fields are

$$\mathcal{L}_g = -\frac{R}{16\pi G}, \tag{253}$$

$$\mathcal{L}_\gamma = -\frac{1}{16\pi} F_{\mu\nu} F^{\mu\nu}, \tag{254}$$

$$\mathcal{L}_\sigma = \frac{1}{2} \nabla_\mu \sigma \nabla^\mu \sigma - U(\sigma), \tag{255}$$

$$\mathcal{L}_\omega = -\frac{1}{4} \Omega_{\mu\nu} \Omega^{\mu\nu} + \frac{1}{2} m_\omega^2 \omega_\mu \omega^\mu, \tag{256}$$

$$\mathcal{L}_\rho = -\frac{1}{4} \mathcal{R}_{\mu\nu} \mathcal{R}^{\mu\nu} + \frac{1}{2} m_\rho^2 \rho_\mu \rho^\mu, \tag{257}$$

where $\Omega_{\mu\nu} \equiv \partial_\mu \omega_\nu - \partial_\nu \omega_\mu$, $\mathcal{R}_{\mu\nu} \equiv \partial_\mu \rho_\nu - \partial_\nu \rho_\mu$, $F_{\mu\nu} \equiv \partial_\mu A_\nu - \partial_\nu A_\mu$ are the field strength tensors for the ω^μ, ρ and A^μ fields respectively, ∇_μ stands for covariant derivative and R is the Ricci scalar. We adopt the Lorenz gauge for the fields A_μ, ω_μ, and ρ_μ.

The Lagrangian density for the three fermion species is

$$\mathcal{L}_f = \sum_{i=e,N} \bar{\psi}_i \left(i\gamma^\mu D_\mu - m_i \right) \psi_i, \tag{258}$$

where ψ_N is the nucleon isospin doublet, ψ_e is the electronic singlet, m_i states for the mass of each particle species and $D_\mu = \partial_\mu + \Gamma_\mu$, being Γ_μ the Dirac spin connections.

The interacting part of the Lagrangian density is, in the minimal coupling assumption, given by

$$\mathcal{L}_{\rm int} = -g_\sigma \sigma \bar{\psi}_N \psi_N - g_\omega \omega_\mu J_\omega^\mu - g_\rho \rho_\mu J_\rho^\mu + e A_\mu J_{\gamma,e}^\mu - e A_\mu J_{\gamma,N}^\mu, \tag{259}$$

where the conserved currents are

$$J_\omega^\mu = \bar{\psi}_N \gamma^\mu \psi_N, \tag{260}$$

$$J_\rho^\mu = \bar{\psi}_N \tau_3 \gamma^\mu \psi_N, \tag{261}$$

$$J_{\gamma,e}^\mu = \bar{\psi}_e \gamma^\mu \psi_e, \tag{262}$$

$$J_{\gamma,N}^\mu = \bar{\psi}_N \left(\frac{1+\tau_3}{2} \right) \gamma^\mu \psi_N. \tag{263}$$

The coupling constants of the σ, ω and ρ-fields are g_σ, g_ω and g_ρ, and e is the fundamental electric charge. The Dirac matrices γ^μ and the isospin Pauli matrices satisfy

the Dirac algebra in curved spacetime (see, *e.g.*, [3, 74] for details)

$$\{\gamma^\mu, \gamma^\nu\} = 2g^{\mu\nu}, \tag{264}$$

$$\{\gamma_\mu, \gamma_\nu\} = 2g_{\mu\nu}, \tag{265}$$

$$\{\gamma^\mu, \gamma_\nu\} = 2\delta^\mu_\nu, \tag{266}$$

$$[\tau_i, \tau_j] = 2\imath\epsilon_{ijk}\tau^k. \tag{267}$$

The equations of the motion of the above Lagrangians lead to the Einstein-Maxwell-Dirac system of equations

$$G_{\mu\nu} + 8\pi G T_{\mu\nu} = 0, \tag{268}$$

$$\nabla_\mu F^{\mu\nu} - eJ^\nu_{ch} = 0, \tag{269}$$

$$\nabla_\mu \Omega^{\mu\nu} + m^2_\omega \omega^\nu - g_\omega J^\nu_\omega = 0, \tag{270}$$

$$\nabla_\mu \mathcal{R}^{\mu\nu} + m^2_\rho \rho^\nu - g_\rho J^\nu_\rho = 0, \tag{271}$$

$$\nabla_\mu \nabla^\mu \sigma + \partial_\sigma U(\sigma) + g_s n_s = 0, \tag{272}$$

$$\left[\gamma_\mu \left(iD^\mu - V^\mu_N\right) - \tilde{m}_N\right] \psi_N = 0, \tag{273}$$

$$\left[\gamma_\mu \left(iD^\mu + eA^\mu\right) - m_e\right] \psi_e = 0, \tag{274}$$

where the scalar density $n_s = \bar{\psi}_N \psi_N$, the nucleon effective mass $\tilde{m}_N \equiv m_N + g_\sigma \sigma$, and

$$V^\mu_N \equiv g_\omega \omega^\mu + g_\rho \tau \rho^\mu + e\left(\frac{1+\tau_3}{2}\right) A^\mu, \tag{275}$$

is the effective four potential of nucleons. The energy-momentum tensor of free-fields and free-fermions $T^{\mu\nu}$ of the system (254)–(257) is

$$T^{\mu\nu} = T^{\mu\nu}_f + T^{\mu\nu}_\gamma + T^{\mu\nu}_\sigma + T^{\mu\nu}_\omega + T^{\mu\nu}_\rho, \tag{276}$$

where

$$T^{\mu\nu}_\gamma = F^\mu{}_\alpha F^{\alpha\nu} + \frac{1}{4} g^{\mu\nu} F_{\alpha\beta} F^{\alpha\beta}, \tag{277}$$

$$T^{\mu\nu}_\sigma = \nabla^\mu \sigma \nabla^\nu \sigma - g^{\mu\nu}\left[\frac{1}{2}\nabla_\sigma \sigma \nabla^\sigma \sigma - U(\sigma)\right], \tag{278}$$

$$T^{\mu\nu}_\omega = \Omega^\mu{}_\alpha \Omega^{\alpha\nu} + \frac{1}{4} g^{\mu\nu} \Omega_{\alpha\beta}\Omega^{\alpha\beta} + m^2_\omega \left(\omega^\mu \omega^\nu - \frac{1}{2} g^{\mu\nu} \omega_\alpha \omega^\alpha\right), \tag{279}$$

$$T^{\mu\nu}_\rho = \mathcal{R}^\mu{}_\alpha \mathcal{R}^{\alpha\nu} + \frac{1}{4} g^{\mu\nu} \mathcal{R}_{\alpha\beta}\mathcal{R}^{\alpha\beta} + m^2_\rho \left(\mathcal{R}^\mu \mathcal{R}^\nu - \frac{1}{2} g^{\mu\nu} \mathcal{R}_\alpha \omega^\alpha\right), \tag{280}$$

are the contribution of free-fields and $T^{\mu\nu}_f$ is the contribution of free-fermions which we discuss below.

12˙1. *The thermodynamic laws and the field equations in the spherically symmetric case*. – We first introduce the non-rotating spherically symmetric spacetime metric

$$ds^2 = \mathrm{e}^{\nu(r)}dt^2 - \mathrm{e}^{\lambda(r)}dr^2 - r^2 d\theta^2 - r^2\sin^2\theta d\varphi^2, \tag{281}$$

where the $\nu(r)$ and $\lambda(r)$ are only functions of the radial coordinate r.

For very large number of fermions, we can adopt the mean-field approximation in which fermion-field operators are replaced by their expectation values (see *e.g.* [3] for details).

We write the nucleon doublet and the electronic spinor as $\psi_i = \psi_i(k)\mathrm{e}^{-ik_\mu x^\mu}$ in the phase-space. Suppose that neutrons, protons and electrons, and the corresponding antiparticles, are in thermodynamic equilibrium with a finite temperature T. The occupation fermion-number operators of the "k"-state, $\mathcal{N}_i(k) = \psi_i^\dagger(k)\psi_i(k)$ with $i = e, p, n$, are replaced by their Fermi-distributions

$$f_i^\pm(k) = \langle\psi_i^\pm(k)^\dagger\psi_i^\pm(k)\rangle = \left[\exp\left(\frac{\epsilon_i(k)\mp\mu_i}{k_B T}\right) + 1\right]^{-1}, \tag{282}$$

where k_B is the Boltzmann constant, μ_i and $\epsilon_i(k) = \sqrt{k^2 + \tilde{m}_i^2}$ denote the single-particle chemical potential and energy-spectrum (we recall that for electrons $\tilde{m}_e = m_e$). The sign "+" correspond to particles and "−" to antiparticles. We do not consider "real" bosons to be present in the system; the only distribution functions involved in the computation are due to fermions and antifermions and therefore phenomena as Bose-Einstein condensation does not occur within this theory (see, *e.g.*, [61] for details).

It is worth to recall that all the thermodynamic quantities, *e.g.*, $k, \epsilon, T\ldots$, are written here in the local frame which is related to the coordinate frame by the Lorentz "boost"

$$\Lambda_\alpha^{(a)} = (u_\alpha, \chi_\alpha, \Theta_\alpha, \Phi_\alpha), \tag{283}$$

where $u_\alpha = e^{\nu/2}\delta_\alpha^0$, $\chi_\alpha = e^{\lambda/2}\delta_\alpha^1$, $\Theta_\alpha = r\delta_\alpha^2$, and $\Phi_\alpha = r\sin\theta\delta_\alpha^3$, being δ_β^α the usual Kronecker delta symbol.

The number-density n_i of the i-specie, taking into account the antiparticle contribution is, within the mean-field approximation, given by

$$n_i = \frac{2}{(2\pi)^3}\int \mathrm{d}^3k[f_i^+(k) - f_i^-(k)]. \tag{284}$$

The contribution of free-fermions and antifermions to the energy-momentum tensor can be then written in the perfect fluid form (see, *e.g.*, [3])

$$T_f^{\mu\nu} = (\mathcal{E} + \mathcal{P})u^\mu u^\nu - \mathcal{P}g^{\mu\nu}, \tag{285}$$

where u^μ is the four-velocity of the fluid which satisfies $u^\mu u_\mu = 1$, and the energy-density $\mathcal{E}$ and the pressure $\mathcal{P}$ are given by

$$\mathcal{E} = \sum_{i=n,p,e}\mathcal{E}_i, \qquad \mathcal{P} = \sum_{i=n,p,e}\mathcal{P}_i, \tag{286}$$

being $\mathcal{E}_i$ and $\mathcal{P}_i$ the single fermion-antifermion fluid contributions

$$\mathcal{E}_i = \frac{2}{(2\pi)^3}\int \mathrm{d}^3k\epsilon_i(k)[f_i^+(k)+f_i^-(k)], \tag{287}$$

$$\mathcal{P}_i = \frac{1}{3}\frac{2}{(2\pi)^3}\int \mathrm{d}^3k\frac{k^2}{\epsilon_i(k)}[f_i^+(k)+f_i^-(k)]. \tag{288}$$

The equation of state (286)–(288) satisfies the thermodynamic law

$$\mathcal{E}+\mathcal{P}-T\mathcal{S} = \sum_{i=n,p,e} n_i\mu_i, \tag{289}$$

where $\mathcal{S}=S/V$ is the entropy per unit volume (entropy density) and $\mu_i = \partial\mathcal{E}/\partial n_i$ is the free-chemical potential of the i-species. At zero-temperature $T=0$, $\mu_i = \sqrt{(P_i^F)^2+\tilde{m}_i^2}$ and $n_i = (P_i^F)^3/(3\pi^2)$, where P_i^F denotes the Fermi momentum of the i-species.

The scalar density n_s, within the mean-field approximation, is given by the following expectation value:

$$n_s = \langle\bar{\psi}_N\psi_N\rangle = \frac{2}{(2\pi)^3}\sum_{i=n,p}\int \mathrm{d}^3k\frac{\tilde{m}_N}{\epsilon_i(k)}[f_i^+(k)+f_i^-(k)]. \tag{290}$$

In the static case, only the temporal components of the covariant currents survive, *i.e.* $\langle\bar{\psi}(x)\gamma^i\psi(x)\rangle = 0$. Thus, by taking the expectation values of eqs. (260)–(263), we obtain the non-vanishing components of the currents

$$J_0^{ch} = n_{ch}u_0 = (n_p-n_e)u_0, \tag{291}$$

$$J_0^{\omega} = n_b u_0 = (n_n+n_p)u_0, \tag{292}$$

$$J_0^{\rho} = n_3 u_0 = (n_p-n_n)u_0, \tag{293}$$

where n_b, n_p, n_n and n_e are the baryon, proton, neutron and electron number densities which are functions only of the spatial coordinates, and $u_0 = \sqrt{g_{00}} = e^{\nu/2}$.

Making a variation of eq. (289) and using eqs. (286)–(288) and (290), we obtain the generalized Gibbs-Duhem relation

$$\mathrm{d}\mathcal{P} = \sum_{i=n,p,e} n_i\mathrm{d}\mu_i - g_\sigma n_s\mathrm{d}\sigma + \mathcal{S}\mathrm{d}T, \tag{294}$$

which can be rewritten as

$$\mathrm{d}\mathcal{P} = \sum_{i=n,p,e} n_i\mathrm{d}\mu_i - g_\sigma n_s\mathrm{d}\sigma + \left(\mathcal{E}+\mathcal{P}-\sum_{i=n,p,e} n_i\mu_i\right)\frac{\mathrm{d}T}{T}, \tag{295}$$

where we have used eq. (289) to eliminate $\mathcal{S}$, and we have used the relation between the scalar density and the fluid energy-density

$$n_s = \langle \bar{\psi}_N \psi_N \rangle = \frac{2}{(2\pi)^3} \sum_{i=n,p} \int \mathrm{d}^3 k \frac{\tilde{m}_N}{\epsilon_i(p)} = \frac{\partial \mathcal{E}}{\partial \tilde{m}_N}\,, \tag{296}$$

which follows from eqs. (286)–(288) and (290).

Therefore, the Einstein-Maxwell equations (268)–(272), within the mean-field approximation, become

$$\mathrm{e}^{-\lambda(r)} \left(\frac{1}{r^2} - \frac{\lambda'}{r} \right) - \frac{1}{r^2} = -8\pi G T_0^0, \tag{297}$$

$$\mathrm{e}^{-\lambda(r)} \left(\frac{1}{r^2} + \frac{1}{r} \frac{\mathrm{d}\nu}{\mathrm{d}r} \right) - \frac{1}{r^2} = -8\pi G T_1^1, \tag{298}$$

$$\mathrm{e}^{-\lambda(r)} \left[\frac{1}{2} \left(\frac{\mathrm{d}\nu}{\mathrm{d}r} - \frac{\mathrm{d}\lambda}{\mathrm{d}r} \right) \left(\frac{1}{r} + \frac{1}{2} \frac{\mathrm{d}\nu}{\mathrm{d}r} \right) + \frac{1}{2} \frac{\mathrm{d}^2\nu}{\mathrm{d}r^2} \right] = -8\pi G T_3^3, \tag{299}$$

$$\frac{\mathrm{d}^2 V}{\mathrm{d}r^2} + \frac{\mathrm{d}V}{\mathrm{d}r} \left[\frac{2}{r} - \frac{1}{2} \left(\frac{\mathrm{d}\nu}{\mathrm{d}r} + \frac{\mathrm{d}\lambda}{\mathrm{d}r} \right) \right] = -\mathrm{e}^{\lambda} e J_0^{ch}, \tag{300}$$

$$\frac{\mathrm{d}^2 \sigma}{\mathrm{d}r^2} + \frac{\mathrm{d}\sigma}{\mathrm{d}r} \left[\frac{2}{r} + \frac{1}{2} \left(\frac{\mathrm{d}\nu}{\mathrm{d}r} - \frac{\mathrm{d}\lambda}{\mathrm{d}r} \right) \right] = \mathrm{e}^{\lambda} \left[\partial_\sigma U(\sigma) + g_s n_s \right], \tag{301}$$

$$\frac{\mathrm{d}^2 \omega}{\mathrm{d}r^2} + \frac{\mathrm{d}\omega}{\mathrm{d}r} \left[\frac{2}{r} - \frac{1}{2} \left(\frac{\mathrm{d}\nu}{\mathrm{d}r} + \frac{\mathrm{d}\lambda}{\mathrm{d}r} \right) \right] = -\mathrm{e}^{\lambda} \left[g_\omega J_0^\omega - m_\omega^2 \omega \right], \tag{302}$$

$$\frac{\mathrm{d}^2 \rho}{\mathrm{d}r^2} + \frac{\mathrm{d}\rho}{\mathrm{d}r} \left[\frac{2}{r} - \frac{1}{2} \left(\frac{\mathrm{d}\nu}{\mathrm{d}r} + \frac{\mathrm{d}\lambda}{\mathrm{d}r} \right) \right] = -\mathrm{e}^{\lambda} \left[g_\rho J_0^\rho - m_\rho^2 \rho \right], \tag{303}$$

where we have introduced the notation $\omega_0 = \omega$, $\rho_0 = \rho$, and $A_0 = V$. The metric function λ is related to the mass $M(r)$ and the electric field $E(r) = -\mathrm{e}^{-(\nu+\lambda)/2} V'$ through

$$\mathrm{e}^{-\lambda(r)} = 1 - \frac{2GM(r)}{r} + Gr^2 E^2(r) = 1 - \frac{2GM(r)}{r} + \frac{GQ^2(r)}{r^2}\,, \tag{304}$$

where we have introduced also the conserved charge $Q(r) = r^2 E(r)$.

An important equation, although not independent of the Einstein-Maxwell equations (297)–(303), is given the energy-momentum conservation law

$$\nabla_\mu T^{\mu\nu} = g_\omega J_\mu^\omega \Omega^{\mu\nu} + g_\rho J_\mu^\rho \mathcal{R}^{\mu\nu} + e J_\mu^{ch} F^{\mu\nu}, \tag{305}$$

from which we have

$$\frac{\mathrm{d}\mathcal{P}}{\mathrm{d}r} = -\frac{(\mathcal{E}+\mathcal{P})}{2} \frac{\mathrm{d}\nu}{\mathrm{d}r} - g_\sigma n_s \frac{\mathrm{d}\sigma}{\mathrm{d}r} - g_\omega J_\omega^0 \frac{\mathrm{d}\omega}{\mathrm{d}r} - g_\rho J_\rho^0 \frac{\mathrm{d}\rho}{\mathrm{d}r} - e J_{ch}^0 \frac{\mathrm{d}V}{\mathrm{d}r}\,, \tag{306}$$

where we have used the energy-momentum tensor $T^{\mu\nu}$ given by eq. (276).

12˙2. *Constancy of the Klein potentials and β-equilibrium.* – Introducing the nucleon doublet and the electronic spinor in the waveform $\psi_i = \psi_i(k)\mathrm{e}^{-ik_\mu x^\mu}$ in phase-space, the Dirac equations (274) become

$$(\gamma_\mu \mathcal{K}_i^\mu - \tilde{m}_i)\psi_i(k) = 0, \tag{307}$$

where

$$\mathcal{K}_i^\mu \equiv k^\mu - V_i^\mu, \quad V_e^\mu = -eA^\mu. \tag{308}$$

In the mean-field approximation, making the quadrature of Dirac operators in eq. (307) and averaging over all states "k", we obtain the generalized chemical potentials or, for short Klein potentials for electrons E_e, neutrons E_n and protons E_p

$$E_e = \sqrt{g_{00}}\mu_e - eV = \mathrm{e}^{\nu/2}\mu_e - eV, \tag{309}$$

$$E_p = \sqrt{g_{00}}\mu_p + g_\omega\omega + g_\rho\rho + eV = \mathrm{e}^{\nu/2}\mu_p + g_\omega\omega + g_\rho\rho + eV, \tag{310}$$

$$E_n = \sqrt{g_{00}}\mu_n + g_\omega\omega - g_\rho\rho = \mathrm{e}^{\nu/2}\mu_n + g_\omega\omega - g_\rho\rho, \tag{311}$$

where we have used eqs. (264)–(267) and eqs. (282), (284), (286)–(288). In the zero-temperature case, they are generalized Fermi energies for electrons $E_e = E_e^F$, neutrons $E_n = E_n^F$ and protons $E_p = E_p^F$.

Using the equations of motion for the fields ρ, ω and σ, and using the generalized Gibbs-Duhem relation (295), the energy-momentum conservation equation (306) can be rewritten as

$$\mathrm{e}^{\nu/2}\sum_{i=n,p,e} n_i\left(\mathrm{d}\mu_i - \frac{\mathrm{d}T}{T}\mu_i\right) + (\mathcal{E}+\mathcal{P})\mathrm{e}^{\nu/2}\left(\frac{\mathrm{d}T}{T} + \frac{1}{2}\mathrm{d}\nu\right) + g_\omega n_b \mathrm{d}\omega + g_\rho n_3 \mathrm{d}\rho + e n_{ch}\mathrm{d}V = 0. \tag{312}$$

The isothermal Tolman condition [39] (see also [21]) demands the constancy of the gravitationally red-shifted temperature

$$\frac{\mathrm{d}T}{T} + \frac{1}{2}\mathrm{d}\nu = 0, \qquad \text{or} \qquad \mathrm{e}^{\nu/2}T = \text{const.} \tag{313}$$

Such a condition can be used into eq. (312) to obtain

$$\sum_{i=n,p,e} n_i \mathrm{d}(\mathrm{e}^{\nu/2}\mu_i) + g_\omega n_b \mathrm{d}\omega + g_\rho n_3 \mathrm{d}\rho + e n_{ch}\mathrm{d}V = 0. \tag{314}$$

Moreover, using the expressions (309)–(310) of the generalized chemical potentials, eq. (314) can be rewritten as

$$\sum_{i=n,p,e} n_i \mathrm{d}E_i = 0, \tag{315}$$

which leads for independent and non-zero particle number densities $n_i \neq 0$ to the constancy of the Klein potentials (309)–(311) for each particle species, *i.e.*

$$E_e = \mathrm{e}^{\nu/2}\mu_e - eV = \text{const}, \tag{316}$$

$$E_p = \mathrm{e}^{\nu/2}\mu_p + \mathcal{V}_p = \text{const}, \tag{317}$$

$$E_n = \mathrm{e}^{\nu/2}\mu_n + \mathcal{V}_n = \text{const}, \tag{318}$$

where

$$\mathcal{V}_p = g_\omega\omega + g_\rho\rho + eV, \tag{319}$$

$$\mathcal{V}_n = g_\omega\omega - g_\rho\rho. \tag{320}$$

In the case of nuclear matter in β-equilibrium (assuming not trapped neutrinos), the values of the constant Klein potentials (316)–(318) are linked by the condition (see *e.g.* [75])

$$E_n = E_p + E_e. \tag{321}$$

We have presented the self-consistent equations of equilibrium at finite temperatures for a system of neutrons, protons and electrons in β-equilibrium within the framework of general relativity including quantum statistics, electro-weak, and strong interactions. In the mean-field approximation, we obtained the generalized particle chemical potentials from the Dirac equations for nucleons and electrons.

From the Einstein-Maxwell equations, the thermodynamic laws and energy-momentum conservation, we obtain the constancy of the Klein potential of each particle-specie and of the gravitationally red-shifted temperature throughout the configuration, *i.e.* the first Klein integrals and the Tolman isothermal condition respectively. In the non-interacting degenerate case, following a minimization energy procedure, it was demonstrated that the thermodynamic equilibrium condition of constancy of the generalized particle Fermi energy of all particle species holds (see E. Olson and M. Bailyn [23]). Such a procedure can be straightforwardly applied to the present case, being the final result given by the equilibrium conditions (316) and (317).

The precise values of such constants are linked, in the case of nuclear matter in β-equilibrium, by eq. (321), and their full determination needs the inclusion of additional constraints to the system, *e.g.* global charge neutrality (see *e.g.* [15]).

The correct implementation of such generalized Thomas-Fermi equilibrium conditions needs the self-consistent solution of the global problem of equilibrium of the configuration following from the solution of the Einstein-Maxwell equations (297), (298), (300)–(304), the general relativistic thermodynamic equilibrium conditions (313), (316) and (317), together with the constraints, *e.g.* β-equilibrium and global charge neutrality.

Thus, the full system of Einstein-Maxwell-Thomas-Fermi equations can be rewritten in the form

$$\mathrm{e}^{-\lambda(r)}\left(\frac{1}{r^2} - \frac{1}{r}\frac{\mathrm{d}\lambda}{\mathrm{d}r}\right) - \frac{1}{r^2} = -8\pi G T_0^0, \tag{322}$$

$$\mathrm{e}^{-\lambda(r)}\left(\frac{1}{r^2} + \frac{1}{r}\frac{\mathrm{d}\nu}{\mathrm{d}r}\right) - \frac{1}{r^2} = -8\pi G T_1^1, \tag{323}$$

$$\frac{\mathrm{d}^2V}{\mathrm{d}r^2}+\frac{\mathrm{d}V}{\mathrm{d}r}\left[\frac{2}{r}-\frac{1}{2}\left(\frac{\mathrm{d}\nu}{\mathrm{d}r}+\frac{\mathrm{d}\lambda}{\mathrm{d}r}\right)\right]=-e\,\mathrm{e}^{\nu/2}\mathrm{e}^{\lambda}(n_p-n_e), \tag{324}$$

$$\frac{\mathrm{d}^2\sigma}{\mathrm{d}r^2}+\frac{\mathrm{d}\sigma}{\mathrm{d}r}\left[\frac{2}{r}+\frac{1}{2}\left(\frac{\mathrm{d}\nu}{\mathrm{d}r}-\frac{\mathrm{d}\lambda}{\mathrm{d}r}\right)\right]=\mathrm{e}^{\lambda}\left[\partial_\sigma U(\sigma)+g_s n_s\right], \tag{325}$$

$$\frac{\mathrm{d}^2\omega}{\mathrm{d}r^2}+\frac{\mathrm{d}\omega}{\mathrm{d}r}\left[\frac{2}{r}-\frac{1}{2}\left(\frac{\mathrm{d}\nu}{\mathrm{d}r}+\frac{\mathrm{d}\lambda}{\mathrm{d}r}\right)\right]=-\mathrm{e}^{\lambda}\left[g_\omega J_0^\omega-m_\omega^2\omega\right], \tag{326}$$

$$\frac{\mathrm{d}^2\rho}{\mathrm{d}r^2}+\frac{\mathrm{d}\rho}{\mathrm{d}r}\left[\frac{2}{r}-\frac{1}{2}\left(\frac{\mathrm{d}\nu}{\mathrm{d}r}+\frac{\mathrm{d}\lambda}{\mathrm{d}r}\right)\right]=-\mathrm{e}^{\lambda}\left[g_\rho J_0^\rho-m_\rho^2\rho\right], \tag{327}$$

$$E_e=\mathrm{e}^{\nu/2}\mu_e-eV=\mathrm{const}, \tag{328}$$

$$E_p=\mathrm{e}^{\nu/2}\mu_p+\mathcal{V}_p=\mathrm{const}, \tag{329}$$

$$E_n=\mathrm{e}^{\nu/2}\mu_n+\mathcal{V}_n=\mathrm{const}, \tag{330}$$

$$\mathrm{e}^{\nu/2}T=\mathrm{const}, \tag{331}$$

where the constants E_n, E_p and E_e are linked by eq. (321) and $\mathcal{V}_{p,n}$ is given by eq. (319). In particular, in the degenerate case $T=0$, eq. (324) becomes

$$\frac{\mathrm{d}^2\hat{V}}{\mathrm{d}r^2}+\frac{\mathrm{d}\hat{V}}{\mathrm{d}r}\left[\frac{2}{r}-\frac{1}{2}\left(\frac{\mathrm{d}\nu}{\mathrm{d}r}+\frac{\mathrm{d}\lambda}{\mathrm{d}r}\right)\right]= -4\pi\alpha\,\mathrm{e}^{\nu/2}\mathrm{e}^{\lambda}\left\{n_p-\frac{\mathrm{e}^{-3\nu/2}}{3\pi^2}[\hat{V}^2+2m_e\hat{V}-m_e^2(\mathrm{e}^{\nu}-1)]^{3/2}\right\}, \tag{332}$$

where $\hat{V}\equiv eV+E_e$ and we have used eq. (328) into eq. (324). This equation is the general relativistic extension of the relativistic Thomas-Fermi equation recently introduced in [12] for the study of compressed atoms. In addition, eq. (332) has been recently used to obtain the globally neutral configurations in the simpler case of degenerate neutrons, protons and electrons in β-equilibrium (see [15] and sect. **10** for details).

13. – Neutron stars with strong, weak, electromagnetic, and gravitational interactions within general relativity

We have formulated the theory of a system of neutrons, protons and electrons fulfilling strong, electromagnetic, weak and gravitational interactions [16] (see sect. **12** for details). The role of the Klein first integrals (Klein potentials) has been evidenced and their theoretical formulation in the Einstein-Maxwell background and in the most general case of finite temperatures has been presented. Such a treatment generalizes the previous results for the "non-interacting" case [15] (see sect. **10**). In this section we construct for the first time the equilibrium configurations of non-rotating neutron stars following the new approach, [15, 16], including the presence of a crust at subnuclear densities. The full set of the Einstein-Maxwell-Thomas-Fermi equations is solved numerically for zero temperatures and for selected parameterizations of the nuclear model.

13˙1. *The constitutive relativistic equations*

13˙1.1. Core equations. The parameters of the nuclear model, namely the coupling constants g_s, g_ω and g_ρ, and the meson masses m_σ, m_ω and m_ρ are usually fixed by fitting experimental properties of nuclei such as saturation density, binding energy per

TABLE IV. – *Selected parameter sets of the σ-ω-ρ model.*

	NL3	NL-SH	TM1	TM2
m_σ (MeV)	508.194	526.059	511.198	526.443
m_ω (MeV)	782.501	783.000	783.000	783.000
m_ρ (MeV)	763.000	763.000	770.000	770.000
g_s	10.2170	10.4440	10.0289	11.4694
g_ω	12.8680	12.9450	12.6139	14.6377
g_ρ	4.4740	4.3830	4.6322	4.6783
g_2 (fm^{-1})	−10.4310	−6.9099	−7.2325	−4.4440
g_3	−28.8850	−15.8337	0.6183	4.6076
c_3	0.0000	0.0000	71.3075	84.5318

nucleon (or experimental masses), symmetry energy, surface energy, and nuclear incompressibility. In table IV we present selected fits of the nuclear parameters: NL3 [76], NL-SH [77], TM1 [78], and TM2 [79].

The constants g_2 and g_3 are the third- and fourth-order constants of the self-scalar interaction as given by the scalar self-interaction potential

$$U(\sigma) = \frac{1}{2}m_\sigma^2\sigma^2 + \frac{1}{3}g_2\sigma^3 + \frac{1}{4}g_3\sigma^4. \tag{333}$$

The non-zero constant c_3 that appears in the TM1 and TM2 models corresponds to the self-coupling constant of the non-linear vector self-coupling $\frac{1}{4}c_3(\omega_\mu\omega^\mu)^2$. We have not include such a self-coupling vector interaction in the general formulation presented in sect. **12**. However, we will also show the results of the integration when such a self-interaction is taken into account and we refer to [78,79] for details about the motivations of including such a coupling.

Inside the core of the star we can safely apply the mean-field approximation by replacing the massive meson fields by their expectation values and considering them as microscopically homogeneous. In such a case, eqs. (322)-(330) reduce to

$$\mathrm{e}^{-\lambda(r)}\left(\frac{1}{r^2} - \frac{1}{r}\frac{\mathrm{d}\lambda}{\mathrm{d}r}\right) - \frac{1}{r^2} = -8\pi G T_0^0, \tag{334}$$

$$\mathrm{e}^{-\lambda(r)}\left(\frac{1}{r^2} + \frac{1}{r}\frac{\mathrm{d}\nu}{\mathrm{d}r}\right) - \frac{1}{r^2} = -8\pi G T_1^1, \tag{335}$$

$$\frac{\mathrm{d}^2V}{\mathrm{d}r^2} + \frac{\mathrm{d}V}{\mathrm{d}r}\left[\frac{2}{r} - \frac{1}{2}\left(\frac{\mathrm{d}\nu}{\mathrm{d}r} + \frac{\mathrm{d}\lambda}{\mathrm{d}r}\right)\right] = -e\,\mathrm{e}^{\nu/2}\mathrm{e}^{\lambda}(n_p - n_e), \tag{336}$$

$$\partial_\sigma U(\sigma) + g_s n_s = 0, \tag{337}$$

$$g_\omega J_0^\omega - m_\omega^2\omega = 0, \tag{338}$$

$$g_\rho J_0^\rho - m_\rho^2\rho = 0, \tag{339}$$

$$E_e = \mathrm{e}^{\nu/2}\mu_e - eV = \text{const}, \tag{340}$$

$$E_p = \mathrm{e}^{\nu/2}\mu_p + \mathcal{V}_p = \text{const}, \tag{341}$$

$$E_n = \mathrm{e}^{\nu/2}\mu_n + \mathcal{V}_n = \text{const}. \tag{342}$$

The numerical integration of the core equations can be started given a central density and the regularity conditions at the origin. At nuclear density the phase-transition to the "solid" crust takes place. Thus, the radius of the core $R_{\rm core}$ is given by $\mathcal{E}(r = R_{\rm core})/c^2 = \rho_{\rm nuc} \sim 2.7 \times 10^{14}\,{\rm g/cm^3}$. These equations must be solved with the boundary conditions given by the fulfillment of the condition of global charge neutrality and the continuity of the Klein potentials of particles between the core and the crust.

13˙2. *Core-crust transition layer equations.* – In the core-crust interface, the mean-field approximation for the meson-fields is not valid any longer and thus a full numerical integration of the meson-field equations of motion, taking into account all gradient terms, must be performed. We expect the core-crust transition boundary-layer to be a region with characteristic length scale of the order of the electron Compton wavelength $\sim \lambda_e = \hbar/(m_e c) \sim 100\,{\rm fm}$ corresponding to the electron screening scale. Then, in the core-crust transition layer, the system of equations is reduced to

$$\frac{{\rm d}^2 V}{{\rm d}r^2} + \frac{2}{r}\frac{{\rm d}V}{{\rm d}r} = -e^{\lambda_{\rm core}} e J_0^{ch}, \tag{343}$$

$$\frac{{\rm d}^2 \sigma}{{\rm d}r^2} + \frac{2}{r}\frac{{\rm d}\sigma}{{\rm d}r} = e^{\lambda_{\rm core}} \left[\partial_\sigma U(\sigma) + g_s n_s\right], \tag{344}$$

$$\frac{{\rm d}^2 \omega}{{\rm d}r^2} + \frac{2}{r}\frac{{\rm d}\omega}{{\rm d}r} = -e^{\lambda_{\rm core}} \left[g_\omega J_0^\omega - m_\omega^2 \omega\right], \tag{345}$$

$$\frac{{\rm d}^2 \rho}{{\rm d}r^2} + \frac{2}{r}\frac{{\rm d}\rho}{{\rm d}r} = -e^{\lambda_{\rm core}} \left[g_\rho J_0^\rho - m_\rho^2 \rho\right], \tag{346}$$

$$E_e = e^{\nu_{\rm core}/2}\mu_e - eV = {\rm const}, \tag{347}$$

$$E_p = e^{\nu_{\rm core}/2}\mu_p + eV + g_\omega \omega + g_\rho \rho = {\rm const}, \tag{348}$$

$$E_n = E_p + E_e, \tag{349}$$

where we have used the fact that the metric functions are with high level of accuracy constant throughout the core-crust transition layer and thus we can take their values at the core radius $e^{\nu_{\rm core}} \equiv e^{\nu(R_{\rm core})}$ and $e^{\lambda_{\rm core}} \equiv e^{\lambda(R_{\rm core})}$.

The system of equations of the transition layer has a stiff nature due to the existence of two different scale lengths. The first one is associated with the nuclear interactions $\sim \lambda_\pi = \hbar/(m_\pi c) \sim 1.5\,{\rm fm}$ and the second one is due to the aforementioned screening length $\sim \lambda_e = \hbar/(m_e c) \sim 100\,{\rm fm}$. Thus, the numerical integration of eqs. (343)–(349) has been performed subdividing the core-crust transition layer in the following three regions: (I) a mean-field–like region where all the fields vary slowly with length scale $\sim \lambda_e$, (II) a strongly interacting region of scale $\sim \lambda_\pi$ where the surface tension due to nuclear interactions dominate producing a sudden decrease of the proton and the neutron densities and, (III) a Thomas-Fermi–like region of scale $\sim \lambda_e$ where only a layer of opposite charge made of electrons is present producing the total screening of the positively charged core. The results of the numerical integration of the equilibrium equations are shown in fig. 29 for the NL3-model.

We have integrated numerically eqs. (334)–(342) for the models listed in table IV. The boundary conditions for the numerical integration are fixed through the following procedure. We start assuming a value for the central baryon number density $n_b(0) = n_n(0) + n_p(0)$. From the regularity conditions at the origin we have $e^{-\lambda(0)} = 1$ and $n_e(0) = n_p(0)$.

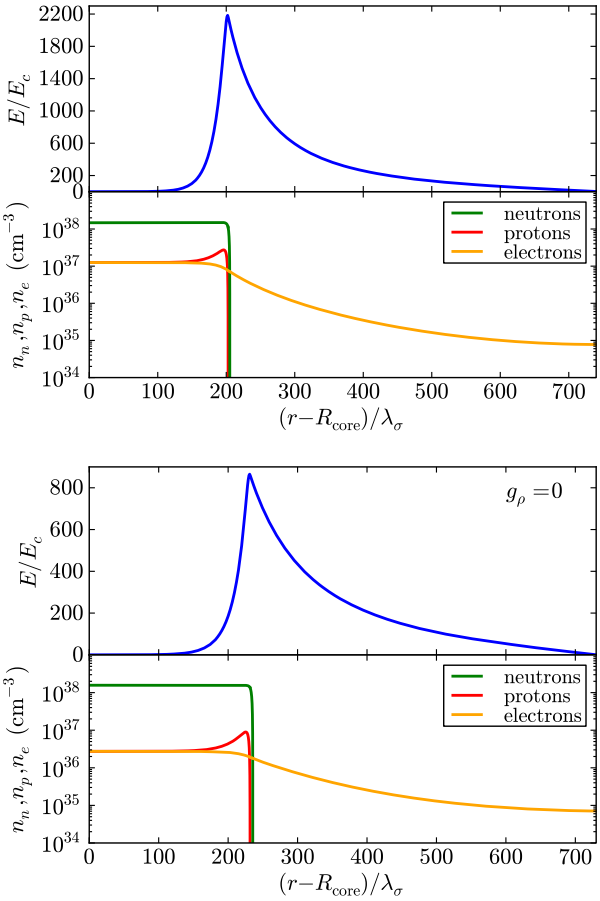

Fig. 29. – Upper panel: electric field in the core-crust transition layer in units of the critical field E_c. Lower panel: particle density profiles in the core-crust boundary interface in units of cm^{-3}. Here we use the NL3-model of table IV and $\lambda_\sigma = \hbar/(m_\sigma c) \sim 0.4\,\text{fm}$ denotes the sigma-meson Compton wavelength. The density at the edge of the crust in this example is $\rho_{\rm crust} = \rho_{\rm drip} = 4.3 \times 10^{11}\,\text{g/cm}^3$. In the right panel plot we have set $g_\rho = 0$ in order to see the effects of the ρ-meson with respect to the case $g_\rho \neq 0$.

The metric function ν at the origin can be chosen arbitrarily, *e.g.* $\nu(0) = 0$, due to the fact that the system of equations remain invariant under the shift $\nu \to \nu +$ constant. The right value of ν is obtained once the end of the integration of the core has been accomplished and duly matched to the crust, by fulfilling the following identity at the surface of the neutron star,

$$e^{\nu(R)} = e^{-\lambda(R)} = 1 - \frac{2GM(R)}{c^2 R}\,, \tag{350}$$

being $M(R)$ and R the total mass and radius of the star. Then, taking into account the above conditions, we solve the system (337)–(342) at the origin for the other unknowns $\sigma(0)$, $\omega(0)$, $\rho(0)$, $n_n(0)$, $n_p(0)$, $n_e(0)$.

The initial conditions for the numerical integration of the core-crust transition layer equations are determined by the final values given by the numerical integration of the core equations, *i.e.* we take the values of all the variables at the core-radius $R_{\rm core}$.

In region I the effect of the Coulomb interaction is clear: on the proton profile we can see a bump due to Coulomb repulsion while the electron-profile decreases as expected. Such a Coulomb effect is indirectly felt also by the neutrons due to the coupled nature of the system of equations. However, the neutron-bump is much smaller than the one of protons and it is not appreciable in fig. 29 due to the plot-scale. In region II we see clearly the effect of the surface tension due to nuclear interaction which produces a sharp decrease of the neutron and proton profiles in a characteristic scale $\sim \lambda_\pi$. In addition, it can be seen a neutron skin effect, analogous to the one observed in heavy nuclei, which makes the scale of the neutron density falloff slightly larger with respect to the proton one, in close analogy to the neutron skin effect observed in neutron rich nuclei, see *e.g.* [80]. Region III is characterized by a smooth decreasing of the electron density which resembles the behavior of the electrons surrounding a nucleus in the Thomas-Fermi model.

The matching to the crust must be done at a radius $R_{\rm core} + \delta R$ where full charge neutrality of the core is reached. Different thicknesses δR correspond to different electron Fermi energies E_e^F. The thickness of the core-crust transition boundary layer δR as well as the value of the electron density at the edge of the crust, $n_e^{\rm crust} = n_e(R_{\rm core} + \delta R)$, depend on the nuclear parameters, especially on the nuclear surface tension.

The equilibrium conditions given by the constancy of the Klein potentials (340)–(342) throughout the configuration, impose in the transition layer the following continuity condition

$$E_e^F = e^{\nu_{\rm core}/2}\mu_e^{\rm core} - eV^{\rm core} = e^{\nu_{\rm crust}/2}\mu_e^{\rm crust}, \tag{351}$$

where $\mu_e^{\rm core} = \mu_e(R_{\rm core})$, $eV^{\rm core} = eV(R_{\rm core})$, and $\mu_e^{\rm crust} = \mu_e(R_{\rm core} + \delta R)$, and $e^{\nu_{\rm crust}} \simeq e^{\nu_{\rm core}}$.

In the boundary interface, the electron chemical potential and the density decrease: $\mu_e^{\rm crust} < \mu_e^{\rm core}$ and $\rho_{\rm crust} < \rho_{\rm core}$. For each central density, an entire family of core-crust interface boundaries exist each one with a specific value of δR: the larger the $\rho_{\rm crust}$, the smaller the δR. Correspondingly, an entire family of crusts with different mass and thickness, exist. From the continuity of the electron Klein potential in the boundary interface given by eq. (351), it follows that different values of $\rho_{\rm crust} \geq 0$ correspond to different values of the electron Fermi energy $E_e^F \geq 0$. In close analogy to the compressed atoms studied in [12], the case $E_e^F = 0$ corresponds to the "free" (uncompressed) configuration, where $\delta R \to \infty$ and $\rho_{\rm crust} = 0$, *i.e.* a bare core. In this configuration the electric field reaches its maximum value. The case $E_e^F > 0$ is analogous to the one of the compressed atom [12]. In fig. 30 we have plotted the electron distribution in the core-crust boundary interface for selected densities at the edge of the crust $\rho_{\rm crust} = [\rho_{\rm drip}, 10^{10}, 10^9]\,{\rm g/cm^3}$, where $\rho_{\rm drip} \sim 4.3 \times 10^{11}\,{\rm g/cm^3}$ is the neutron drip density.

The configuration with $\rho_{\rm crust} = \rho_{\rm drip}$ separates neutron stars with and without inner crust. In the so-called inner crust, the neutrons dripped from the nuclei in the crust form a fluid that coexist with the nuclei lattice and the degenerate electrons [58]. For definiteness, we present in this article the results for configurations $\rho_{\rm crust} \leq \rho_{\rm drip}$, *i.e.* for neutron stars possessing only outer crust. The construction of configurations with $\rho_{\rm crust} > \rho_{\rm drip}$ needs to be studied in more detail and will be the subject of a forthcoming work.

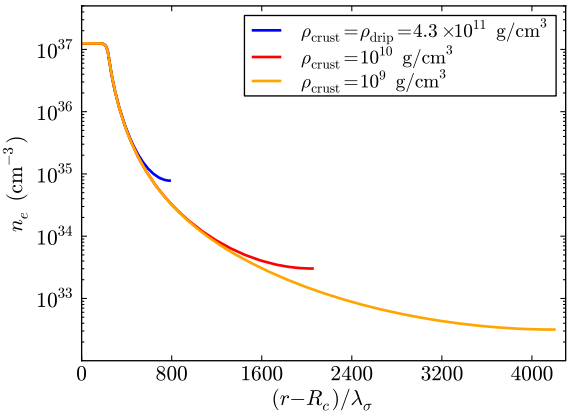

Fig. 30. – Distribution of electrons in the core-crust boundary interface for different densities at the edge of the crust, $\rho_{\rm crust}$. The larger the $\rho_{\rm crust}$, the smaller the electric field E and the smaller the thickness of the interface δR.

In fig. 29 we show the core-crust transition layer for the NL3 model of table IV with and without the presence of the ρ-meson respectively. The presence of the ρ-meson is responsible for the nuclear asymmetry within this nuclear model. The relevance of the nuclear symmetry energy on the structure of nuclei and neutron stars is continuously stressed in literature; see, *e.g.*, [81-85]. The precise value of the nuclear symmetry energy plays here a crucial in determining the precise value of the ρ-meson coupling which, in the present case, is essential in the determination of the intensity of the electric field in the core-crust boundary interface; as can be seen from the comparison of fig 29.

13˙3. *Crust equations.* – Turning now to the crust, it is clear from our recent treatment of white dwarfs [14] that also this problem can be solved by the adoption of Wigner-Seitz cells and from the relativistic FMT approach [12] it follows that the crust is clearly neutral. Thus, the structure equations to be integrated are the TOV equations

$$\frac{\mathrm{d}\mathcal{P}}{\mathrm{d}r} = -\frac{G(\mathcal{E}+\mathcal{P})(M+4\pi r^3\mathcal{P})}{r^2(1-\frac{2GM}{r})}\,, \tag{352}$$

$$\frac{\mathrm{d}M}{\mathrm{d}r} = 4\pi r^2\mathcal{E}, \tag{353}$$

where $M = M(r)$ is the mass enclosed at the radius r.

The effects of the Coulomb interaction in "solid"-like electron-ion systems appears only at the microscopic level, *e.g.*, Debye-Hueckel screening in classical systems [86] and Thomas-Fermi screening in the degenerate case [87]. In order to analyze the effects of the microscopic screening on the structure of the configuration we will consider two equations of state for the crust: the locally neutral case or uniform approximation (see, *e.g.*, [29]) and, for simplicity, instead of using the RFMT EoS [12], we use as second EoS the one due to Baym, Pethick and Sutherland (BPS) [58], which is by far the most used equation of state in literature for the description of the neutron star crust (see, *e.g.*, [19]).

In the uniform approximation, both the degenerate electrons and the nucleons distribution are considered constant inside each cell of volume $V_{\rm ws}$. This kind of configuration

TABLE V. – *$\rho_{\max}$ is the maximum density at which the nuclide is present; $\Delta\ R_1$, $\Delta\ R_2$ and R.A.1(%), R.A.2(%) are respectively the thickness of the layer where a given nuclide is present and their relative abundances in the outer crust for two different cases: $M_{\rm core} = 2.56 M_\odot$, $R_{\rm core} = 12.79\,{\rm km}$; $M_{\rm core} = 1.35 M_\odot$, $R_{\rm core} = 11.76\,{\rm km}$.*

Equilibrium Nuclei Below Neutron Drip						
Nucleus	Z	$\rho_{\max}({\rm g\,cm^{-3}})$	$\Delta\ R_1$ (km)	R.A.1(%)	$\Delta\ R_2$ (km)	R.A.2(%)
^{56}Fe	26	8.1×10^6	0.0165	7.56652×10^{-7}	0.0064	6.96927×10^{-7}
^{62}Ni	28	2.7×10^8	0.0310	0.00010	0.0121	0.00009
^{64}Ni	28	1.2×10^9	0.0364	0.00057	0.0141	0.00054
^{84}Se	34	8.2×10^9	0.0046	0.00722	0.0017	0.00683
^{82}Ge	32	2.2×10^{10}	0.0100	0.02071	0.0039	0.01983
^{80}Zn	38	4.8×10^{10}	0.1085	0.04521	0.0416	0.04384
^{78}Ni	28	1.6×10^{11}	0.0531	0.25635	0.0203	0.25305
^{76}Fe	26	1.8×10^{11}	0.0569	0.04193	0.0215	0.04183
^{124}Mo	42	1.9×10^{11}	0.0715	0.02078	0.0268	0.02076
^{122}Zr	40	2.7×10^{11}	0.0341	0.20730	0.0127	0.20811
^{120}Sr	38	3.7×10^{11}	0.0389	0.23898	0.0145	0.24167
^{118}Kr	36	4.3×10^{11}	0.0101	0.16081	0.0038	0.16344

can be obtained only imposing microscopically the condition of local charge neutrality

$$n_e = \frac{Z}{V_{\rm ws}}\,. \tag{354}$$

The total pressure of the system is assumed to be entirely due to the electrons, *i.e.*

$$\mathcal{P} = \mathcal{P}_e = \frac{2}{3\,(2\pi\hbar)^3} \int_0^{P_e^F} \frac{c^2 p^2 4\pi p^2}{\sqrt{c^2 p^2 + m_e^2 c^4}} {\rm d}p, \tag{355}$$

while the total energy-density of the system is due to the nuclei, *i.e.* $\mathcal{E}{=}(A/Z) m_N n_e$, where m_N is the nucleon mass.

We turn now to the BPS equation of state. The first correction to the uniform model, corresponds to abandon the assumption of the electron-nucleon fluid through the so-called "lattice" model which introduces the concept of Wigner-Seitz cell: each cell of radius $R_{\rm ws}$ contains a point-like nucleus of charge $+Ze$ with A nucleons surrounded by a uniformly distributed cloud of Z fully-degenerate electrons.

The sequence of the equilibrium nuclides present at each density in the BPS equation of state is obtained by looking for the nuclear composition that minimizes the energy per nucleon for each fixed nuclear composition (Z, A) (see table V and [58] for details). The

pressure $\mathcal{P}$ and the energy-density $\mathcal{E}$ of the system are, within this model, given by

$$\mathcal{P} = \mathcal{P}_e + \frac{1}{3} W_L n_N, \tag{356}$$

$$\frac{\mathcal{E}}{n_b} = \frac{W_N + W_L}{A} + \frac{\mathcal{E}_e(n_b Z/A)}{n_b}\,, \tag{357}$$

where the electron energy-density is given by

$$\mathcal{E}_e = \frac{2}{(2\pi)^3} \int_0^{P_e^F} \sqrt{p^2 + m_e^2}\, 4\pi p^2 \mathrm{d}p, \tag{358}$$

and $W_N(A, Z)$ is the total energy of an isolated nucleus given by the semi-empirical formula

$$W_N = m_n c^2 (A - Z) + m_p c^2 Z - bA, \tag{359}$$

with b being the Myers and Swiatecki binding energy per nucleon [88]. The lattice energy per nucleus W_L is given by

$$W_L = -\frac{1.819620 Z^2 e^2}{a}\,, \tag{360}$$

where the lattice constant a is related to the nucleon density n_N by $n_N a^3 = 2$.

14. – Neutron star structure

In the traditional TOV treatment the density and the pressure are a priori assumed to be continuous as well as the local charge neutrality of the system. The distinguishing feature of our new solution is that the Klein potentials are constant throughout the three regions; the core, the crust and the transition interface boundary. An overcritical electric field is formed and consequently a discontinuity in density is found with a continuous total pressure including the surface tension of the boundary. In fig. 31, we compare and contrast the density profiles of configurations obtained from the traditional TOV treatment and with the treatment presented here.

In figs. 32, 33 we show the results of the numerical integration of the system of the general relativistic constitutive equations of the configuration from the center all the way up to the surface with the appropriate boundary conditions between the involved phases. In particular, we have plotted the mass-radius relation as well as the compactness of the neutron stars obtained with the models listed in table IV.

It is worth to note that the inclusion of the Coulomb interaction and in particular the presence of the negative lattice energy W_L results in a decreasing of the pressure of the cells. Such an effect, as shown in figs. 34, 35, leads to a decreasing of the mass and the thickness of the crust with respect to the uniform-approximation case where no Coulomb interactions are taken into account.

Comparing the mass and the thickness of the crust obtained with these two different EoS, we obtain systematically crusts with smaller mass and larger thickness when Coulomb interactions are taken into account. This results are in line with the recent

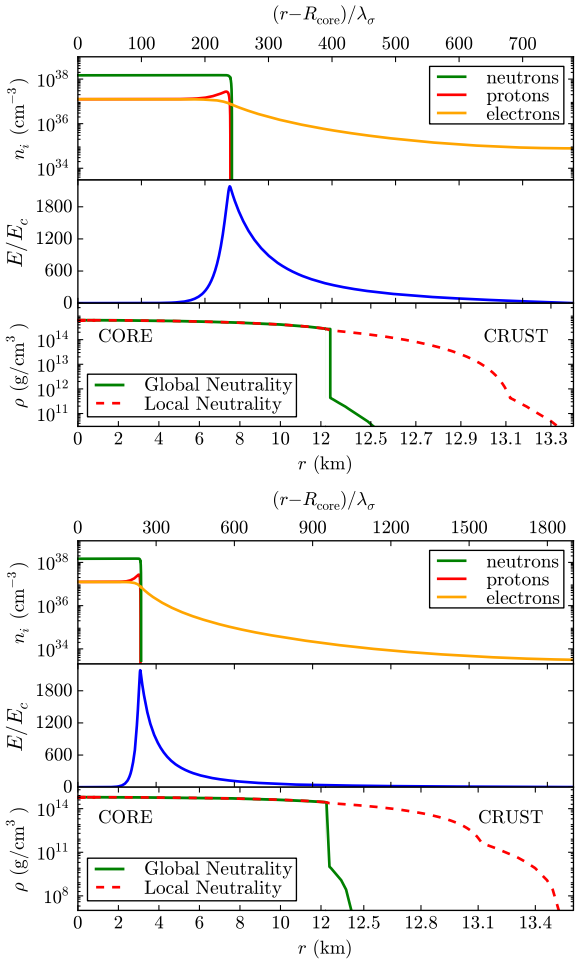

Fig. 31. – Top panel: particle density profiles in the core-crust boundary interface, in units of cm^{-3}. Middle panel: electric field in the core-crust transition layer, in units of the critical field E_c. Lower panel: density profile inside a neutron star with central density $\rho(0) \sim 5\rho_{\rm nuc}$. We compare and contrast the structural differences between the solution obtained from the traditional TOV equations (locally neutral case) and the globally neutral solution presented here. We use here the NL3 nuclear parametrization of table IV and $\lambda_\sigma = \hbar/(m_\sigma c) \sim 0.4\,$fm, denotes the sigma-meson Compton wavelength. The density at the edge of the crust is $\rho_{\rm crust} = \rho_{\rm drip} = 4.3 \times 10^{11}\,{\rm g/cm^3}$ (top plot) and $\rho_{\rm crust} = 10^{10}\,{\rm g/cm^3}$ (bottom plot).

results in [14], where the mass-radius relation of white-dwarfs has been calculated using an EoS based on the relativistic FMT model for compressed atoms [12].

In the case of the BPS EoS, the average nuclear composition in the outer crust, namely the average charge to mass ratio of nuclei Z/A, is obtained by calculating the contribution of each nuclear composition present to the mass of the crust. We exemplified the analysis for two different cores: $M_{\rm core} = 2.56 M_\odot$, $R_{\rm core} = 12.79\,$km; $M_{\rm core} = 1.35 M_\odot$, $R_{\rm core} = 11.76\,$km. The relative abundance of each nuclide within the crust of the star

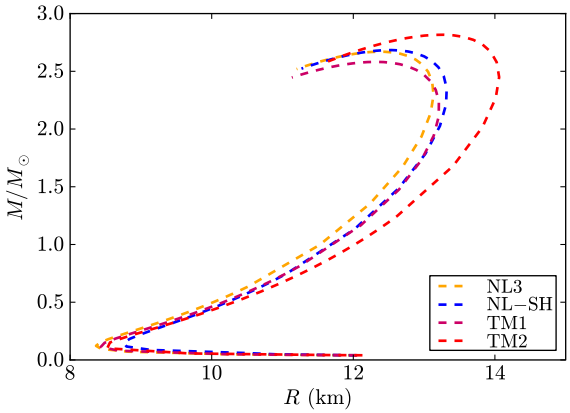

Fig. 32. – Mass-Radius relation for the neutron stars obtained with the nuclear models listed in table IV. In the crust we have used the BPS equation of state. The mass is given in solar masses and the radius in km.

can be obtained as

$$\text{R.A.} = \frac{1}{M_{\text{crust}}^{\text{BPS}}} \int_{\Delta r} 4\pi r^2 \mathcal{E} \mathrm{d}r, \tag{361}$$

where the integration is carried out in the layer of thickness Δr where the particular nuclide is present; see table V and fig. 36. Our results are in agreement with the analysis on the neutron star crust composition obtained in [55, 56]. In both cases we obtain as average nuclear composition $^{105}_{35}$Br. The corresponding crusts with fixed nuclear composition $^{105}_{35}$Br for the two chosen cores are calculated neglecting Coulomb interactions (*i.e.* using the first EoS). The mass and the thickness of these crusts with fixed $^{105}_{35}$Br are different with respect to the ones obtained using the full BPS EoS, leading to such average nuclear composition. For the two selected examples we obtain that the mass

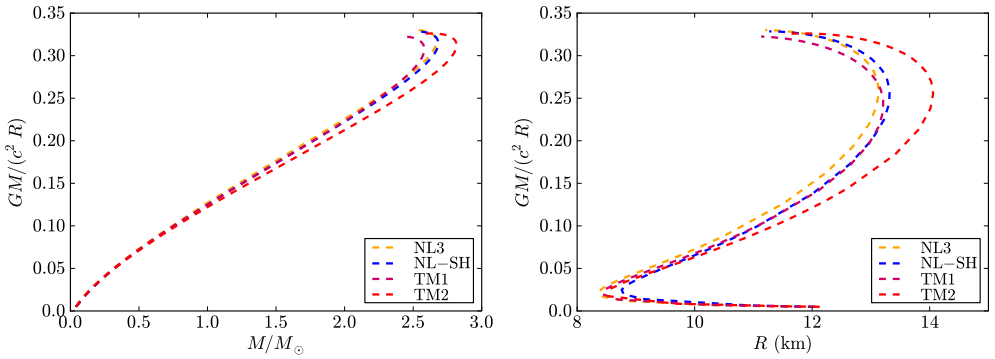

Fig. 33. – Compactness of the star $GM/(c^2R)$ as a function of the star mass M (left panel) and the radius (right panel). In the crust we have used the BPS equation of state and the nuclear models are in table IV.

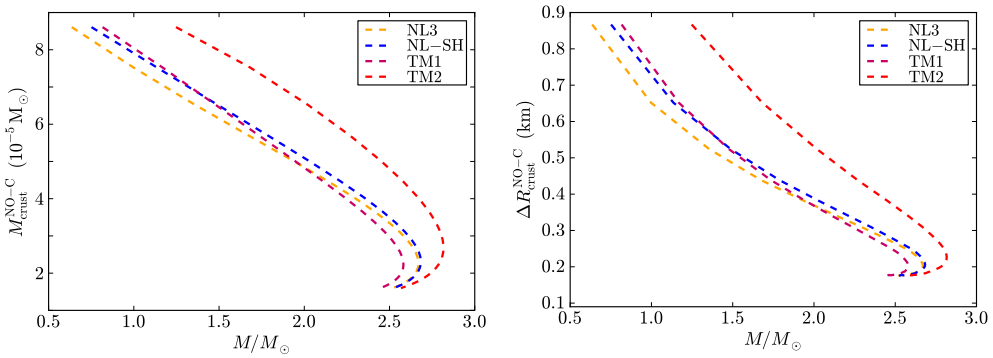

Fig. 34. – Left panel: mass of the crust as a function of the total mass of the star for the crust EoS without Coulomb interactions. Right panel: crust-thickness as a function of the total mass of the star.

and the thickness of the crust with average $^{105}_{35}$Br are, respectively, 18% larger and 5% smaller with respect to the ones obtained with the corresponding BPS EoS. This result shows how small microscopic effects due to the Coulomb interaction in the crust of the neutron star leads to quantitative not negligible effects on the macroscopic structure of the configuration.

15. – Observational constraints on the mass-radius relation

It has been recently pointed out that the most up-to-date stringent constraints to the mass-radius relation of neutron stars are provided by the largest mass, the largest radius, the highest rotational frequency, and the maximum surface gravity, observed for pulsars [89].

So far, the highest neutron star mass measured with a high level of experimental confidence is the mass of the 3.15 millisecond pulsar PSR J1614-2230, $M = 1.97 \pm 0.04 M_\odot$, obtained from the Shapiro time delay and the Keplerian orbital parameters of the binary system [90]. The fitting of the thermonuclear burst oscillation light curves

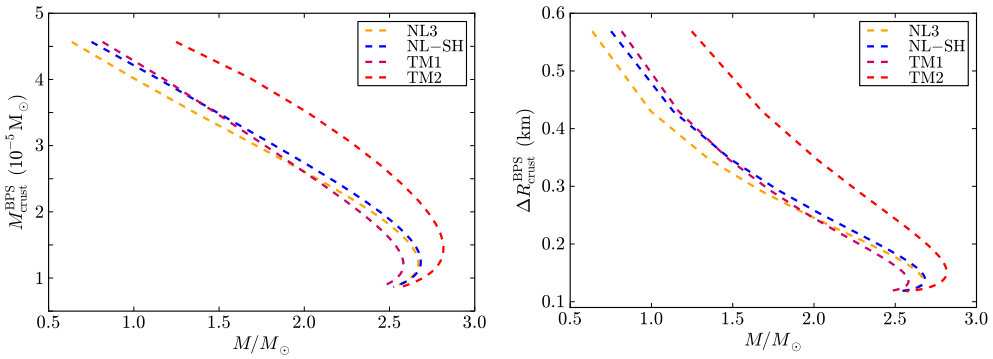

Fig. 35. – Same as fig. 34 but for the BPS EoS.

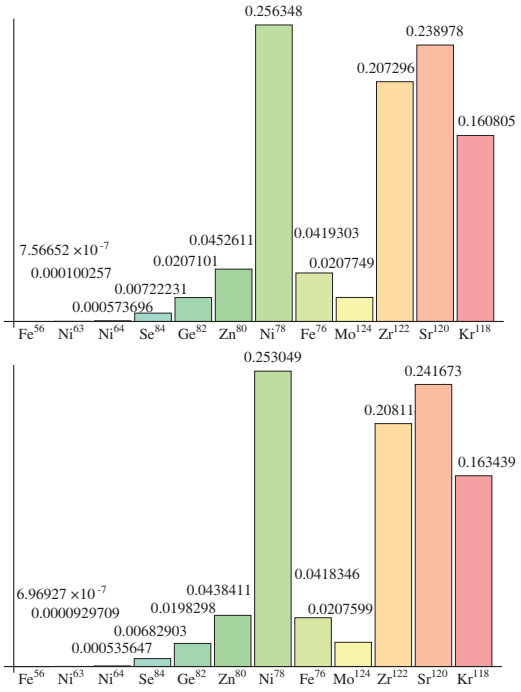

Fig. 36. – Relative abundances of chemical elements in the crust for the two cores analyzed in table V.

from the accreting millisecond pulsar XTE J1814-338 weakly constrain the mass-radius relation imposing an upper limit to the surface gravity of the neutron star, $GM/(c^2R) < 0.24$ [91]. A lower limit of the radius of RX J1856-3754, as seen by an observer at infinity $R_\infty = R[1 - 2GM/(c^2R)]^{-1/2} > 16.8\,\mathrm{km}$, has been obtained from the fit of the optical and X-ray spectra of the source [92]; it gives the constraint $2GM/c^2 > R - R^3/(R_\infty^{\min})^2$, being $R_\infty^{\min} = 16.8\,\mathrm{km}$. Assuming a neutron star of $M = 1.4M_\odot$ to fit the Chandra data of the low-mass X-ray binary X7, it turns out that the radius of the star satisfies $R = 14.5^{+1.8}_{-1.6}\,\mathrm{km}$, at 90% confidence level, corresponding to $R_\infty = [15.64, 18.86]\,\mathrm{km}$, respectively (see [93] for details). The maximum rotation rate of a neutron star taking into account both the effects of general relativity and deformations has been found to be $\nu_{\max} = 1045(M/M_\odot)^{1/2}(10\,\mathrm{km}/R)^{3/2}\,\mathrm{Hz}$, largely independent of the equation of state [94]. The fastest observed pulsar is PSR J1748-2246ad with a rotation frequency of 716 Hz [95], which results in the constraint $M \geq 0.47(R/10\,\mathrm{km})^3 M_\odot$. In fig. 37 we show all these constraints and the mass-radius relation presented in this article.

As discussed by J. E. Trümper in [89], the above constraints strongly favor stiff equations of state which provide high maximum masses for neutron stars. In addition, putting all of them together, the radius of a canonical neutron star of mass $M = 1.4M_\odot$ is highly constrained to the range $R \gtrsim 12\,\mathrm{km}$ disfavoring, at the same time, the strange quark hypothesis for these specific objects. It is clear from fig. 37 that the mass-radius relation presented here is consistent with all the observation constraints, for all the nuclear parametrizations of table IV. We present in table VI, the radii predicted by our mass-radius relation for a canonical neutron star of $M = 1.4M_\odot$ as well as for the millisecond pulsar PSR J1614-2230, $M = 1.97 \pm 0.04M_\odot$.

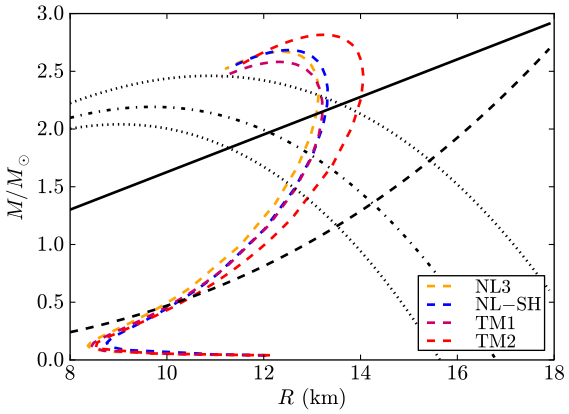

Fig. 37. – Constraints on the mass-radius relation given by J. E. Trümper in [89] and the theoretical mass-radius relation presented in this article in fig. 32. The solid line is the upper limit of the surface gravity of XTE J1814-338, the dotted-dashed curve corresponds to the lower limit to the radius of RX J1856-3754, the dashed line is the constraint imposed by the fastest spinning pulsar PSR J1748-2246ad, and the dotted curves are the 90% confidence level contours of constant R_∞ of the neutron star in the low-mass X-ray binary X7. Any mass-radius relation should pass through the area delimited by the solid, the dashed and the dotted lines and, in addition, it must have a maximum mass larger than the mass of PSR J1614-2230, $M = 1.97 \pm 0.04 M_\odot$.

16. – Comparison with the traditional TOV treatment

In the traditional TOV treatment local charge neutrality as well as the continuity of the pressure and the density in the core-crust transition are assumed. This leads to explicit violation of the constancy of the Klein potentials throughout the configuration (see, *e.g.*, [15]). In such a case there is a smooth transition from the core to the crust without any density discontinuity and therefore the density at the edge of the crust is $\sim \rho_{\rm nuc} \sim 2.7 \times 10^{14}\,{\rm g/cm^3}$. The so-called inner crust in those configurations extends in the range of densities $\rho_{\rm drip} \lesssim \rho \lesssim \rho_{\rm nuc}$ while, at densities $\rho \lesssim \rho_{\rm drip}$, there is the so-called outer crust.

In fig. 38 we compare and contrast the mass and the thickness of the crust as obtained from the traditional TOV treatment with the new configurations presented here in the case $\rho_{\rm crust} = \rho_{\rm drip}$.

TABLE VI. – *Radii (in km) predicted by the nuclear parametrizations NL3, NL-Sh, TM1 and TM2 of table IV, for a canonical neutron star of* $M = 1.4 M_\odot$ *and for the millisecond pulsar PSR J1614-2230,* $M = 1.97 \pm 0.04 M_\odot$.

$M(M_\odot)$	$R_{\rm NL3}$	$R_{\rm NL-SH}$	$R_{\rm TM1}$	$R_{\rm TM2}$
1.40	12.31	12.47	12.53	12.93
1.93	12.96	13.14	13.13	13.73
2.01	13.02	13.20	13.17	13.82

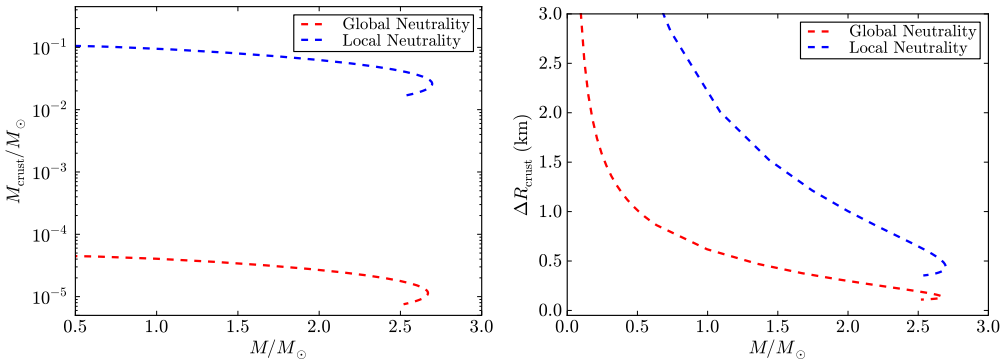

Fig. 38. – Mass (left panel) and thickness (right panel) of the crust given by the traditional locally neutral Tolman-Oppenheimer-Volkoff treatment and by the new globally neutral equilibrium configurations presented in this article. We use here the NL3 nuclear model, see table IV.

The markedly differences both in mass and thickness of the crusts (see fig. 38) obtained from the traditional Tolman-Oppenheimer-Volkoff approach and the new equilibrium configurations presented here, leads to a very different mass-radius relations which we compare and contrast in fig. 39.

We have formulated the equations of equilibrium of neutron stars based on our recent works [16] and [12, 14, 15]. The strong, weak, electromagnetic, and gravitational interactions are taken into due account within the framework of general relativity. In particular, the strong interactions between nucleons is described by the exchange of the σ, ω, and ρ mesons. The equilibrium conditions are given by the set of Einstein-Maxwell-Thomas-Fermi equations and by the constancy of the general relativistic Fermi energies of particles, the Klein potentials, throughout the configuration.

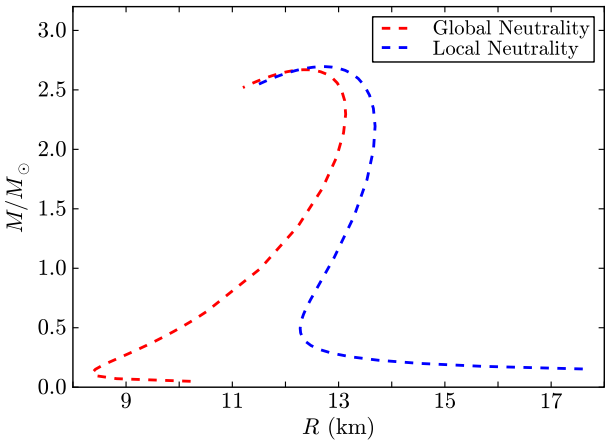

Fig. 39. – Mass-Radius relation obtained with the traditional locally neutral TOV treatment and with the new globally neutral equilibrium configurations presented here. We use here the NL3 nuclear model, see table IV.

We have solved these equilibrium equations numerically, in the case of zero temperatures, for the nuclear parameter sets NL3 [76], NL-SH [77], TM1 [78], and TM2 [79]; see table IV for details.

A new structure of the star is found: the positively charged core at supranuclear densities is surrounded by an electronic distribution of thickness $\gtrsim \hbar/(m_e c) \sim 10^2 \hbar/(m_\pi c)$ of opposite charge and, at lower densities, a neutral ordinary crust.

In the core interior the Coulomb potential well is $\sim m_\pi c^2/e$ and correspondingly the electric field is $\sim (m_p/m_{\rm Planck})(m_\pi/m_e)^2 E_c \sim 10^{-14} E_c$. Due to the equilibrium condition given by the constancy of the Klein potentials, there is a discontinuity in the density at the transition from the core to the crust, and correspondingly an overcritical electric field $\sim (m_\pi/m_e)^2 E_c$ develops in the boundary interface; see fig. 29.

The continuity of the Klein potentials at the core-crust boundary interface leads to a decreasing of the electron chemical potential and density, until values $\mu_e^{\rm crust} < \mu_e^{\rm core}$ and $\rho_{\rm crust} < \rho_{\rm core}$ at the edge of the crust, where global charge neutrality is achieved. For each central density, an entire family of core-crust interface boundaries and, correspondingly, an entire family of crusts with different mass and thickness, exist. The larger $\rho_{\rm crust}$, the smaller the thickness of the interface, the peak of the electric field, and the larger the mass and the thickness of the crust. The configuration with $\rho_{\rm crust} = \rho_{\rm drip} \sim 4.3 \times 10^{11}\,{\rm g/cm^3}$ separates neutron stars with and without inner crust. The neutron stars with $\rho_{\rm crust} > \rho_{\rm drip}$ deserve a further analysis in order to account for the reduction of the nuclear tension at the core-crust transition due to the presence of dripped neutrons from the nuclei in the crust.

All the above new features lead to crusts with masses and thickness smaller than the ones obtained from the traditional TOV treatment, and we have shown specifically neutron stars with $\rho_{\rm crust} = \rho_{\rm drip}$; see fig. 38. The mass-radius relation obtained in this case have been compared and contrasted with the one obtained from the locally neutral TOV approach; see fig. 39. We have shown that our mass-radius relation is in line with observations, based on the recent work by J. E. Trümper [89]; see fig. 37 for details.

The electromagnetic structure of the neutron star presented here is of clear astrophysical relevance. The process of gravitational collapse of a core endowed with electromagnetic structure leads to signatures and energetics markedly different from the ones of a core endowed uniquely of gravitational interactions; see, *e.g.*, [96-99].

It is clear that the release of gravitational energy in the process of gravitational collapse of the core, following the classic work of Gamow and Schoenberg (see [100,101]), is carried away by neutrinos. The additional nuclear and electromagnetic energy $\sim 10^{51}$ erg of the collapsing core introduced in this article are expected to be carried away by electron-positron plasma created in the overcritical electromagnetic field in the collapsing core.

REFERENCES

[1] Gombás P., *Die Statistischie Theorie des Atoms und Ihre Anwendungen* (Springer-Verlag, Wien) 1949.
[2] Lieb E. H., *Rev. Mod. Phys.*, **53** (1981) 603.
[3] Ruffini R. and Bonazzola S., *Phys. Rev.*, **187** (1969) 1767.
[4] Ruffini R., in *Black holes (Les astres occlus)* (Gordon and Breach Science Publishers, New York) 1973.
[5] Migdal A. B., Voskresenskii D. N. and Popov V. S., *JETP Lett.*, **24** (1976) 163; *JETP*, **45** (1977) 436.

[6] Ferreirinho J., Ruffini R. and Stella L., *Phys. Lett. B*, **91** (1980) 314.
[7] Ruffini R. and Stella L., *Phys. Lett. B*, **102** (1981) 442.
[8] Ruffini R., Rotondo M. and Xue S.-S., *Int. J. Mod. Phys. D*, **16** (2007) 1.
[9] Ruffini R., *Proceedings of the 9th International Conference on "Path Integrals"* (World Scientific) 2008, p. 207.
[10] Popov V. S., *AIP Conf. Proc.*, **1205** (2010) 127.
[11] Rotondo M., Ruffini R., Xue S.-S. and Popov V. S., *Int. J. Mod. Phys. D*, **20** (2011) 1995.
[12] Rotondo M., Jorge A. Rueda, Ruffini R. and Xue S.-S., *Phys. Rev. C*, **83** (2011) 045805.
[13] Feynman R. P., Metropolis N. and Teller E., *Phys. Rev.*, **75** (1949) 1561.
[14] Rotondo M., Jorge A. Rueda, Ruffini R. and Xue S.-S., *Phys. Rev. D*, **84** (2011) 084007.
[15] Rotondo M., Jorge A. Rueda, Ruffini R. and Xue S.-S., *Phys. Lett. B*, **701** (2011) 667.
[16] Jorge A. Rueda, Ruffini R. and Xue S.-S., *Nucl. Phys. A*, **872** (2011) 286.
[17] Tolman R. C., *Phys. Rev.*, **55** (1939) 364.
[18] Oppenheimer J. R. and Volkoff G., *Phys. Rev.*, **55** (1939) 374.
[19] Haensel P., Potekhin A. Y. and Yakovlev D. G., *Neutron Stars 1: Equation of State and Structure* (Springer, New York) 2007.
[20] Evans R., *Fundamentals of Inhomogeneous Fluids* (Dekker, New York) 1992.
[21] Klein O., *Rev. Mod. Phys.*, **21** (1949) 531.
[22] Kodama T. and Yamada M., *Prog. Theor. Phys.*, **47** (1972) 444.
[23] Olson E. and Bailyn M., *Phys. Rev. D*, **12** (1975) 3030.
[24] Rosseland S., *Mon. Not. R. Astron. Soc.*, **84** (1924) 720.
[25] Belvedere R., Pugliese D., Jorge A. Rueda, Ruffini R. and Xue S.-S., *Nucl. Phys. A* (2012), http://dx.doi.org/10.1016/j.nuclphysa.2012.02.018.
[26] Thomas L. H., *Proc. Camb. Philos. Soc.*, **23** (1927) 542.
[27] Fermi E., *Rend. Accad. Lincei*, **6** (1928) 602.
[28] Emden R., *Gaskugeln Anwendungen der Mechanischen Wärmetheorie auf Kosmologische und Meteorologische Probleme* (Teubner, Leipzig) 1907.
[29] Chandrasekhar S., *Astrophys. J.*, **74** (1931) 81.
[30] Landau L. D., *Phys. Z. Sowjetunion*, **1** (1932) 285.
[31] Landau L. D. and Lifshitz E. M., *Statistical Physics*. Part 1 (Pergamon Press, Oxford) 1980.
[32] Stoner E. C., *Philos. Mag.*, **7** (1929) 63.
[33] Fowler R. H., *Mon. Not. R. Astron. Soc.*, **87** (1926) 114.
[34] Milne E. A., *Mon. Not. R. Astron. Soc.*, **91** (1930) 4.
[35] Eddington A. S., *Mon. Not. R. Astron. Soc.*, **95** (1935) 194.
[36] Salpeter E. E., *Astrophys. J.*, **134** (1961) 669.
[37] Frenkel Y. I., *Z. Phys.*, **50** (1928) 234.
[38] Dirac P. A. M., *Proc. Cambridge Philos. Soc.*, **26** (1930) 376.
[39] Tolman R., *Phys. Rev.*, **35** (1930) 904.
[40] Chandrasekhar S., *An Introduction to the Study of Stellar Structure* (The University of Chicago Press, Chicago) 1939.
[41] Ciufolini I. and Ruffini R., *Astrophys. J.*, **275** (1983) 867.
[42] Hund F., *Erg. d. exacten Natwis.*, **15** (1936) 189.
[43] Landau L. D., *Nature*, **19** (1938) 333.
[44] Zel'Dovich I. B., *Sov. Phys. JETP*, **6** (1958) 760.
[45] Harrison B. K., Thorne K. S., Wakano M. and Wheeler J. A., *Gravitation Theory and Gravitational Collapse* (The University of Chicago Press, Chicago) 1965.
[46] Audi G., Wapstra A. H. and Thibault C., *Nucl. Phys. A*, **729** (2003) 337.
[47] Wapstra A. H. and Bos K., *Atomic Data and Nuclear Data Tables*, **19** (1977) 175.
[48] Shapiro S. L. and Teukolsky S. A., *Black Holes, White Dwarfs, and Neutron Stars: The Physics of Compact Objects* (Wiley-Interscience, New York) 1983.

[49] Hamada T. and Salpeter E. E., *Astrophys. J.*, **134** (1961) 683.
[50] Phillips M., *Astrophys. J.*, **413** (1993) L105.
[51] Riess A. G. *et al.*, *Astrophys. J.*, **116** (1998) 1009.
[52] Perlmutter S. *et al.*, *Astrophys. J.*, **517** (1999) 565.
[53] Riess A. G. *et al.*, *Astrophys. J.*, **607** (2004) 665.
[54] Hoyle F. and Fowler W. A., *Astrophys. J.*, **132** (1960) 565.
[55] Goriely S., Chamel N., Janka H.-T. and Pearson J. M., *Astron. Astrophys.*, **531** (2011) A78.
[56] Pearson J. M., Goriely S. and Chamel N., *Phys. Rev. C*, **83** (2011) 065810.
[57] Alcock C., Farhi E. and Olinto A., *Astrophys. J.*, **310** (1986) 261.
[58] Baym G., Bethe H. A. and Pethick C. J., *Nucl. Phys. A*, **175** (1971) 225.
[59] Haensel P., Potekhin A. Y. and Yakovlev D. G., *Neutron Stars 1: Equation of State and Structure* (Springer, New York) 2007.
[60] Olson E. and Bailyn M., *Phys. Rev. D*, **18** (1978) 2175.
[61] Bowers R. L., Campbell J. A. and Zimmerman R. .L., *Phys. Rev. D*, **7** (1973) 2278.
[62] Bowers R. L., Campbell J. A. and Zimmerman R. .L., *Phys. Rev. D*, **7** (1973) 2289.
[63] Johnson M. H. and Teller E., *Phys. Rev.*, **98** (1955) 783.
[64] Duerr H. P., *Phys. Rev.*, **103** (1956) 469.
[65] Miller L. D. and Green A. E. S., *Phys. Rev. C*, **5** (1972) 241.
[66] Lee T. D. and Wick G. C., *Phys. Rev. D*, **9** (1974) 2291.
[67] Lee T. D. and Margulies M., *Phys. Rev. D*, **11** (1974) 1591.
[68] Boguta J. and Rafelski J., *Phys. Lett. B*, **71** (1977) 22.
[69] Boguta J. and Bodmer A. R., *Nucl. Phys. A*, **292** (1977) 413.
[70] Walecka J. D., *Ann. Phys.*, **83** (1974) 491.
[71] Boguta J. and Stocker H., *Phys. Lett. B*, **120** (1983) 289.
[72] Boguta J. and Moszkowski S. A., *Nucl. Phys. A*, **403** (1983) 445.
[73] Boguta J., *Nucl. Phys. A*, **501** (1989) 637.
[74] Lee T. D. and Pang Y., *Phys. Rev. D*, **35** (1987) 3678.
[75] Boguta J., *Phys. Lett. B*, **106** (1981) 255.
[76] Lalazissis G. A., König J. and Ring P., *Phys. Rev. C*, **55** (1997) 540.
[77] Sharma M. M., Nagarajan M. A. and Ring P., *Phys. Lett. B*, **312** (1993) 377.
[78] Sugahara Y. and Toki H., *Nucl. Phys. A*, **579** (1994) 557.
[79] Hirata D., Toki H. and Tanihata I., *Nucl. Phys. A*, **589** (1995) 239.
[80] Tamii A. *et al.*, *Phys. Rev. Lett.*, **107** (2011) 062502.
[81] Müther H., Prakash M. and Ainsworth T. L., *Phys. Lett. B*, **199** (1987) 469.
[82] Kubis S., *Phys. Rev. C*, **76** (2007) 025801.
[83] Sharma B. K. and Pal S., *Phys. Lett. B*, **682** (2009) 23.
[84] Hebeler K., Lattimer J. M., Pethick C. J. and Schwenk A., *Phys. Rev. Lett.*, **105** (2010) 161102.
[85] Loan D. T., Ngo N. H., Khoa D. T. and Margueron J., *Phys. Rev. C*, **83** (2011) 065809.
[86] Debye P. and Hueckerl E., *Phyz. Zeitschr.*, **24** (1923) 185.
[87] Mott N., *Proc. Camb. Philos. Soc.*, **32** (1936) 281.
[88] Myers W. D., *Nucl. Phys.*, **81** (1966) 1.
[89] Trümper J. E., *Prog. Part. Nucl. Phys.*, **66** (2011) 674.
[90] Demorest P. B., Pennucci T., Ransom S. M., Roberts M. S. E. and Hessels J. W. T., *Nature*, **467** (2010) 1081.
[91] Bhattacharyya S., Strohmayer T. E., Miller M. C. and Markwardt C. B., *Astrophys. J.*, **619** (2005) 483.
[92] Trümper J., Burwitz V., Harberl F. and Zavlin V. E., *Nucl. Phys. B Proc. Suppl.*, **132** (2004) 560.
[93] Heinke C. O., Rybicki G. B., Narayan R. and Grindlay J. E., *Astrophys. J.*, **644** (2006) 1090.
[94] Lattimer J. M. and Prakash M., *Science*, **304** (2004) 536.

[95] Hessels J. W. T., Ransom S. M., Stairs I. H., Freire P. C. C., Kaspi V. M. and Camilo F., *Science*, **311** (2006) 1901.
[96] Ruffini R., Vitagliano L. and Xue S.-S., *Phys. Lett. B*, **573** (2003) 33.
[97] Ruffini R., Vitagliano L. and Xue S.-S., *Phys. Lett. B*, **559** (2003) 12.
[98] Ruffini R. and Xue S.-S., *AIP Conf. Proc.*, **1059** (2008) 68.
[99] Ruffini R., Vereshchagin G. V. and Xue S.-S., *Phys. Rep.*, **487** (2010) 1.
[100] Gamow G. and Schoenberg M., *Phys. Rev.*, **59** (1941) 539.
[101] Arnett D., *Supernovae and Nucleosynthesis: An Investigation of the History of Matter from the Big Bang to the Present* (Princeton University Press, Princeton) 1996.